SEATOS

2005 Cruise Report

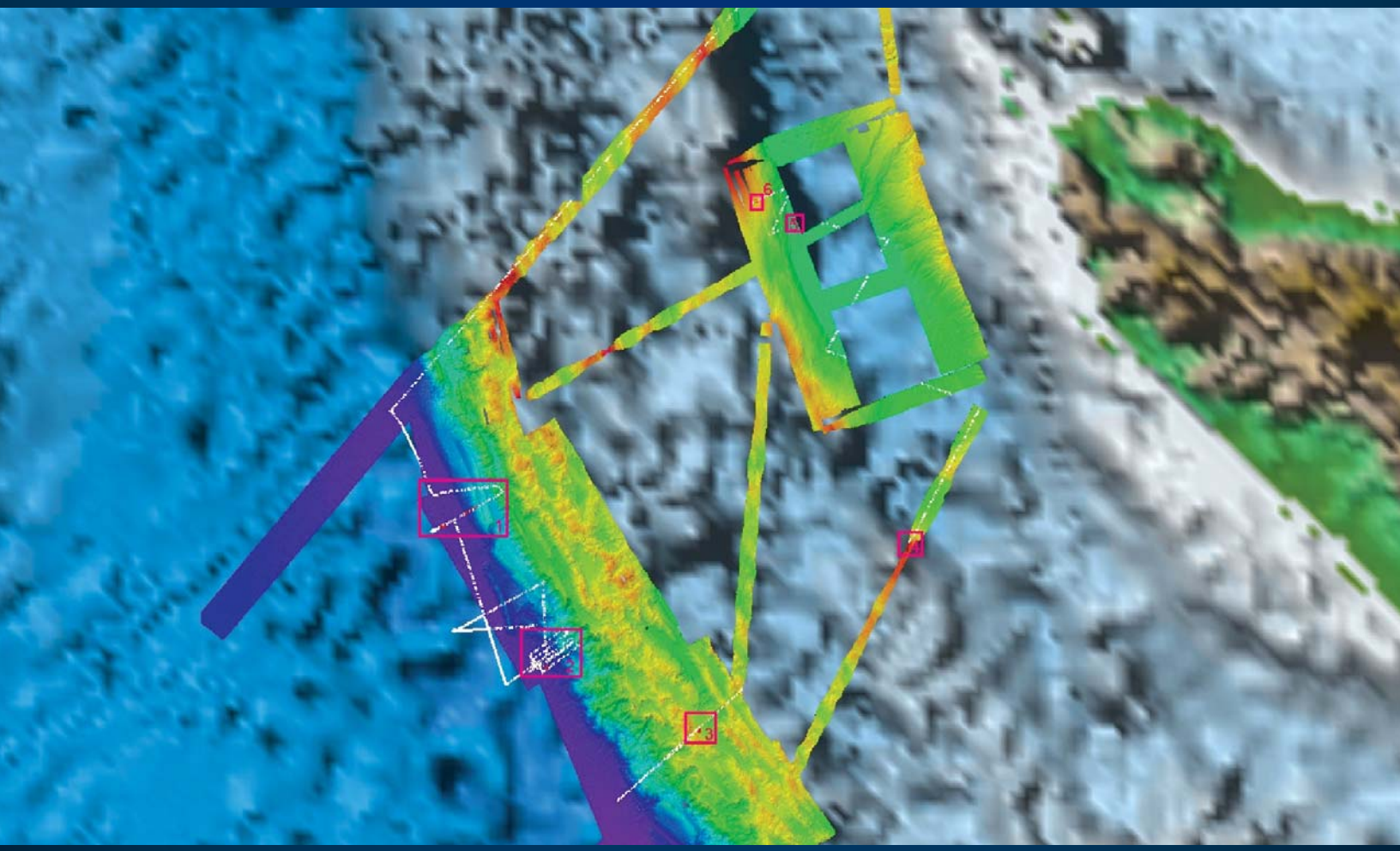

Sumatra Earthquake and Tsunami Offshore Survey (SEATOS)

SEATOS

2005 Cruise Report

Sumatra Earthquake and Tsunami Offshore Survey (SEATOS)

Contents

Summary 1

1. Background 2

2. Methods & Approaches 4
   - Geophysics 4
   - Biology 9
   - Earthquake Modeling 10
   - Tsunami Modeling 11
   - Survey Planning 16
   - Geotechnical and Slope Stability 18

3. Survey Results 19
   - Cross-Margin Transect 19
     - Site 1: Landslide Site 20
     - Site 2: The Block 25
     - Site 3: The "Ditch" 26
     - Site 3A: The Proto-Ditch 29
     - Site 4: The "Frog Pond" 29
     - Site 5: Southern Forearc High ("Sweet Spot") 30
   - Forearc Basin Survey 32
     - Forearc Basin ROV Survey 34
     - Site 6: Forearc Basin Survey ("Mosher's Mystery Tour") 36
     - Site 7: Northern Forearc High ("Mosher's Toe") 37
     - Site 8: Don's Volcano 37

4. References 40

Appendix A: Tsunami Wave Modeling Results A-1

Appendix B: SEATOS Data Logs B-1

ACKNOWLEDGEMENTS

Primary funding was provided by the British Broadcasting Corporation and The Discovery Channel. Supplemental funding for additional shiptime and fuel was provided by Science Applications International Corporation and BP Marine Limited.

Science support funding was provided by the University of Rhode Island, British Geological Survey, Geological Survey of Canada, Alfred P. Sloan Foundation's Census of Marine Life, University of New Hampshire Center for Coastal and Ocean Mapping, Institute for Geophysics at the University of Texas Austin, Pennsylvania State University, Institut de Recherche pour le Dévelopement–"Géosciences Azur"–Observatoire Océanologique, and L'ecole Normale Superieure de Cachan. Oceaneering International Corporation provided extensive support and provision of the M/V *The Performer*. Special thanks to the Captain and crew.

SEATOS results were used in several TV documentaries, aired by BBC and Discovery Channel and produced by Darlow Smithson Productions. Special thanks to Julian Ware and Ed Wardle for their strong support of science in the TV shows. Thanks also to David Mearns, Bluewater Recoveries for oversight, coordination, and developing the concept for the documentaries. We thank the United Kingdom Ministry of Defence and Hydrographic Office for Dave Tappin's access to the HMS *Scott* data, the British Embassy Jakarta for assistance with offshore permitting, and The Republic of Indonesia for granting permits for the survey.

Editing and design by Geosciences Professional Services.

PREFERRED CITATION

Moran, K. and D. Tappin. 2006. *SEATOS 2005 Cruise Report: Sumatra Earthquake and Tsunami Offshore Survey (SEATOS)*. 92 pp. [Online] available at http://ocean.oce.uri.edu/seatos.

SEATOS Participants

SHIPBOARD SCIENCE PARTY

The science party was selected to represent experts across a broad range of disciplines and to maximize international representation. The party was divided into five teams: geophysics, biology, earthquake modeling, tsunami modeling, and visualization, listed below.

Co-chief Scientists
Kate Moran, University of Rhode Island (USA)
David Tappin, British Geological Survey (UK)

Biology
Paul Tyler, National Oceanography Centre, Southampton (UK)
Jon Copley, National Oceanography Centre, Southampton (UK)
Joelle Galeron, IFREMER (France)
Baban Ingole, Institute of Oceanography (India)

Earthquake Modeling
Don Fisher, Pennsylvania State University (USA)
Tim Masterlark, SAIC (USA)
Yang Shen, University of Rhode Island (USA)

Geophysics
David Mosher, Geological Survey of Canada (Canada)
Jamie Austin, University of Texas (USA)
Aaron Bradshaw, University of Rhode Island (USA)
Borden Chapman, Geological Survey of Canada (Canada)
Steffen Saustrup, University of Texas (USA)

Tsunami Modeling
Frederic Dias, Ecole Normale Superieure de Cachan (France)
Stephan Grilli, University of Rhode Island (USA)
Mansour Ioualelen, Geoscience Azur, Institut de Recherche pour le Development, IRD (France)

Visualization
Larry Mayer, University of New Hampshire (USA)
Colin Ware, University of New Hampshire (USA)
Roland Arseneault, University of New Hampshire (USA)
Kate Collins, University of British Columbia (Canada)

LAND BASED SCIENTISTS

In addition to the shipboard participants there were land based scientists contributing to the survey:

Cindy van Dover, William and Mary University, Biologist (USA)
Tim Henstock, University of Southampton, Geophysicist (UK)
Lisa McNeill, University of Southampton, Geologist (UK)
Phil Watts, Applied Fluids Engineering, Modeller (USA)

PRODUCTION TEAM

David Mearns, Client Representative, Bluewater Recoveries (UK)
Josh Talbot, Darlow Smithson (Singapore/Australia)
Dudley Sargeant, Darlow Smithson (UK)
Matt Green, Darlow Smithson (UK)
Jim Mercer, Bluewater Recoveries (UK)
Vicki Young, Darlow Smithson (UK)
Ed Wardle, Darlow Smithson (UK)

M/V *THE PERFORMER* CREW

Gregg Dayton Baptiste ..... Captain
Christina Maria Aguiar ..... 3rd Assistant Engineer
Girvle Dewey Brandon III..... Crane Operator
David Wayne Casey..... Inventory Specialist
Robert William Fisher ..... Motorman
Omar Flores ..... Galleyhand
Jill Paige Friedman ..... 2nd Mate
Chad Norbert Fuhrmann ..... 1st Assistant Engineer
Kenneth Carl Guthjahar ..... ROV navigator
William Thomas Innes..... Chief Mate
Stanley Raymond Jandura ..... ROV Electrician
Donald Dale Kammerzell..... ROV Electrician
Russell Cameron Keltner..... A/B
Troy Kriesch ..... ROV Mechanic
Hugh Burbank MacLeod..... Chief Engineer
George Franklin Myers..... ROV Mechanic
Daniel Wade Oden ..... Electrician
John Pizzariello..... 3rd Mate
Steven Curtis Powers..... ROV Supervisor
Patrick Allen Purington..... A/B
Raymond Salo ..... Bosun
Glenn Thomas Schulten ..... ROV Mechanic
Eric Stephen Smith..... ROV Engineer
Michael James Soroczak ..... O/S
Rayburn Scott Stewart ..... 2nd Cook
William D. Varquez..... 1st Cook
Arnel Samson Vasquez ..... Motorman
Marciele Lois Woodard..... C/S

Summary

In May 2005, an international, interdisciplinary team of scientists conducted a detailed survey of the seafloor in the vicinity of the epicenter of the Great Sumatra earthquake of December 26, 2004. The survey was named the Sumatra Earthquake and Tsunami Offshore Survey (SEATOS). The December 26 tsunami was one of the most devastating in recorded history. It was generated in the Indian Ocean off of the Indonesian island of Sumatra by one of the largest earthquakes ever recorded, with a moment magnitude M_w= 9.1–9.3 (Ammon et al., 2005; Lay et al., 2005; Stein and Okal, 2005). The number of fatalities caused by the tsunami is an estimated 300,000 (http://portal.unesco.org/en/ev.php-URL_ID=24838&URL_DO=DO_TOPIC&URL_SECTION=201.html), spread over more than 10 countries located on the coast of the Indian Ocean. Over 130,000 of those who died lived on the Indonesian island of Sumatra in the region of Banda Aceh. The other most affected countries included Thailand, Sri Lanka, and India.

The earthquake and tsunami had a global impact. The earthquake shook the Earth's axis and slowed down Earth's rotation by 2.68 μs per day. The tsunami wave traveled around the world for three days. The widespread destruction resulted in one of the largest emergency relief efforts ever mounted. Scientists had previously warned that a major earthquake and tsunami could strike the region off Sumatra, although the exact location and impact was not accurately identified. In all the countries affected by the tsunami, the absence of any effective tsunami education or warning system increased the number of fatalities, although victims on the island of Sumatra, closest to the earthquake epicenter, had little chance of escaping the waves.

The overall goal of the SEATOS was to gather data to improve models of seafloor displacement and the resulting tsunami wave. To achieve this aim, single channel seismic (SCS) data and seabed images and cores from a remotely operated vehicle (ROV) were acquired. The SEATOS survey was planned using the results of HMS *Scott* multibeam data acquired in February 2005 (Henstock et al., in press). Eight sites were selected from the HMS *Scott* data for SEATOS detailed investigations: a large underwater landslide (two sites) and a ~20-km-long trench feature (the "Ditch") located at the deformation front, both of which were interpreted as possibly due to the December 26 earthquake; two locations on the forearc high to investigate evidence of recent seabed movement; two locations on the margin of the Aceh forearc basin, which may be the sites of recent strike slip faulting; and a steep mound north of Sumatra, interpreted as a volcano.

SCS data were also acquired across the margin in the north of the study area and between detailed study sites to characterize the style of subduction in this area.

Data acquisition began after a 30-hour steam from Phuket, Thailand to the northeastern edge of the plate margin offshore Sumatra where the high-resolution seismic system was deployed to acquire a cross-margin transect. SCS data, ROV imagery (high-definition television quality video), biological core data, and sedimentological cores were acquired at sites located at the accretionary complex deformation front, at one site in the forearc fold regions, and at sites along the forearc high. Early results suggest a likelihood of significant seafloor disturbance from the December 26, 2004 earthquake at least at one site at the deformation front. The forearc high is characterized mainly by stable seafloor conditions. The sites on the western margin of the forearc basin revealed no visible evidence of recent movement. To the north of the Aceh forearc basin, and north of Sumatra, the 200-m high conical shaped structure proved to be a volcano with no evidence of recent activity.

This cruise report includes a background chapter describing the rationale for the expedition; methods chapters for each scientific team; and eight site/transect chapters that include descriptions of survey operations, site data acquired, and initial interpretations. There is also a separate appendix on tsunami wave modeling.

1. Background

During earthquakes greater than Ms > 7, there is the potential to generate large tsunamis by the co-seismic displacement of the seafloor. In the deep open ocean, tsunamis take the form of small amplitude (~0.5–1 m), long period waves (~100 km), which are difficult to discern. Such waves propagate at great speed (>300 km/hr) and travel over great distances. As they approach the shore, and water depth decreases, bottom friction results in wave deceleration and a transfer of energy that leads to the formation of taller and shorter-wavelength (~5 km) waves that can be over 10-m high and very destructive.

Co-seismic displacement waves are usually generated over a larger source area, have a longer wavelength and greater energy, but have lower energy per unit area (and are thus smaller on a local scale) than landslide-generated waves. The initial wave heights of co-seismic tsunamis correlate with earthquake magnitudes.

On December 26, 2004 at 0058 GMT, an earthquake of M_w = ~9.1–9.3 (Ammon et al., 2005) occurred along the Sumatra subduction zone rupturing 1300 km of crust and creating a teleseismic tsunami that, on striking adjacent coastlines, resulted in the deaths of an estimated 300,000 people and caused billions of dollars of damage.

In January 2005, as one response to the disaster, the British government dispatched the Royal Navy's hydrographic research vessel, HMS *Scott*, to the region. Off the northwest coast of Sumatra, the ship mapped, using a 12 kHz multibeam system, over 40,000 km^2 of seabed on the margin of the subduction zone and over the Aceh forearc basin (Figure 1). The objectives of the multibeam

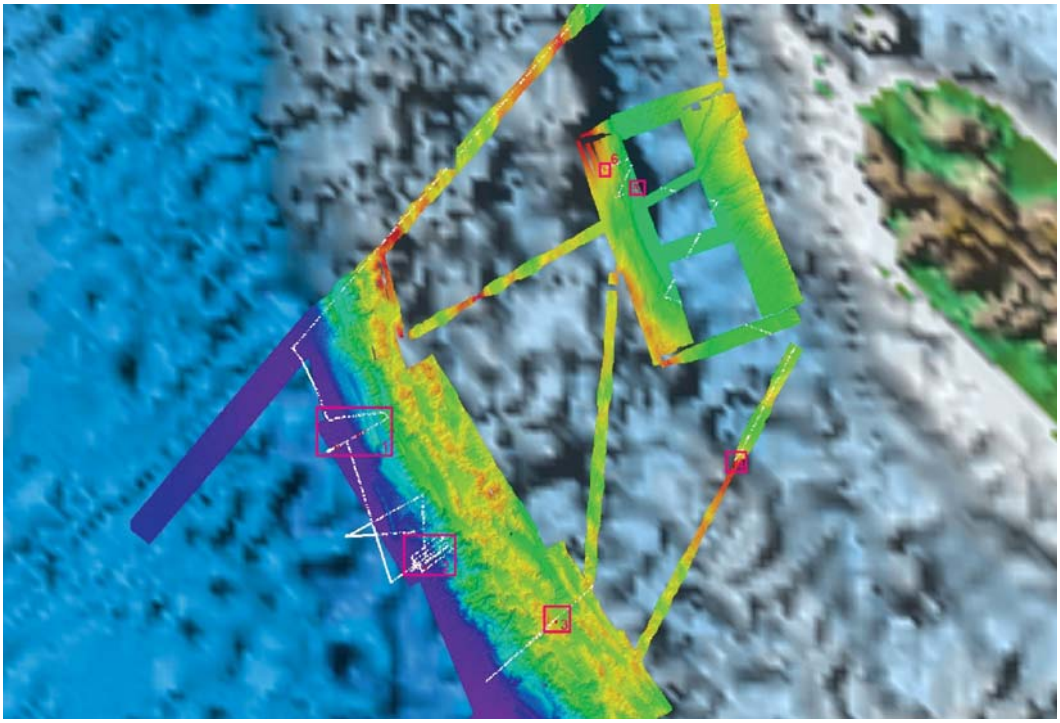

Figure 1. Basemap of the study area showing the northern tip of Sumatra (green/brown) and the adjacent continental margin. Overlying the ETOPO2 bathymetry data is an image of the multibeam data collected by HMS *Scott*. White lines are single channel seismic lines. SEATOS 2005 study sites (red boxes) were selected from the multibeam data. Site 1 is the landslide; 2 is the "Ditch;" 3 is "Frog Pond;" 4, 5, 6 are forearc high sites; and 7 (not shown), located norht of Sumatra, is the volcano.

survey were to investigate the regional morphology and underlying subductions zone structure, and identify areas of recent seabed movement and submarine mass failures that may have been caused by the earthquake.

SEATOS scientific program targets were based on interpretations of the HMS *Scott* multibeam data (Henstock et al., in press) (Figure 1). Most survey sites were chosen where it looked like recent, large-scale deformation had taken place. From May 9 to May 25, 2005, the SEATOS program acquired SCS and ROV imagery, although initial survey plans included acquisition of high-resolution deep-tow Huntec sparker data, side-scan sonar data, and sediment cores. SEATOS program objectives were to investigate the seafloor near the great Sumatra earthquake epicenter. Previous to the survey, five main locations were selected for detailed investigation: a large young, underwater landslide (two sites); a~20-km-long trench feature (the "Ditch") located at the deformation front, both of which were interpreted as possibly due to the December 26 earthquake; a location on the forearc high to investigate for evidence of recent seabed movment; and the western margin of the Aceh forearc basin, which may have been the site of recent strike-slip faulting. Two more locations were added during the survey, another site on the forearc high (Sweet Spot) and a steep mound north of Sumatra, interpreted as a volcano.

Data collected would enable reconstruction of seafloor displacement, which could then be incorporated into new earthquake models because an additional and important SEATOS objective was to improve existing models of the tsunami source, propagation, and runup. Early estimates of seafloor displacements used in tsunami wave models to hindcast the event did not accurately reconstruct all of the observations of the tsunami generated on December 26, including those from tide gage records, satellite observations, and coastal run-up measured by field survey teams along the impacted coasts of the Indian Ocean.

Regional models of seafloor displacement (along the entire rupture zone) with vertical uplift of 5–10 m calculated from the earthquake magnitude were used as a basis for modeling the tsunami source. The feature, termed the "Ditch," identified in the HMS *Scott* data, displayed a similar order-of-magnitude vertical movement and may have formed coseismically during the 2004 earthquake (Henstock et al., in press)

2. Methods & Approaches

GEOPHYSICS

The Geological Survey of Canada (Atlantic) provided most of the mechanical equipment used in the collection of seismic reflection data for the cruise. The University of Rhode Island provided the air compressors. Two reflection systems were mobilized: a single channel seismic reflection profiling system and a high-resolution Huntec DTS sparker system received on an internal and external hydrophone array. However, the Huntec system had extremely limited application in SEATOS due to water depth limitations.

The seismic reflection profiling system consisted of a pneumatic source, supplied with pressurized air from two onboard compressors, a firing system, a receiving hydrophone array, a digital data recorder, and a hard-copy recorder.

The sound source used for seismic operations on SEATOS was the Seismic Systems Inc. Generator Injector (GI) gun (or a two GI gun array) (Figure 2). The two guns were mounted horizontally below a 3-m-long I-beam tow frame that, in turn, was suspended from two Norwegian Floats. Tow depth was 1.25 m below the sea surface and 50 m behind the fantail. When operating two GI guns, the blast phones were used to synchronize the guns. The Long Shot firing unit automatically adjusts fire delays to synchronize the two guns.

The concept behind the GI gun is that an initial pressure wave is generated by the release of compressed air (the generator), as in a conventional airgun. This sudden re-lease of compressed air produces the primary pulse and the resulting volume of air (the bubble) starts to expand. When the bubble approaches its maximum size, it encompasses the injector ports and its internal pressure

Figure 2. The two air gun array on the fantail of M/V *The Performer*

is far below the outside hydrostatic pressure. In a conventional airgun, the bubble would now collapse and it is this expansion and collapse that gives rise to the bubble pulse. In the GI gun, the injector is fired at this time, injecting air directly inside the bubble, increasing the internal pressure of the bubble and preventing its violent collapse. The oscillations of the bubble and the resulting secondary pressure pulses are thus reduced and reshaped.

With two air guns, the source amplitude is nearly doubled. The resulting power spectral density of the two gun array (Figure 3) shows the power.

There are two modes of operation of the GI gun. For this expedition, the gun was operated in harmonic mode (recommended for high-resolution surveying). In harmonic mode, the generator and injector volumes are each 105 in^3, so the sum total volume for both guns combined is 420 in^3.

The GI gun is equipped with a blast phone. Through monitoring the blast phone and varying the delay between the generator and injector pulses, the optimum bubble cancellation was achieved. The optimum delay was found to be 16 ms.

Compressed air, maintained between 1,750 and 1,820 psi (12,065 and 12,548 kPa), was supplied to the GI guns from 2 Price Model W2 electric. These compressors are driven by two diesel generators producing approximately 80-85 SCFI of compressed air, at pressures up to 2,500 PSI. Cooling water for the compressor intercoolers comes from a pump in the engine room of the vessel. Because of the complexity of the Price diesel compressor, an operator must be constantly available to monitor the functions of both the diesel engine and the compressor. All machine statistics were inspected at 15-min intervals by watch keepers.

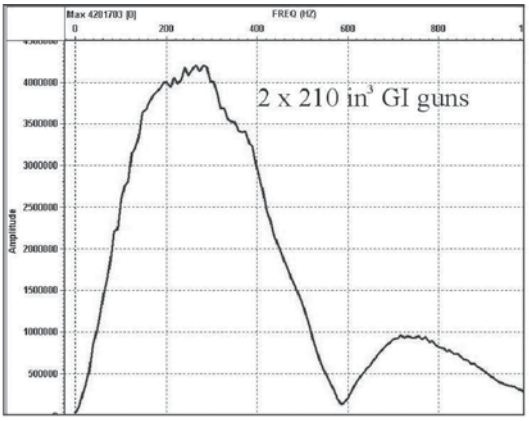

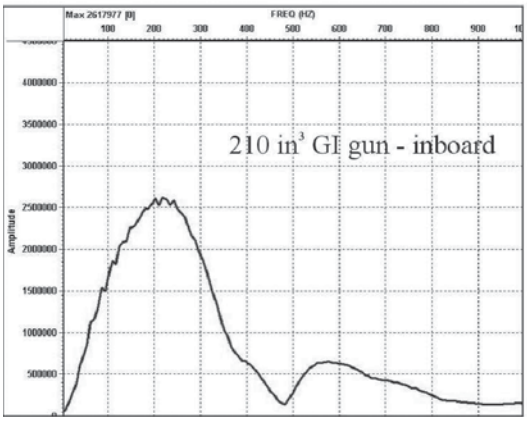

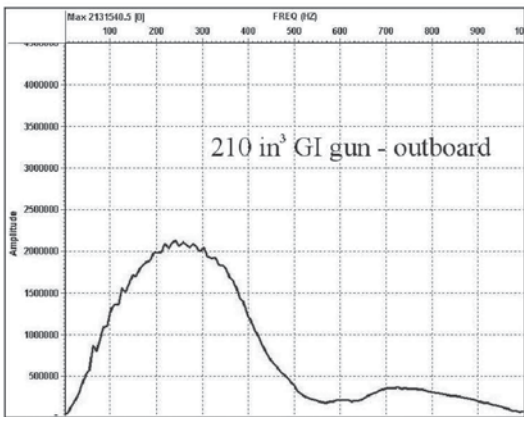

Figure 3. Power spectra for the source signatures shown in the above signature tests. Relative energy in the two-gun array is nearly double that of each single gun separately. The frequency bandwidths are nearly equivalent, however, so no high frequencies are lost.

Airgun (GI and sleeve) firing was controlled by the MITS system to fire on time intervals. The trigger signal was supplied to the RTS Long Shot firing box that sent a voltage to the gun solenoids to trigger firing. The time interval between the generator and the injector firing for the GI gun was set by the software of the Long Shot gun controller. We observed that the optimal interval between "G" and "I" firing was 16 ms for the gun tow depth of approximately 1 m (3.14 ft). The fire rate was 8 s throughout the cruise.

The Teledyne model 28420 streamer is 61 m (200 ft) in length, which includes an 8 m (27 ft) lead in dead section and a 4.9 m (16 ft) dead section at the tail. The active section is 45.2 m (148.33 ft) long, consisting of two interlaced sets of three groups, comprising a total of six groups of Teledyne B-1 acceleration-canceling hydrophone cartridges. There are 16 individual hydrophones within a group, each element separated by 1 m (3.14 ft). The companion, interlaced group is equivalent in dimensions and is offset from the first group by 0.23 m (0.75 ft). For all operations, signals from the active groups in the streamer were summed into a single channel. This capability is provided by a deck-unit switching board into which the signal feeds. This unit also provides some gain control on signal levels.

The Teledyne hydrophone streamer was outfitted with a DigiCourse DigiBird Model 9000-5010 for each deployment, mounted at the lead dead section. This "bird" allows for actively setting and maintaining hydrophone streamer tow depth. It can be controlled and monitored from the shipboard lab with the DigiScan system and it is self-correcting (dynamic) to maintain depth of flight. To remain compatible with the tow depth of the sound source array, the bird was set to fly at 4 m (12 ft). The streamer was towed 50 m astern of the fantail (Figure 4). It was noted that the length of the "lead in" cable deployed had a direct affect on the ability of the bird to control the depth. Too much "lead in" cable caused the eel to sink; with too little "lead in" cable deployed, the bird could not "sink" the eel. Further investigation on placing positive buoyancy devices on the lead in cable should be undertaken. It was clear that the optimum tow distance placed the front of the eel adjacent to the GI gun, a distance of 50 m behind the vessel.

Seismic signals were digitally recorded with a GSC-DIGS unit and the parameters shown in Table 1.

The GSCDIGS system is built upon a sigma-delta A/D converter. This converter provides the ability of employing high sample rates and high dynamic range, avoiding the need for anti-alias filtering and constant gain adjustment. The result is ease of use to the end user and higher and consistent data quality. Acquisition and interface software (GDAim v. 1.4) was designed and built by D. Heffler of GSC-A. The software allows for real-time monitoring of signals including time series and power spectral density views. Data are recorded to hard drive in 24-bit long integer SEG-Y format. Deepwater delay times and navigation data are written to the SEGY headers. Data are immediately suitable for commercial seismic processing and interpretation software as a result of

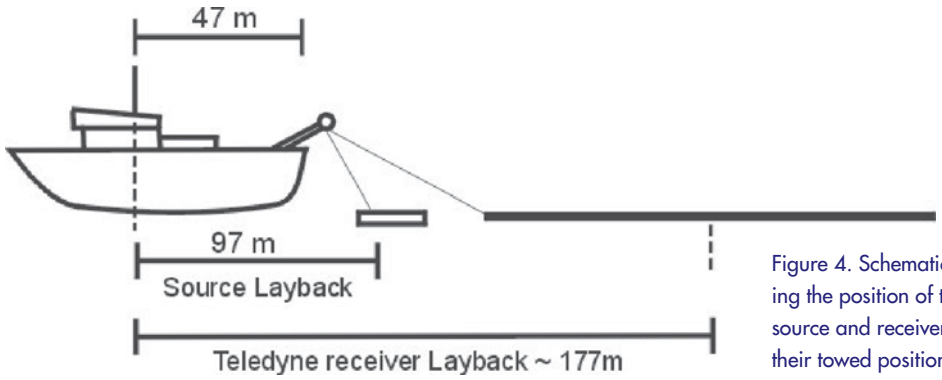

Figure 4. Schematic depicting the position of the air gun source and receiver streamer in their towed positions.

the data format and information in the headers. Data are recorded on commercially available DVD media, providing ease of backup and recovery.

For the Huntec system (Figure 5), the GSCDIGS system manages the master trigger and the fire trigger to accommodate heave compensation, and it integrates the fish depth. It also successfully tracks multiple shots in the water, often used in deep-water data acquisition. The result is that all records are referenced from sea level.

Seismic signals were first passed through a Krohn-Hite Model 3905B multi-channel filter and band passed between 65 and 500 Hz with a 20 dB gain amplification before going to the EPC hardcopy recorder. Signals to the digitizer were unfiltered and unamplified. Post-acquisition, these raw seismic signals were digitally filtered with an Ormsby bandpass filter of 10/35 to 325/350 Hz. An exponential gain (time*e1.5) was applied to compensate for spherical spreading losses. Seismic traces were padded to compensate for deepwater delays and data were compiled into line segments before being imported into interpretation software.

The Huntec (DTS) typically uses a boomer source,

Table 1. GSCDIGS (GDAIMS v. 1.4)

Seismic - Raw (Channel 1)	Sample rate 250 µs (0.25 ms), sample window 2,500 ms, number of samples 10,000
Seismic - Filtered (Channel 2)	Sample rate 250 µs (0.25 ms), sample window 2,500 ms, number of samples 10,000
Deep Water Delays	Managed on the fly through software window and recorded in the SEG-Y header
Data Recording[1]	Data written to hard drive and backed up on DVD media

[1]Seismic digital data log is structured as:

Disk	Start Day	UTC time	End Day	UTC time	Lines
DVD 1	1/31/2005	00:16	132/2005	23:54	1-5

Figure 5. The Huntec fish on the after deck of the M/V *The Performer*

but for deep water or hard seafloor substratum a sparker attachment can be used to increase the source energy. Higher frequencies and source repeatability are sacrificed as a result.

Sparker systems operate by creating an explosive spark arcing between electrodes and the fish body that vaporizes the water. The resulting vapor bubble then collapses under ambient pressure. The sparker signature (Figure 6), therefore, is highly dependent upon energy input (voltage), relative positions of the electrodes, conductivity (salinity) of the medium in which it is immersed, and tow depth (pressure field). At equivalent depths, source characteristics are similar but vary slightly in amplitude as a result of input voltages (Figure 6).

At different water depths, however, the differences in source characteristics are dramatic. At greater depths, the initial amplitude resulting from the spark is smaller, but the vapor bubble collapses much more rapidly under the higher ambient pressure, causing a shortening of the pulse. This rapid collapse also causes oscillations in the bubble resulting in a ringing characteristic. Figure 7 shows the source spectra characteristics of the sparker at

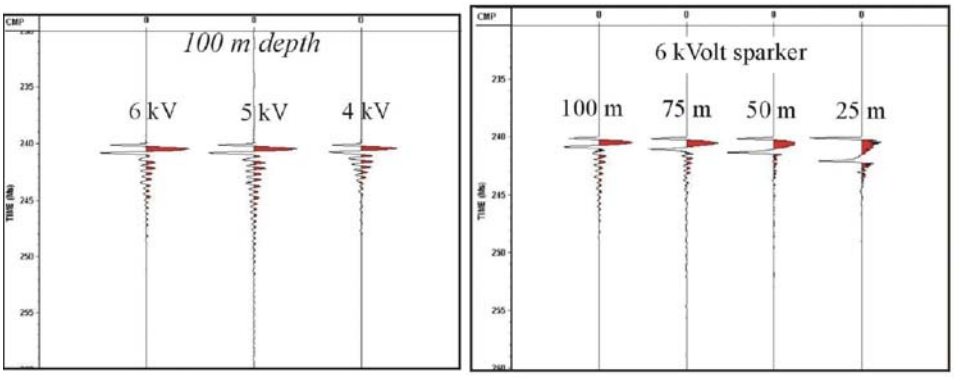

Figure 6. Huntec sparker signatures at 100 m depth with three different voltages (left). The characteristics of these three pulses are similar; amplitudes differ only slightly. Huntec sparker signatures at 6 kV and variable depths (right). Note the extreme difference in pulse characteristics between 100 and 25 m depth.

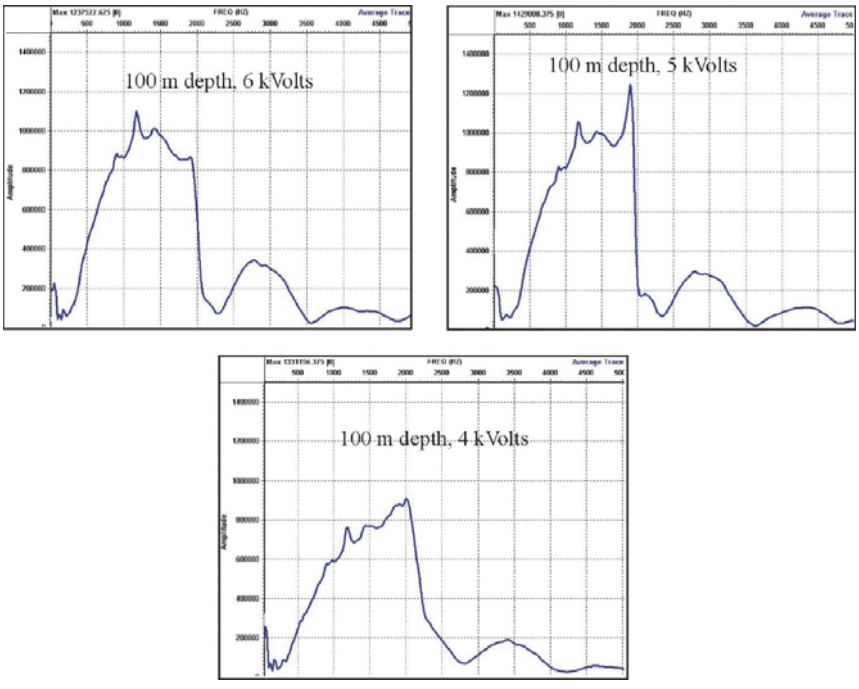

Figure 7. Source spectral characteristics for the Huntec sparker at 100 m and varying voltage inputs.

100 m depth and various voltages. For operations during this mission, the Huntec fish was towed at a depth of about 60 m. Due to the great water depths and steep terrain encountered, few useful Huntec sparker seismic signals were obtained.

BIOLOGY

The primary objectives of the biology team were: (1) to compare the macrofauna and meiofauna inhabiting seafloor features interpreted as "disturbed" by recent seismic activity with "undisturbed" reference sites at comparable depth; and (2) to survey the megafauna of the accretionary prism, with particular attention to any chemosynthetic communities.

ROV Setup

A quadrant frame was attached to the port side of the Magellan 825 ROV (Figure 8) to carry:

1. a mesh sample basket (mesh size 1 mm) with hydraulic lid;
2. three push cores (60 mm diameter) and quivers, supplied by CLVD; and
3. three IFREMER blade corers (200 x 100 mm), carried in sample basket.

The ROV also carried a suction sampler (50 mm tube diameter) connected to a second mesh sample basket (5 mm mesh) at the rear of the vehicle. The ROV was equipped with a three-chip CCD video camera and digital still camera (set at 2,048 x 1,536 resolution) on a pan-and-tilt mount to obtain seafloor images.

Videography

The occurrence and putative identification of benthic and benthopelagic megafauna was logged by biological observers during ROV transects. Digital still images were also obtained for post-dive reference. Approximate scale of specimens and features was provided by the 50 mm width of the suction sampler mounted by the starboard manipulator.

Sampling of Macro- and Meiofauna

IFREMER blade corers were used to collect macrofaunal and meiofaunal samples for analysis and additional samples were collected by push cores. Following recovery of the ROV, cores were photographed prior to extrusion and sectioning into core depths of 0–10 mm, 10–30 mm, 30–50 mm, 50–100 mm, and 100–150 mm. Sections were fixed with 10% buffered seawater formalin. Each

Figure 8. Left photo. ROV setup (left to right): suction sampler hose, pan-and-tilt cameras, sample basket on quadrant frame. Right photo. Sample basket containing blade cores; pushcores and quivers were mounted to the right of basket.

section was sieved into greater than 500 mm, 300–500 mm, and 250–300 mm size fractions. A 63–250 mm fraction was also collected for sections in the top 50 mm of each core sample.

Sampling of Megafauna

The suction sampler attached to the starboard manipulator was used to collect specimens into mesh basket attached to the rear of the vehicle. Epibenthic megafauna were also collected using the blade corers. Specimens were either preserved in 95% ethanol (for genetic studies) or fixed in 10% seawater formalin for 48 hours and preserved in 70% ethanol (for morphology).

EARTHQUAKE MODELING

The main objectives of the SEATOS Tectonics Team were: (1) to characterize the structure and determine the structural evolution across the margin using seismic reflection profiles, and (2) to use the offsets on recent structures identified from seismic reflection profiling and ROV observations to constrain the slip distribution of the earthquake.

Wedge Structure and Kinematics

The forearc of thickly sedimented convergent margins is characterized by a critically tapered wedge that faces the incoming plate. This prism grows seaward through time due to transfer of material from the downgoing plate to the overriding plate by offscraping of material at the toe of the prism and underplating of material along the base. In general, the surface of the prism is convex upward, and the forearc can be subdivided into three domains from the trench to the volcanic arc: (1) the steep lower slope or toe of the prism, (2) the upper slope and fore arc high, and (3) the fore arc basin.

The multibeam bathymetry in the Sumatran forearc acquired by HMS *Scott* depicts a lower slope with ridges parallel to the plate margin that represent the surface expression of fault-related folds. The frontal structure of the margin (i.e., the most recent structure to develop) is unusual when compared to other similar margins (e.g., Nankai, Barbados, eastern Aleutian); ridge segments display a gentle slope facing seaward and a shorter, steeper slope facing landward, a geometry that is suggestive of backthrusting along a fault that is antithetic to the margin(Henstock et al., in press). A segment of the Cascadia accretionary wedge displays similar features that have been attributed to low friction along basal decollement that defines the plate boundary. Another potential explanation along the Sumatran margin is that the shallower sediments of the trench are delaminated from the deeper part of the section as a passive roof that is uplifted and backthrust over a trenchward propagating duplex at depth.

The SCS reflection program investigated the forearc frontal structures in the following manner:

1. The geometry of the faulted folds together with sediments in basins between ridges describe the kinematics of fault-related folding. Growth strata in these basins may record progressive tilting of pre-growth strata that define fold limbs, and these stratal geometries can be used to evaluate how these structures have evolved through time.
2. Using the seismic lines that cross the entire accretionary wedge, we employed similar methods to investigate perched basins on the upper slope to determine whether these older structures record a similar deformation history to those lower down. By comparing the deformation history recorded by different basins across the wedge, we determined the distribution of deformation in time and space.
3. A seismic survey across the fore arc basin was used to determine the geometry of the basement-cover contact, particularly at the margin of the basin proximal to the fore arc high. This boundary was important for evaluating the gross morphology of the wedge and placing the seismic transect in the context of geodynamic models for critical wedge dynamics model that provides an explanation for the location of large subduction megathrust earthquakes.
4. Finally, we attempted to relate any scarps on the seafloor imaged by the ROV biology/geology teams that may be related to recent seabed movement, such as the December 26 earthquake, to subsurface faults imaged by the Geophysics Team.

Deformation, Stress, and Pore Pressure Models

A slip distribution for the December 26, 2004 M_w 9.2 earthquake was estimated by inverse modeling techniques using the available deformation data and Green's functions for deformation due a dislocation in a homogeneous, isotropic, half-space (Okada, 1992). The resulting slip distribution predicts the coseismic as well as the steady-state deformation, stress, and pore pressure in the region. The two poroelastic-states are simulated by using undrained and drained material properties for coseismic and steady-state conditions, respectively (Berryman and Wang, 2000). These calculations not only predict the deformation that drives the tsunami, but also addresses the potentially causal relationship linking the 2004 M_w 9.2 and 2005 M_w 8.7 Sumatra earthquakes via Coulomb stress analyses (Masterlark and Wang, 2002).

TSUNAMI MODELING

General Approach

The two main objectives for the Tsunami Modeling Group were to: (1) refine the tsunami source to perform more accurate simulations of the December 26, 2004 tsunami at the Indian Ocean basin scale based on new information obtained during the cruise; and (2) perform regional simulations on refined grids and better estimate coastal tsunami impact for selected areas (e.g., Ko Phi Phi, Banda Aceh). The latter can be referred to as case studies. A full description of the modeling and results is attached in Appendix A.

The tsunami source used in the modeling was based on existing pre-cruise information, supplemented by seafloor morphology and other information about the earthquake obtained during the cruise and provided by the geophysics and seismology groups. The initial rupture model used in our pre-cruise work (Watts et al., 2005) was made of four separate segments, with different characteristics, along a 1200-km-long rupture zone. Tsunami sources for these segments were obtained using Okada's (1985) method. According to information from existing rupture models (Okada, 1985), we triggered these sources in a time sequence spanning 331 s, and performed a numerical simulation of the tsunami with a higher-order Boussinesq model (i.e., a dispersive long wave model with full nonlinearity up to a certain order). The pre-cruise source gave reasonable agreement of numerical results with a few observed coastal runup values.

During the cruise, as more became known about the tsunami source, we iteratively conducted modeling studies at a number of selected locations aimed at better reproducing tide gage measurements, *Jason I* satellite observations, and runup data collected by a variety of international teams. We also created the topographic and grid data for the regional studies and modeled these in order to perform the selected case studies.

Methods

There were direct instrument observations of the event in and around the Indian Ocean region, including seismometers, tide gages (Figures 9 and 10), buoys, GPS stations, and at least one satellite overpass (*Jason I*) (Figures 11 and 12) (Gower, 2005; Kulikov, 2005). Some of the tide-gage data were processed to estimate the likely location and extension of the tsunami source area (e.g., Figure 13). A similar analysis performed by Lay et al. (2005), using nine additional arrival times around the western Indian Ocean basin, yields a tsunami source area for strong initial tsunami excitation apparently extending 600–800 km north of the epicenter.

These data, after proper correction and interpretation, represent invaluable records of what happened on December 26, 2004 and will help us understand the tsunami event better and calibrate and validate our numerical models. Direct eyewitness observations of the December 26, 2004 tsunami event were numerous, and many of these observations were in the form of still pictures and movies, because some of the regions hit by the wave are popular tourist destinations. These records display a wide variety of waveforms and wave activity that are distinct to each location. In addition, various media recorded numerous eyewitness accounts, and many of these were posted on the web, with a great deal of detail

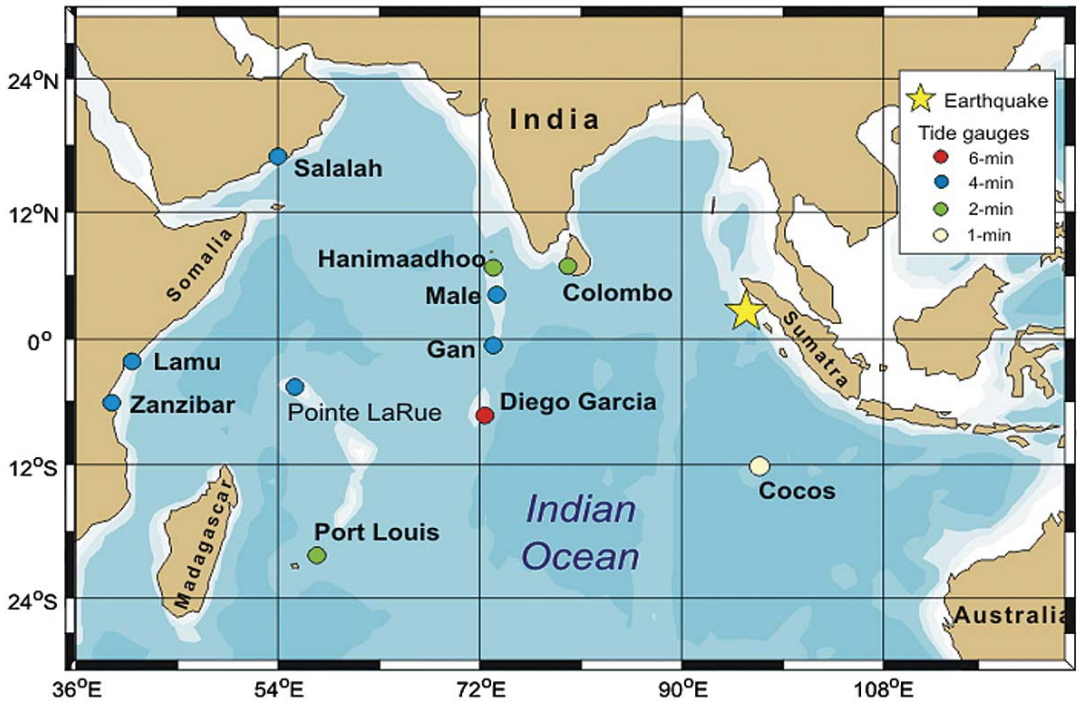

Figure 9. Location of some tide gages in the Indian Ocean basin

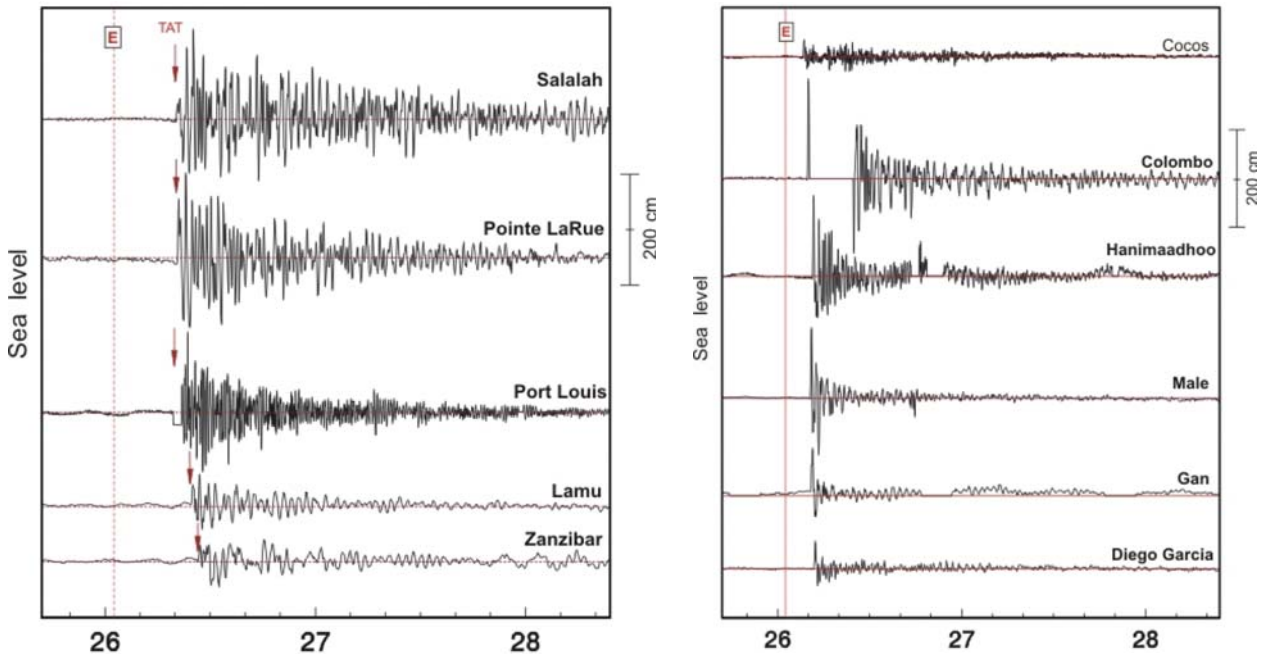

Figure 10. Measurements at tide gages of Figure 11 (source NOAA, 1/05): (a) Western Indian Ocean. (b) Eastern Indian Ocean.

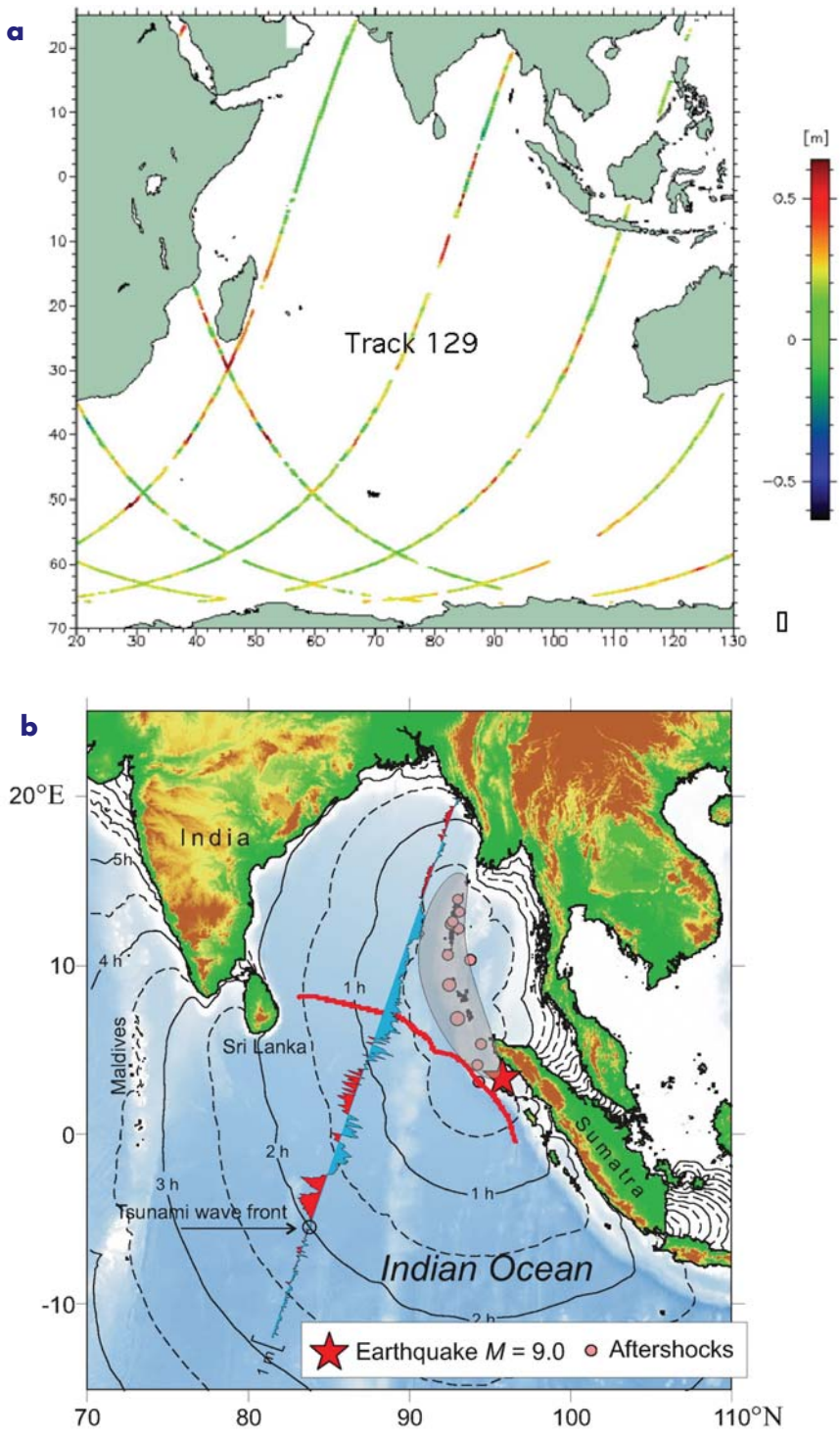

Figure 11. Track and data for *Jason I* satellite on 12/26/04. (a) Track 109 and altimetry (Gower, 2005). (b) Track 109 with tsunami source and propagation time (Kulikov, 2005).

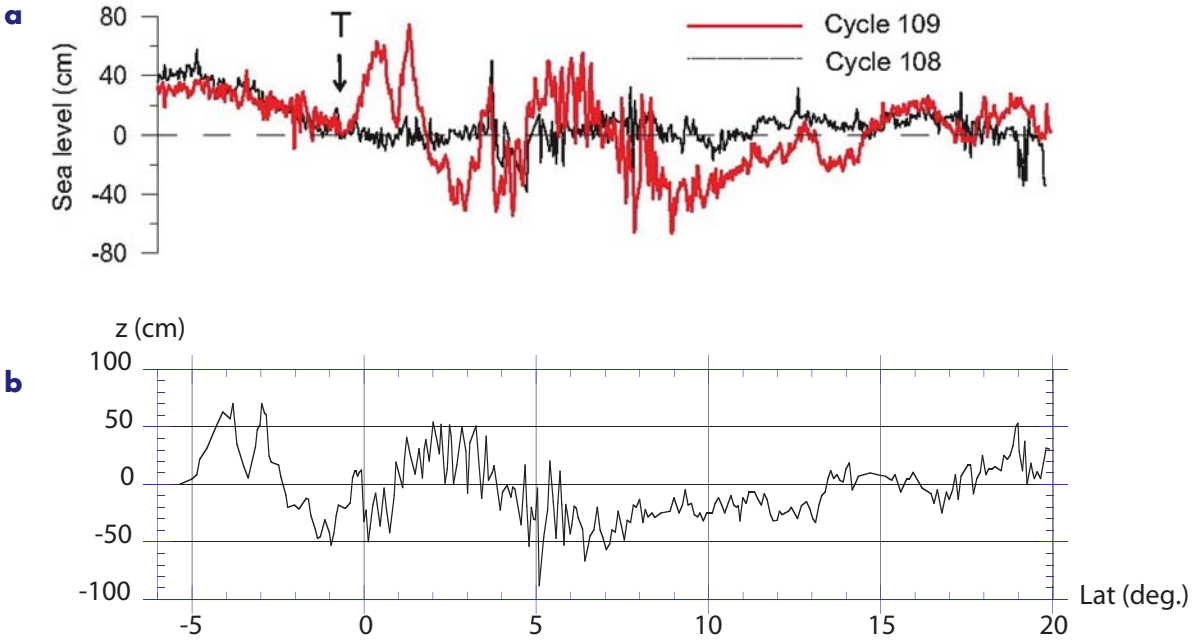

Figure 12. (a) *Jason I* altimetry for tracks 108 and 109 (Kulikov, 2005). (b) Tsunami signal: difference of track 109 and 108.

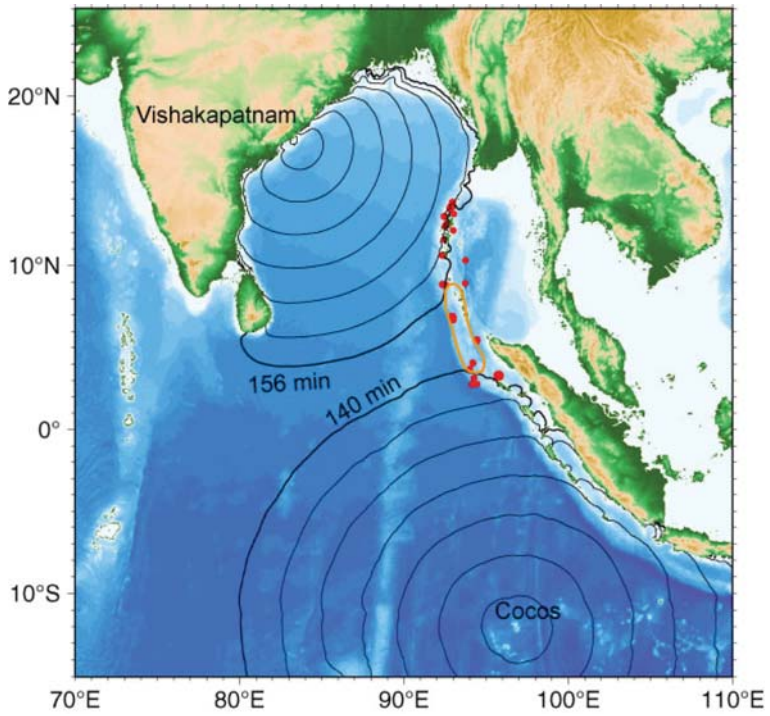

Figure 13. Tsunami source area constraint based on arrival times at Cocos Island and Vishakapatnam tide gages.

provided about the size and timing of the tsunami waves (e.g., http://www.yachtaragorn.com/Thailand.htm). The quantity of such records, along with their unknown quality, makes the processing and collection of these observations a difficult and lengthy task. We devoted significant effort during the cruise in analyzing some of these less-traditional observations in order to reconcile them with the other more absolute data discussed above and to be able to use them with some degree of confidence when validating our models.

Soon after the tsunami, the international scientific community mounted a response to this event through multiple tsunami survey teams. These were largely coordinated by the International Tsunami Information Center, a United Nations agency. These teams of scientists documented damage, measured vertical runup and horizontal inundation, and assembled careful reconstructions of wave activity (e.g., Gusiakov, 2005; Harada, 2005; Yalciner et al., 2005) (e.g., Figure 14). Each team was restricted to a limited geographical region, given the length of damaged coastline and number of countries involved. The runup and inundation data are still becoming available through various publications and web sites, in a piecemeal fashion, region by region.

Prior to this cruise, we conducted initial modeling studies of the tsunami using reasonable sources, based on available seismological and other information, and compared runup results with some of the available observations at a few locations (Watts et al., 2005). The agreement was found reasonable. More detailed analyses and comparisons were conducted during the cruise and additional comparisons with various field data were made. These, however, do not yet include a comprehensive comparison of modeling results with all of the available data and records. Such a lengthy analysis is still premature, pending confirmation of the selected characteristics of the tsunami source. Thus, we focused our efforts on constructing increasingly accurate tsunami sources and

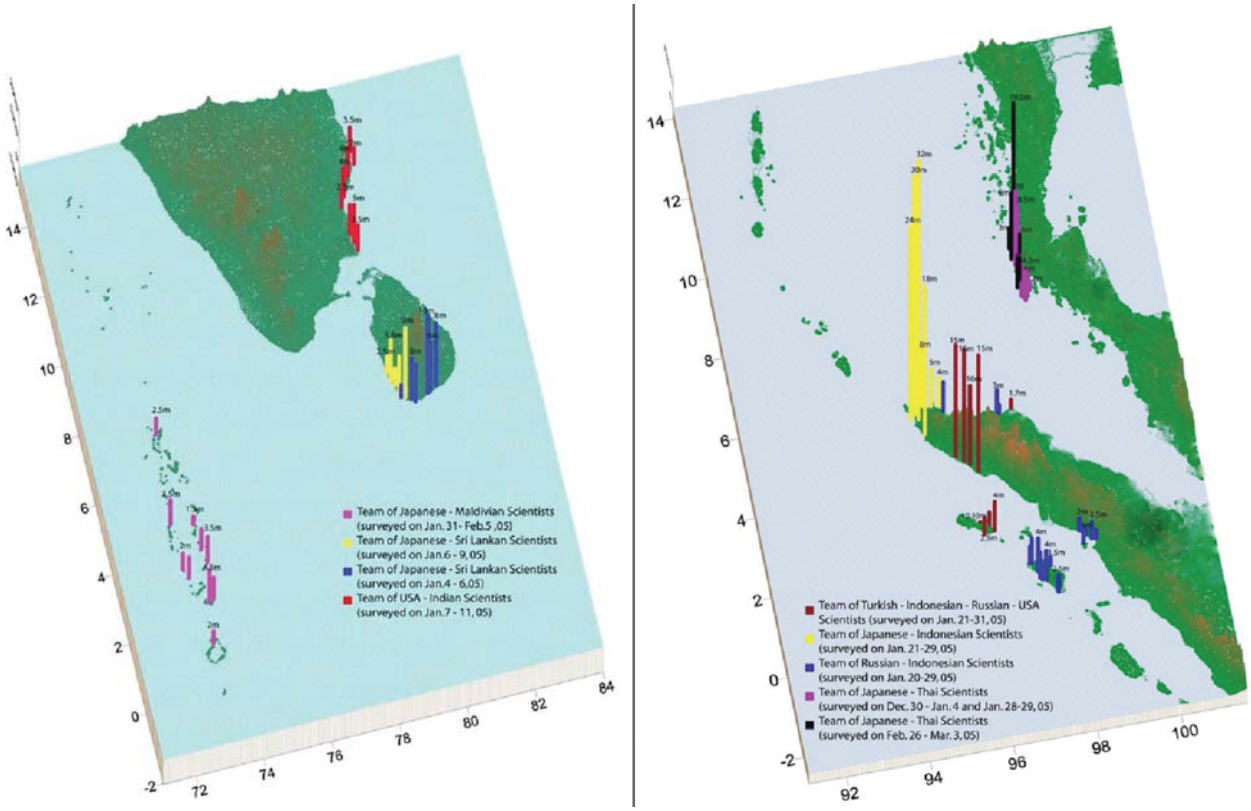

Figure 14. Runup distribution in northern Sumatra (Indonesia), Thailand, India, Sri Lanka, and the Maldives (Yalciner et al., 2005).

tsunami modeling grids (including ocean bathymetry and coastline topography), based on geophysical and seismological data, some of it newly acquired or analyzed during the cruise. Based on these sources, we performed tsunami simulations aimed at explaining the observed large-scale features of tsunami propagation and inundation at the Indian Ocean basin scale.

SURVEY PLANNING

The Visualization Team's efforts focused on the provision of tools and products for the integration, display, analysis, and interpretation of the many complex data sets used on the SEATOS Expedition. Tools included those for real-time planning and decision-making, for scientific analysis and interpretation, and for visualizations aimed at helping the general public understand the science behind the expedition. The general approach was to bring the disparate data sets together in a common georeferenced framework that allows intuitive exploration and manipulation of data in a 3-D environment. This approach was implemented through the use and modification of several software packages and, when necessary, the development of new code.

Multibeam Bathymetry

Multibeam bathymetry collected by the 12 kHz SAS system on the HMS *Scott* provided the basemaps upon which cruise planning was done.

Real-time Ship Navigation (2-D and 3-D)

Real-time navigation was provided to the scientific party in both a 2-D and 3-D environment. Navigation strings were provided via two Trimble 4000RL and one Trimble 4000DS GPS receivers located on the bridge. No differential correction service was available so all receivers operated in non-differential mode. The output of these receivers was sent to the Oceaneering ROV Nav shack where the three independent solutions were combined using the Winfrog software package and a single blended solution derived. Serial input navigation lines were run to the visualization computers (originally in the conference room and then in the "barn"). Two separate data streams were provided: (1) for surface-ship navigation, NMEA GPGGA, GPVGT, and GPHDT telegrams were sent over one line and (2) for ROV navigation, a Winfrog ASCII data stream was sent over the other line.

Real-Time 3-D Display of ROV Position

Real-time navigation of the ROV was based on the serial line sending data from WinFrog, a data-acquisition software packaged used to aggregate the data from instruments on the ROV, GPS, and the LS-5 low-frequency ultra-short baseline acoustic positioning system. GeoZui3D was modified to parse the supplied WinFrog data, project the latitude and longitude into UTM coordinates, and display the ROV data in three dimensions over the bathymetry. Relevant information was also displayed on the screen, including latitude, longitude, depth, time, altitude, and heading.

Software was developed to allowed the real-time display of the video telemetered from the ROV. A video feed was provided from the ROV to the visualization team using a shuttle computer with a video capture card. The video was displayed in real time on a screen in front of the ROV. As the ROV moved, the screen moved synchronously. This tactic proved successful, however, the camera pan, tilt, and zoom settings were not known, requiring a static setting of the camera with a straight-ahead look angle. Knowledge of pan, tilt, and zoom would have allowed more accurate positioning of the video with respect to the ROV.

ROV Track Filtering

Occasionally, the ROV's depth sensor was noisy. The ROV's navigation was noisy, too, jumping up to 70 m between pings. The ROV navigation was smoothed by running a moving average of positions over a period of five minutes. The ROV depth was smoothed by keeping track of the last plausible depth and replacing the intervening noise with a linear interpolation between the known good points. A depth was considered plausible if it was within 1.5 m from the last known good depth.

ROV Launch and Descent Visualization

Real-time track planning tools were created for modifying the 3-D models to build a 3-D visualization of the ROV launch procedure. Real-time navigation tools (2-D and 3-D) were also used for survey planning. Based on interactive 3-D exploration of the region, survey lines were selected. Way points for these lines were recorded in degree, minute format and passed on to the bridge.

Digitization of Bathymetric Data for Tsunami Modeling

The tsunami modeling sought to generate a high-resolution model of wave inundation in the vicinity of Phi Phi Island. This modeling required much more detailed bathymetry than that provided by either the GEBCO or ETOPO-2 data bases. The only available source of more detailed bathymetry (at least on board the vessel) was the paper nautical chart of the region. To digitize the chart we took high-resolution (8 Megapixel) digital photos of small subsets of the chart. These subsets were cropped to known geographic boundaries and then georeferenced (made into GEOTIF images) using the IVS ImageViewer software. Each image thus became a high-resolution georeferenced image that contained soundings and contours. Fledermaus was then used in the "geopicking" mode to move a cursor to the position of the sounding and then manually enter the sounding depth into the position table generated by Fledermaus. The result is an x, y, z file of position and depths that could then be input into the tsunami model.

Interactive 3-D Visualization of the Tsunami Model

The output of the tsunami modeling team's effort was a series of grids each depicting sea surface height at a point in time after the initiation of a tsunamogenic disturbance. These grids were passed to the visualization team in the form of "Surfer" grids. The Surfer grids were then sun-illuminated, shaded, and converted to Fledermaus objects. The Fledermaus objects were then constructed into a time series of surfaces that could be combined with a bathymetric grid (from ETOPO-2), interactively rendered, and explored in the full interactive 3-D environment (Figure 15).

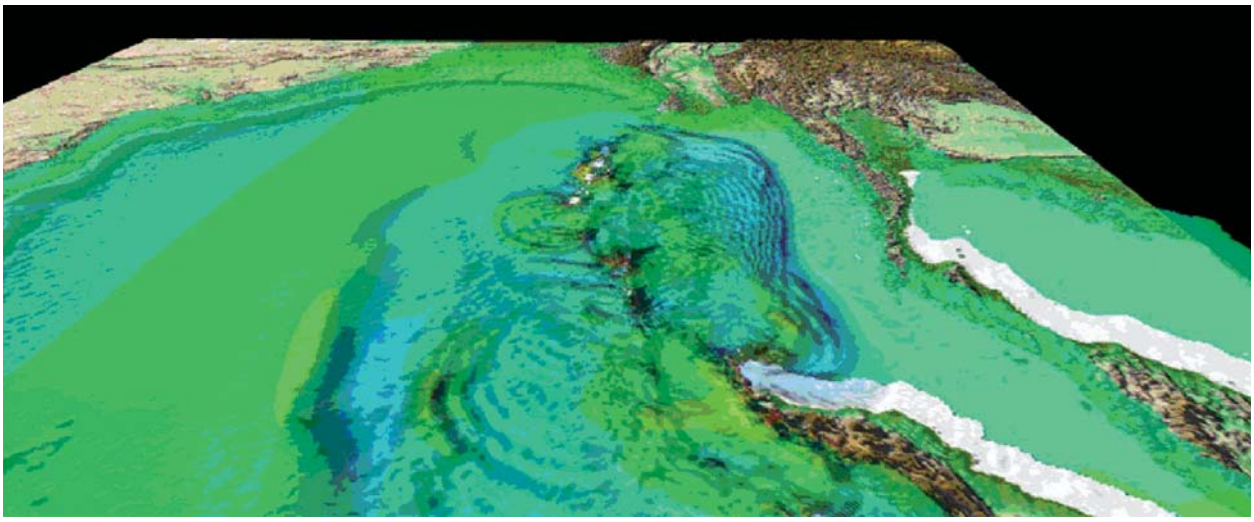

Figure 15. Single frame from a 3-D animation of the tsunami model superimposed over ETOPO-2 bathymetry.

GEOTECHNICAL AND SLOPE STABILITY

Miniature vane-shear tests were performed on select cores recovered with the ROV. A description of the coring equipment is given in the biology sampling section. The miniature vane-shear test provides an estimate of undrained shear strength of clay sediments. The device consists of a 1-cm square blade that is inserted into the sediment and rotated at a rate of about one revolution per minute. The resistance of the blade is measured with a mechanical torque sensor (torque watch). The torque measurements were converted to undrained shear strength in accordance with ASTM 4648.

Both undisturbed and remolded vane measurements were made. The remolded test, which represents a large strain or residual strength condition, was performed by rotating the vane a number of revolutions after an undisturbed measurement was made. The sensitivity was calculated from the ratio of the undisturbed to the remolded strengths. Sensitivity provides a quantitative measure of the loss in strength that can result from sediment disturbance.

Samples of sediment from each core were also placed in sealed containers for transport back to the University of Rhode Island for bulk density and water content determination.

3. Survey Results

CROSS-MARGIN TRANSECT

Data collection began on the expedition with a cross-margin seismic line that collected a continuous single channel air gun profile from 6.8°N 94.9°W to 4.4°N 92.9°E (Figure 16). Seismic data were recovered to approximately 1 s two-way travel time (TWT) penetration beneath the seafloor. The reflection data clearly imaged the sub-seafloor across the margin. A thin sediment cover was observed on the accreted ridge tops with thicker sediment accumulation within the ridge-bounded basins.

SEATOS Line 1 is a single-channel GI-gun profile extending from the outer arc high (~2.5 s water depth) to the abyssal plain seaward of the deformation front (~6.0 s water depth). Profiling began (inboard end) at 1206z, JD 131; the profile was completed at 1100z, JD 132. Most of this profile has undergone F-K migration at water velocity (Figure 17).

Bathymetry crossing the inner trench wall consists of a series of highs (thrust ridges) and sediment-filled lows. The most pronounced high has a local relief of ~1.1 s. Penetration across highs is limited. Sediment thicknesses within ponded basins range from ~200 ms (inboard) to ~500 ms (farther seaward). Preliminary examination suggests that ponded sediments are undergoing progressive deformation with depth, consisting of progressive tilting and folding.

Seaward of the deformation front, in the Sunda Trench, sediment fill exceeds 1.0 s; oceanic crust could not be observed. There is evidence for incipient folding beneath the seafloor increasing toward the deformation front, fluid escape (some sub-seafloor wipeouts), slumping, and perhaps a seaward-verging thrust plane surfacing at the seafloor coincident with the deformation front.

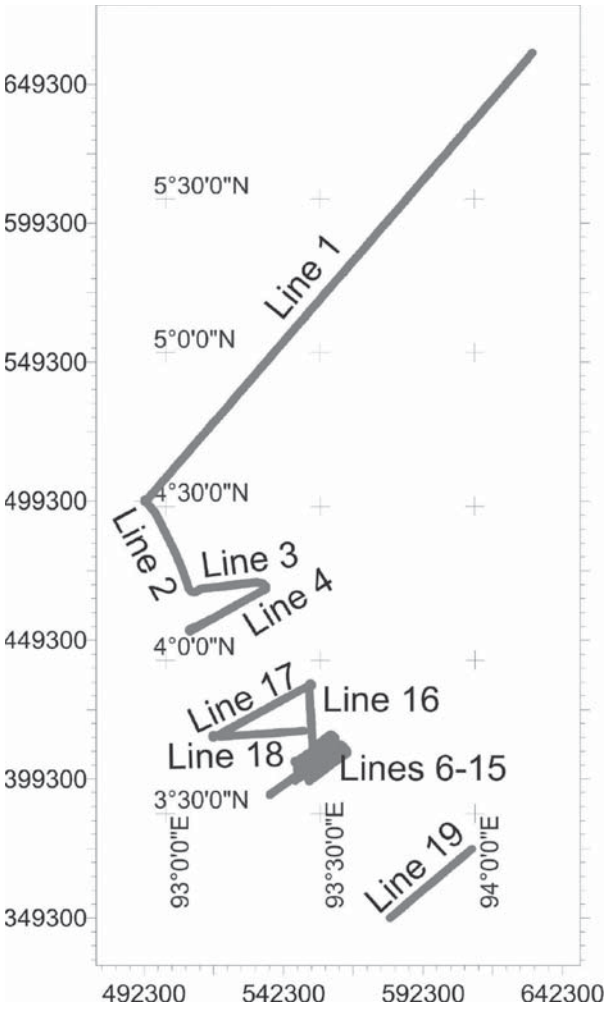

Figure 16. Track plot of seismic lines 1 through 19, which includes the landslide site (2–4), the Ditch (6–18), and the Proto-Ditch (19).

Site 1: Landslide Site

The first site to be investigated in detail was a recent landslide identified in the north of the HMS *Scott* survey area. The *Scott* survey scientists considered it possible that the December 26, 2004 earthquake had caused the landslide. The landslide was characterized as a large debris flow complex with blocks that moved up to 13 km onto the abyssal plain (Figures 1 and 17).

The objective for studying the landslide site was to determine if the landslide was caused by the December 26 earthquake and, if so, to assess the impact of the landslide on the resulting tsunami. Preliminary assessments of the landslide by *Scott* survey scientists suggested that if the landslide had occurred on December 26, 2004, it would have had minimal, if any, impact on the tsunami generated due its location in deep water and the size of the slide when compared with the estimated co-seismic displacement.

Surveys

Several seismic lines were run (Figure 17) parallel to the direction of slope failure. A series of four profiles (Figure 17; Lines 2–5) were collected with the Huntec sparker and the single-channel GI system along and seaward of the toe of the deformation front. Returns from the Huntec sparker were unsatisfactory; power levels at the ambient water depths were too low to resolve much more than the seafloor on flat terrain, and could not even track seafloor on the deformation front. SCS profile quality was generally excellent, with more than 1 s of penetration in sedimentary fill of the Sunda Trench.

Line 2 was parallel to the deformation front and imaged sedimentary fill of the Sunda Trench in ~4.5 km of water. In general, sediments were well stratified with occasional channel cut-and-fill sequences interrupting the flat-lying strata. A normal fault with several meters of offset to the seafloor was observed on this transect.

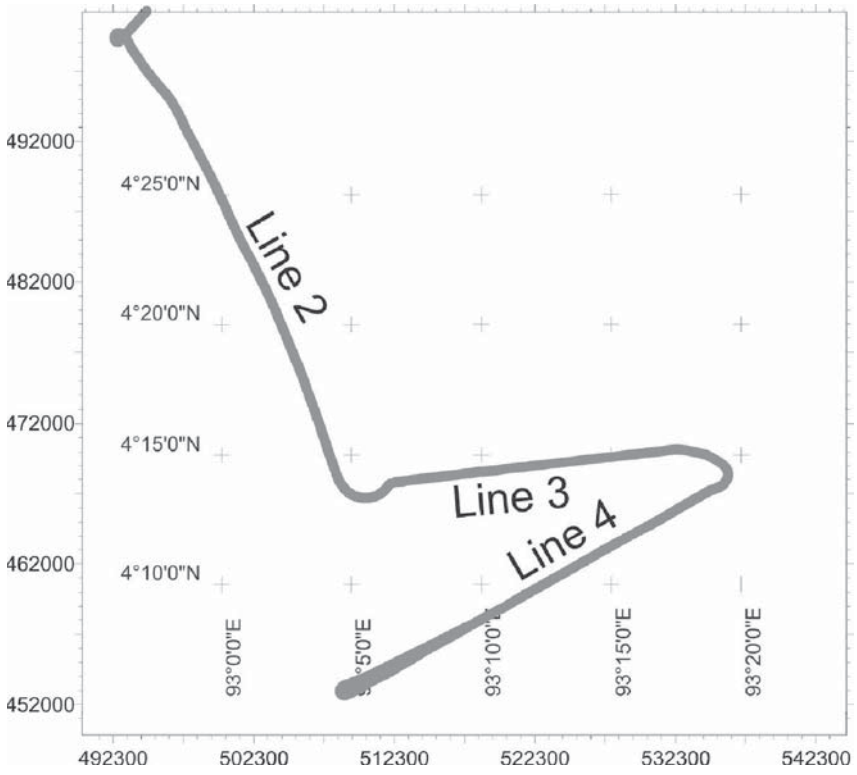

Figure 17. Position of seismic track lines run at the Landslide site.

Lines 3, 4, and 5 (northeastern portion) were designed to image the interpreted landslide scar at the foot of the deformation front. Lines 4 (southwestern portion) and 5 crossed the largest of a series of slide blocks now sitting atop Sunda Trench fill seaward of the deformation front. These crossings showed an interpreted debris flow up to 50 ms beneath the seafloor, with stratified sediments on top. The large slide blocks appear rooted within this debris flow, suggesting the landslide causing them is old.

One ROV survey line was run (Figure 18) along the central upslope transect line that crossed landslide-disturbed sediment and slope failure scars. The survey included continuous video capture of the seafloor. Discrete sampling using push cores and slab cores (six per dive) was planned, but a hydraulic problem occurred and no samples were collected in this manner. The vacuum hose was used to collect living and dead specimen along the transect. Figure 19 summarizes the ROV survey transect in terms of the geological description and the biota.

Landslide Velocity Evaluation

An analysis was performed to estimate the velocity of a block slide that was identified on the outer slope of the margin. A cross section of the slide is shown in Figure 20. As shown, the cohesive block is located approximately 8,600 m from the base of the slope. A deep scarp of comparable thickness, identified about 12,000 m upslope, suggests that the block originated from this location.

In the analysis, the block slide was assumed to be a rigid body having a elliptical shaped top surface in the direction of the slope. It was assumed that the block starts at zero initial velocity at the location of the scarp. Gravitational body forces act to push the block downslope and viscous drag forces on the top surface together with basal friction on the bottom act to oppose its motion. Once the block reaches the base of the slope, gravitational forces no longer act in the direction of motion and the block slows, eventually stopping. Analytical

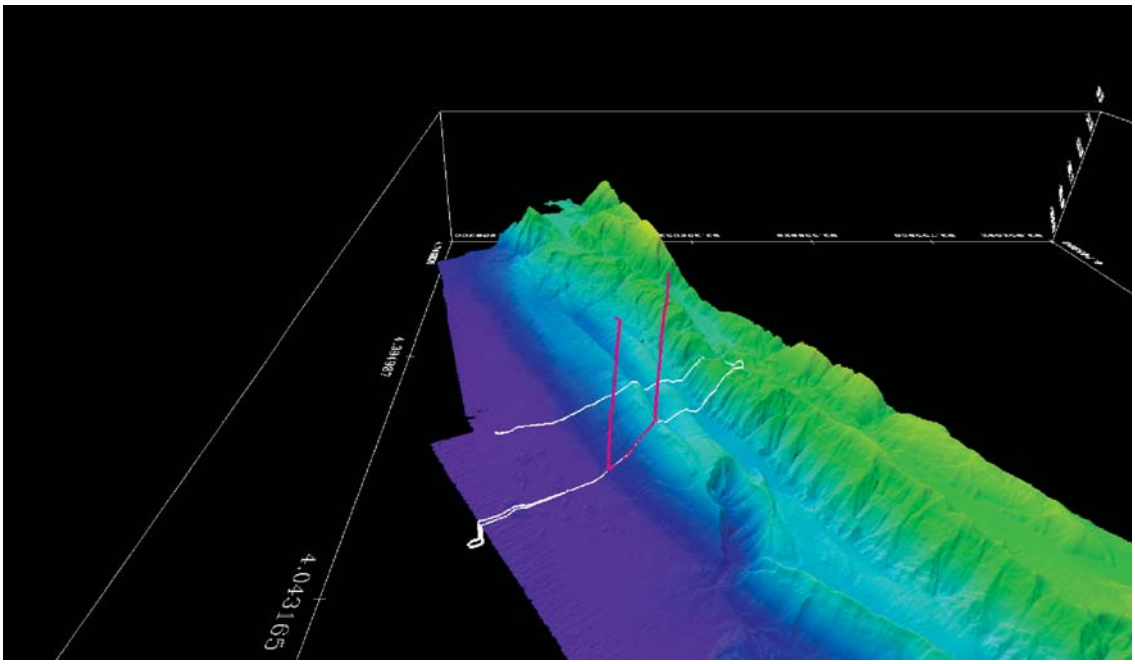

Figure 18. The landslide site multibeam data with the location of the seismic survey lines (white) and the ROV dive (red).

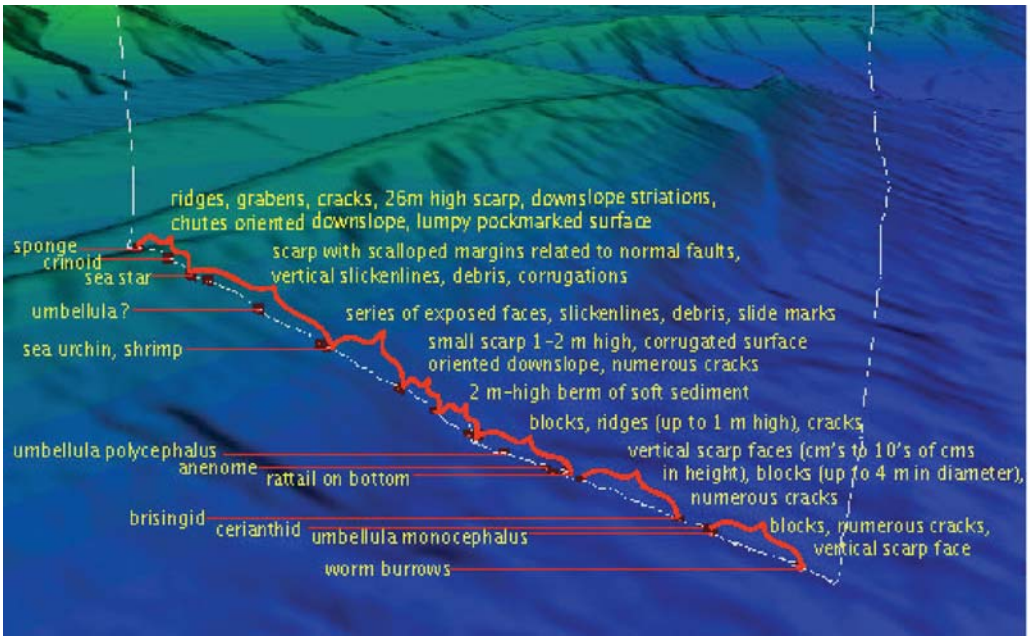

Figure 19. Summary of ROV transect showing geological and biological features observed at the landslide.

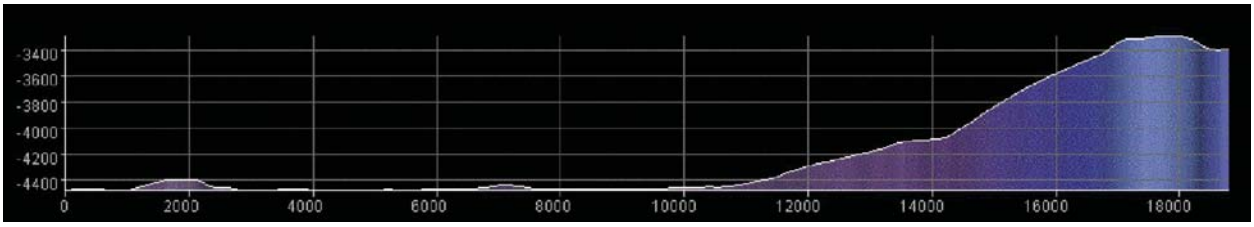

Figure 20. Cross section of the landslide site.

solutions to the equation of motion for the rigid body model were derived.

Using the assumed point of origin, the basal friction in the model was iteratively adjusted until the block stopped at the known run-out distance. The block velocity was calculated from the analytic solutions using the estimated basal friction. The velocity profile calculated along the length of the slope is shown in Figure 21. The analysis suggests that the velocity reached a maximum value of about 35 m/s (126 km/hr) at the base of the slope approximately 3,500 m down-slope of the scarp.

Landslide Block Simulation

A computer simulation was prepared to evaluate and explain how the large blocks, up to 8 km from the foot of the slope, could have originated from region that had been identified as a likely source. This combined computer graphics rendering with numerical simulation. The work was carried out in the following steps.

- Step 1: An editor was constructed to allow for the blocks to be edited out. This enabled the total volume of the blocks to be estimated (~ 0.5 km^3). The largest block had a volume of ~ 0.2 km^3.

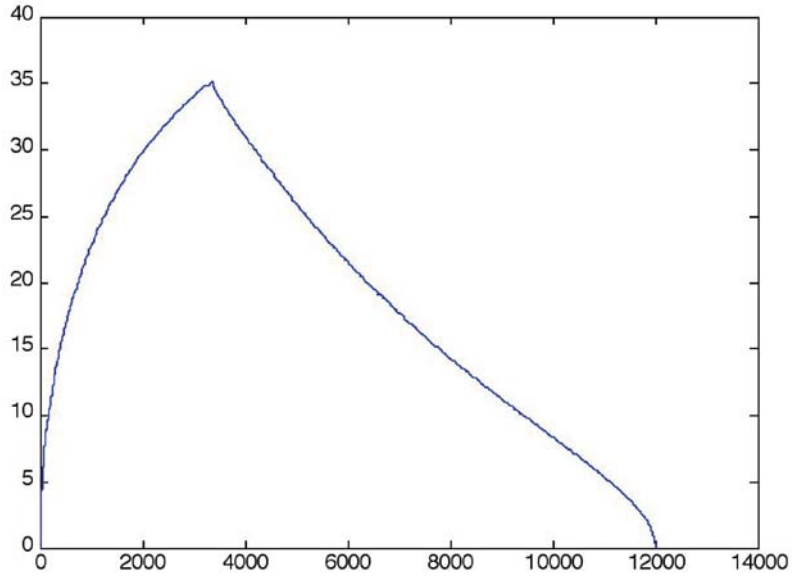

Figure 21. Estimated velocity profile of the slide block. The vertical and horizontal axes are velocity (m/s) and run-out distance (m), respectively.

- Step 2: The conjectured origin region of the landslide was filled in, allowing for the volume of source material to be estimated to be 1.0 km^3.
- Step 3: The source region was packed with 108 hemispheric objects, each having a constant radius of 500 m. These were then simulated to slide down the slope using a simple model that included terms for acceleration due to gravity, momentum, and friction. The resulting spread of the objects closely approximated the distribution of the blocks at the foot of the slope.
- Step 4: To create the visualization, first we discovered which of the 108 hemispheric objects came closest at terminal position to the center of each of the 13 blocks identified from the bathymetry. The motion path of each of these 13 objects was then used to animate its corresponding block. To represent debris flow, each of the remaining 95 objects was rendered as 50 semi-transparent particles having a random Gaussian distribution about its center. The 98 motion paths were used to animate these particle clouds.
- Step 5: The simulation described in Step 3 was modified to incorporate terms provided by the modeling team describing idealized blocks sliding down an inclined plane underwater. In this case, the source region was packed with hemi-ellipsoidal objects having random radii between 250 and 1,000 m. The distribution of radii was biased so that there were more of the smaller sizes. An example of the output is shown in Figure 22.

Geotechnical ROV Results

At the landslide site, the ROV descended to near the base of the landslide at a depth of 4,284 m and then traversed up the slope to the top of the ridge at a depth of 3,289 m. Near the base of the slide, the bottom was smooth with scattered angular blocks up to 4 m in diameter. On the slope, the ROV crossed numerous cracks, berms, and ridges as well as a series of vertical seaward-facing scarp walls with heights of tens of centimeters up to 2 m. Scarp walls were typically striated or corru-

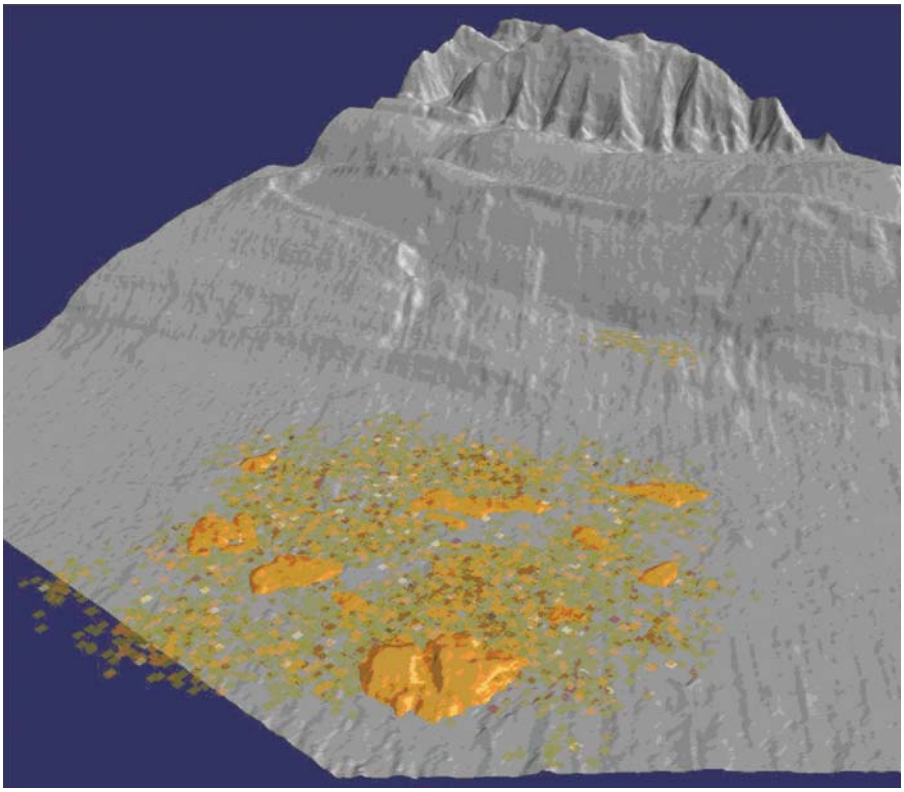

Figure 22. Example from a final frame grab of the block slide simulation.

gated, with a sharp or scalloped upper ledge. The slope surface varied from smooth and littered with scattered biological debris to bumpy with elongate lumps and blocks. Near the top of the slope, the gradient steepened and there were numerous ridges, grabens, cracks, and chutes oriented down-slope. The steeper slope region was marked by a series of striated, stepped scarps with a total height of 26 m. The top of the ridge was lumpy and pockmarked. The presence of abundant biota and the smooth to lumpy sedimented surface of the slide indicate that the landslide was relatively old. The scarps with sharp upper ledges and striations on the scarp wall suggested more recent slope failures that likely could have occurred on December 26, 2004.

Biological Results

Initial observations at Site 1 made during the first part of the dive indicated several bands of flat seafloor covered in ripples and containing infauna. Between these bands were areas of more hummocky sediment, which also showed evidence of small, meter-scale fractures. The middle part of the dive covered a sedimentary zone where we observed the pennatulids *Umbellula monocephalus* and *U. lindahli* and a moribund brisingid seastar. No other megafauna were observed. As the slope steepened sediment clouds in the water column increased although there was a brief observation of possibly fresh fractures on a vertical wall, but this could not be substantiated. Except for the crumple zone at the beginning of the dive there was no positive evidence of a recent landslide.

Site 2: The Block

Seismic Surveys

See description of the landslide site.

Geotechnical ROV Results

The ROV descended to the trench floor on the northeast side of the block (between the block and the trench slope) at a depth of 4,473 m (Figure 23). The seabed was flat and featureless to lumpy and undulating, with roughness increasing up the slope of the block. The surface was broken by three near-vertical walls with heights of 1, 4, and 7 m with associated debris and cracks near the scarp face. The absence of any fresh features, such as slide scars, on the seabed between the block and the landslide face suggested that the block may not have been emplaced recently; however, evidence from elsewhere on the margin and reports from the Japanese JAMSTEC survey (http://www.jamstec.go.jp/jamstec-e/sumatra/natsushima/bm/contents.html) indicate that seabed sediment disturbed by the earthquake may, on settling, have covered seabed features created by the movement of the sliding block from the landslide. An interpretation that the failure is old is consistent with both the presence of biota on the slide surface (see below) and the bumpy seabed surface that suggests a thick sediment cover overlying a debris flow.

Biological Results

The primary objective of Dive 2 was to identify when one of the large landslide blocks moved. The dive plan was to conduct a transect from a point landward of one of the main blocks westward of the deformation front, over the block that was about 100 m high, and down the seaward side. Our hypothesis was that if this block had slid into position recently, the landward side of the block would show evidence of a slide and would contain no fauna, whereas there would be a well-established fauna on the seaward side. To test this hypothesis we observed the megafauna and took samples for infaunal analysis landward, seaward, and on top of the block. Initial data analysis suggests that the blocks did not slide into position recently. There was an established megafuana in

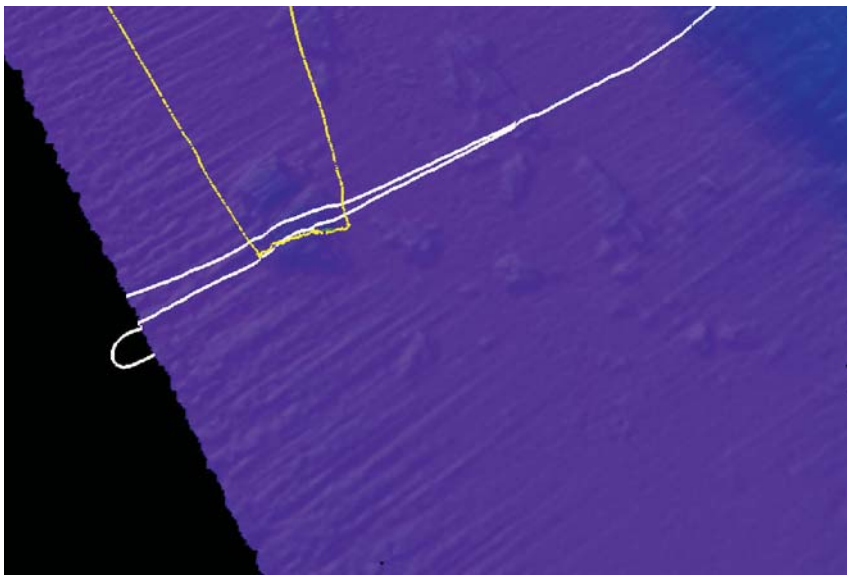

Figure 23. The block: Seismic lines (white) and ROV traverse (yellow)

front of and behind the blocks and on top; the top also had numerous tracks and trails. The hypothesis that the landslide occurred on December 26 is not supported.

Site 3: The "Ditch"

Site 3, dubbed the "Ditch," is a feature that was identified on the HMS *Scott* multibeam data (Figure 1). The Ditch runs parallel to the margin at the deformation front and is ~15–20 m deep and ~200 m wide. It was interpreted by the *Scott* scientists to have possibly formed coseismically and may therefore have been contributed to by slip during the 2004 earthquake.

To investigate the freshness of this feature and its tectonic significance, orthogonal seismic lines were run across and along the feature (Figure 24). Also, an ROV survey was run in the Ditch.

All profiles at this site, located at the toe of the deformation front ~50 km southeast of the landslide site, were collected only with the SCS reflection system.

Profiles 6–15 represent a detailed survey of the Ditch, a steep-sided linear depression at the foot of the deformation front. The first profile (Line 6) was initiated far seaward to attempt to image oceanic crust of the incoming plate beneath thick (> 1 km) sediments filling the Sunda Trench, but oceanic crust was not observed. All profiles were oriented to cross the Ditch at right angles. Profile spacing averaged 2 km; each profile was ~20 km long. Due to large diffractions, the seismic profiles initially did not image the Ditch well, but upon migration, the feature became apparent. Subsurface faults were not readily apparent beneath the Ditch, perhaps due either to strong vertical motion on them or because the Ditch was at the hinge line of the toe thrust where sediment is scraped off the Sunda Plate and thrust onto the accretionary prism. The resulting thrusting results in apparent landward-verging folds within the sedimentary sequence.

Three additional profiles (Lines 16–18) were also collected to image Sunda Trench fill northwest of the Ditch to provide a structural comparison in the same tectonic position at the toe of the deformation front (Figure 24). Line 16 crossed the toe of the front obliquely, Line 17 crossed the toe at right angles to image both the toe and sedimentary fill of the Sunda Trench, and Line 18 com-

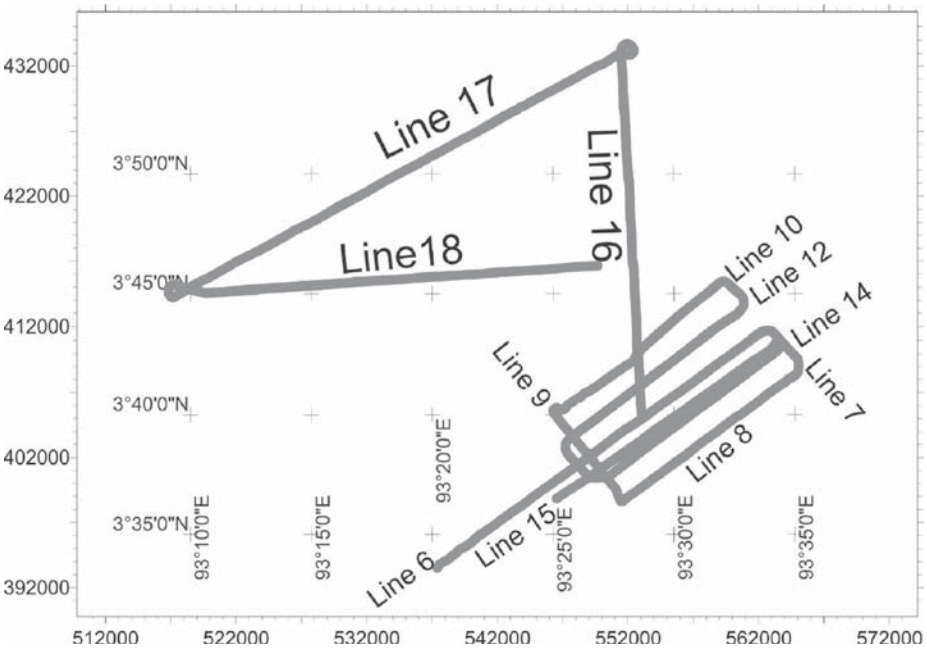

Figure 24. Location of seismic lines at the Ditch Site.

pleted a triangle by tying to the mid-point of Line 16 near the toe of the deformation front. These data show well-stratified sediments with channel cut-and fill-sequences. The toe thrust is a steep structure about 750 m high, consisting of a single steep anticlinal fold (Figure 25). Near-surface faults are apparent on the landward side of the fold. On the seaward side, the slope apron consists of debris giving incoherent reflections. This debris apron appears fault-bounded at its seaward extent.

A summary of the Ditch ROV dive (Figure 26) shows several freshly deformed soft rock features and no marine life, suggesting that the Ditch was very recently formed.

Geotechnical ROV Results

At Site 3, the ROV descended to a depth of 4,425 m on the southwest margin of the Ditch and proceeded across the Ditch to the northeast margin. After traversing the Ditch, the ROV climbed up and back down the northeast Ditch slope (Figure 27). The ROV then crossed the Ditch again and surveyed the southwest margin before returning to the surface. The southwest margin of the Ditch was characterized by ridges with a "cottage-cheese-like" texture and angular cobbles of mudstone lightly dusted with sediment. The bottom of the Ditch displayed bifurcating ripple marks and scalloped ripples and cobble-sized mudstone blocks with a sediment cover. The northeast wall of the Ditch was marked by small (0.5 m), fresh-looking scarps striking parallel to the margin, with up to 10-m-wide gullies that were oriented perpendicular to the margin and increased in abundance up slope. The southwestern wall of the Ditch in the north had multiple rounded benches with a sharp wall at the top. The top of the wall had a jagged edge with orthogonal joints that display plumose features. At its base lay a talus apron formed of angular blocks up to 1 m in

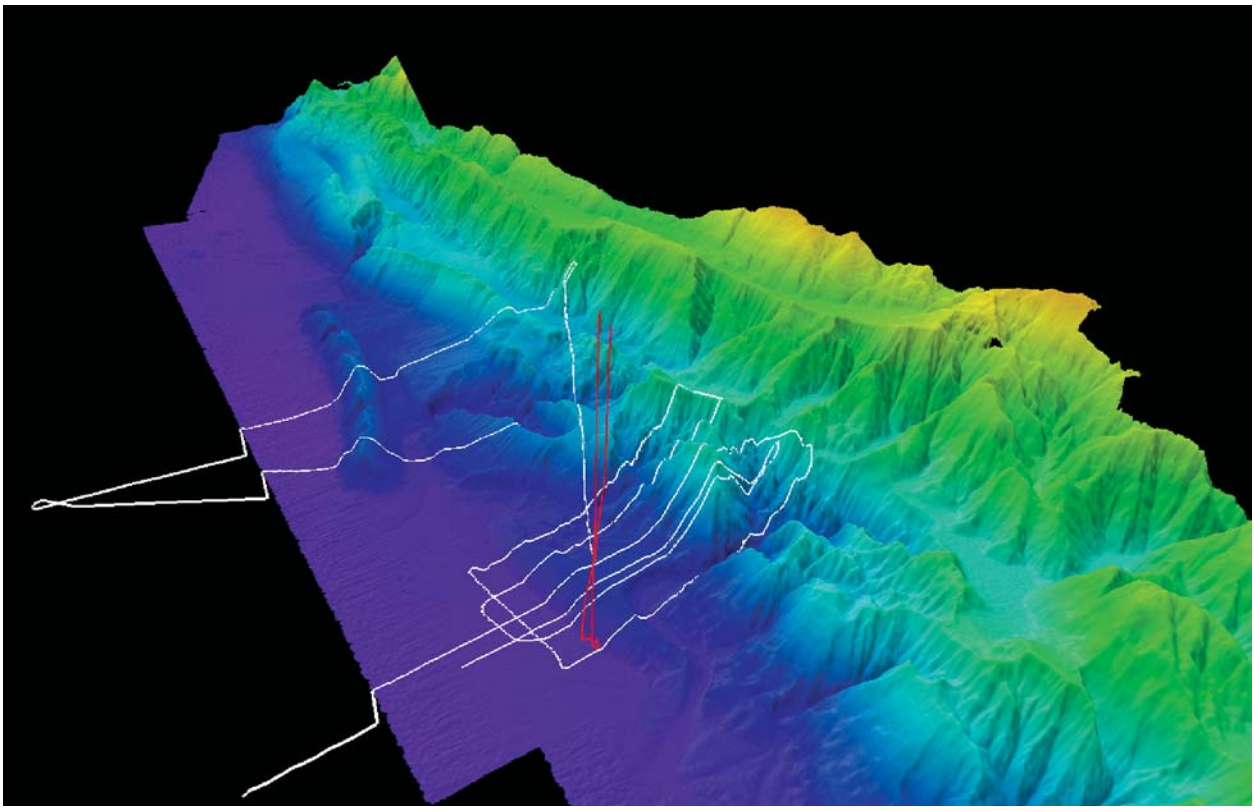

Figure 25. Multibeam image of the Ditch site with seismic lines (white) and ROV survey (red) overlain.

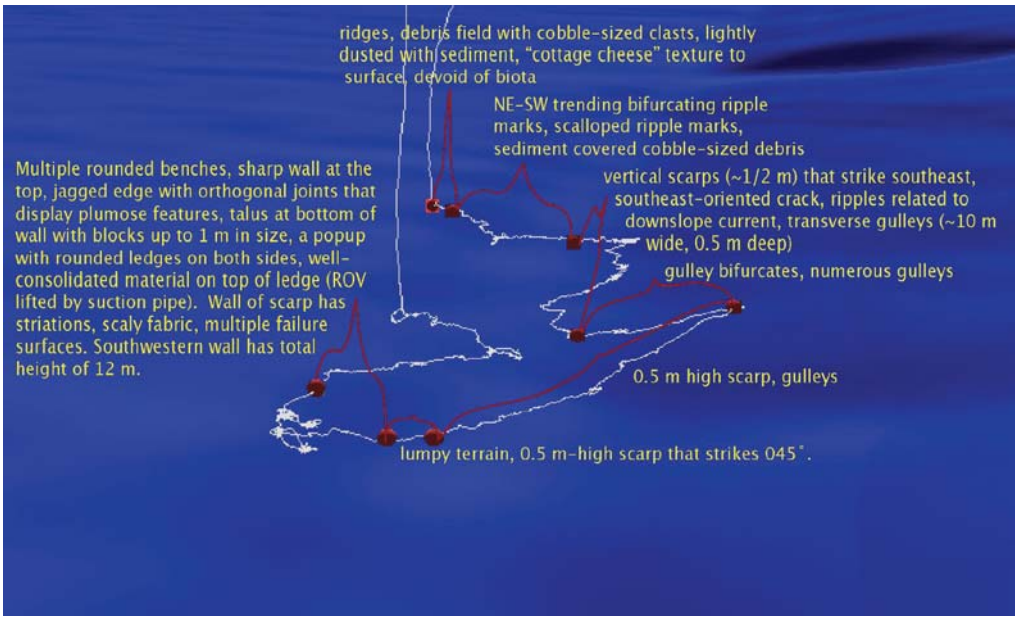

Figure 26. Summary of ROV transect showing features observed at the Ditch.

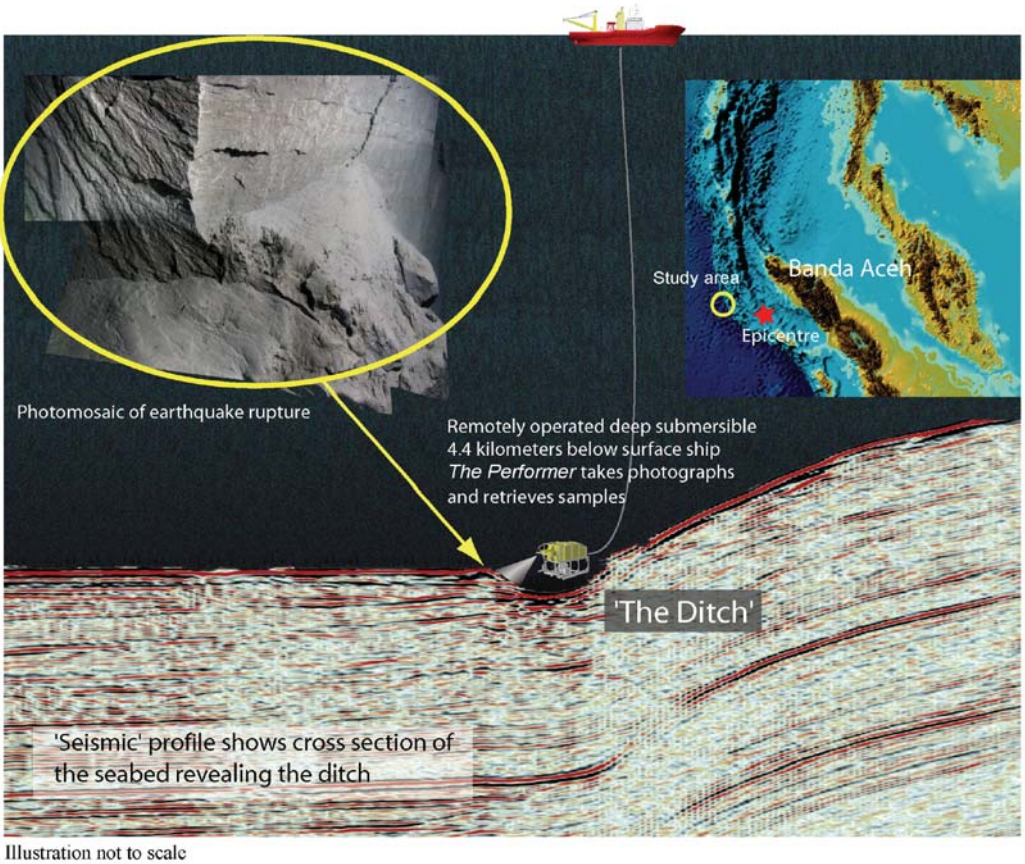

Illustration not to scale

Figure 27. Summary diagram showing a seismic line and a cartoon image of the ROV. A photomosaic constructed from ROV still images in shown in the upper left corner. The general location is shown in the upper right corner.

size. A "popup" was developed on the upper flank and had rounded ledges on both sides. The material on the flank was well consolidated as indicated by the observation that the ROV could be lifted by suction pipe. The wall of the scarp had striations, scaly fabric, and multiple failure surfaces, with a total height of 12 m.

No biota were observed during the Ditch dive. The absence of biota, the sharpness of the scarp wall on both sides of the Ditch, the angular talus blocks, and the well-developed striations on the scarp walls indicate that the margins of the ditch are faults with recent movement, probably due to the earthquake that occurred on December 26, 2004.

Biological Results

Dive 3 concentrated on the Ditch region at ~4,500 m. During the 14-hour dive, not a single megafaunal organism was seen. There was some putative evidence of recent uplift, but the cause of the lack of fauna (either afaunal or defaunal) could not be positively determined. It is possible the lack of fauna may have resulted from tectonic activity or from other factors such as local current activity or sediment instability. We were unable to take any cores for biological analysis on this dive because of the nature of the sediment.

Site 3A: The Proto-Ditch

A single seismic line (Line 19, Figure 26) was run normal to another accretionary toe southeast of the Ditch where there was no outboard longitudinal gully. The objective was to provide a comparison with the Ditch. The profile was similar to the others in a similar position, showing thrusting and folding of the sedimentary package at the toe of the accretionary prism. In this case, a normal-reverse fault was apparent beneath the hinge point of the fold. A small depression, perhaps representing an incipient ditch was imaged.

A complete investigation of the Proto-Ditch site was cut short because of a shipboard medical emergency. The ROV was not deployed.

Site 4: The "Frog Pond"

The "Frog Pond" was targeted by the *Scott* scientists from the multibeam data as a dive site because it was an oblong scarp-bounded feature lying inboard of the plate margin (Figures 1, 28, and 29). Its angular morphology suggested movement on December 26, 2004.

Geotechnical ROV Survey

The objective of Dive 4 was to look for evidence of recent seabed movement due to shaking on December 26, 2004 landward of the deformation front. Here the thrust folds forming the accretionary prism are older than those at the front and the sediment is assumed to be more lithified. The dive traversed a major southwest-facing scarp with approximately 70 m of relief along a heading of 054°.

The ROV landed at 1,689 m on a sediment-covered seabed that had ripples at the surface. The sediment appeared to be micaceous. Lying on the sediment were small displaced blocks with trails. At 1,727 m, a steep (30°), in part almost vertical, scarp was encountered. The scarp was composed of stratified, green, well-lithified mudstone, which was strongly folded and deformed. The scarp face did not look fresh. This interpretation was confirmed by an attached fauna that the biologists estimated at three to five years old. At 1,662 m, the scarp became vertical and formed a cliff that was heavily eroded; bedding was sub-horizontal. The cliff had 20 m of vertical relief. The top of the scarp was at 1,602 m depth where the seabed was a sediment-covered bench. The sediment formed bifurcating ripples. From this point, water depths increased, and the seabed was sediment covered and mainly featureless except for common burrows and associated mounds.

The presence of displaced blocks and lead-in trails at the beginning of the dive at the foot of the scarp suggested recent movement, but this was small scale, no fresh rock faces were observed.

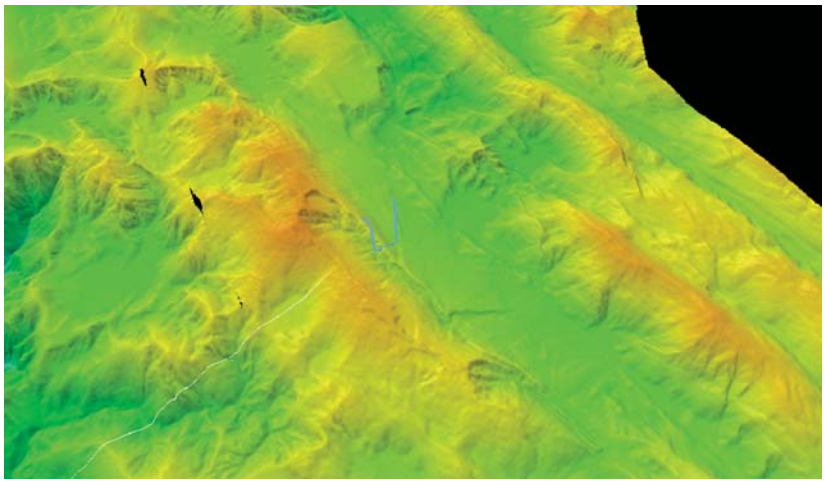

Figure 28. Close-up image of the "Frog Pond" from the multibeam dataset.

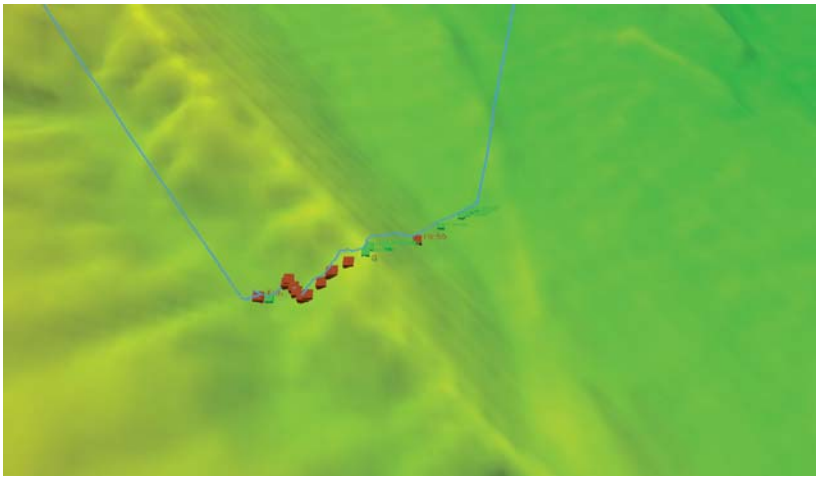

Figure 29. Detail showing the ROV dive observation and sample locations.

Biological Results

Dive 4 at the Frog Pond went to ~1,700 m depth. We observed a relatively rich megafauna throughout the dive. This distribution suggested there was tectonic activity in the recent past. Most of the visible fauna was filter feeding, consisting of anthozoans (anemones, zoanthids, gorgonians, pennatulids) and sponges. A recent origin of the scarps was disproved by the presence of a large bamboo coral, estimated at three to five years old, attached to the middle of the scarp face.

Site 5: Southern Forearc High ("Sweet Spot")

Geotechnical ROV Results

Site 5 was designed to examine structural features near the highest point in the fore arc imaged by multibeam data (Figure 30). The ROV transect crossed two scarps—a small lower scarp and a higher, larger scarp that crested at the highest part of the fore arc imaged in multibeam data. The ROV descended to a depth of 843 m and moved up the lower of the two scarps. The seabed was

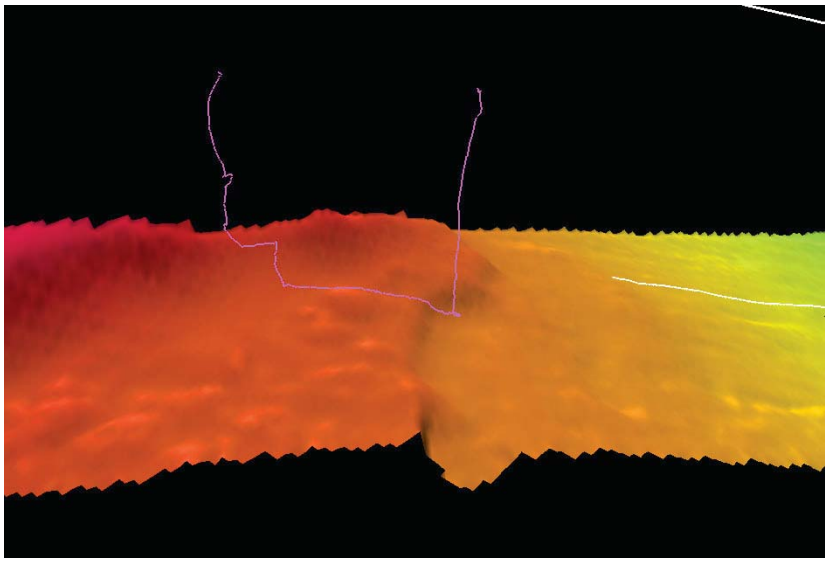

Figure 30. Close-up image of the "Sweet Spot" from the multibeam dataset (ROV traverse in pink).

coarse rippled sand, but blocks were encountered at the bottom of the scarp, which increased in abundance up slope. At a depth of 811 m, ledges composed of continuous outcrops of flat-lying bedrock were encountered. A series of sandy, debris-covered slopes alternating with rock ledges were observed up to a depth of ~720 m where numerous fresh-looking cracks or exposed 10-25-cm-high fault surfaces were observed.

The ROV then crossed a relatively flat sandy, rippled surface with coarser material in the trough of ripples. The heading was changed toward perpendicular to the upper scarp (300˚) until the ROV reached the base of the slope, where the heading was changed again (220˚–245˚) to cross the scarp obliquely to the top. The base of the slope was characterized by a steep sandy surface with ripples and scattered blocks of small white boulders and larger dark brown boulders. The abundance of blocks increased up slope to the base of a cliff of bedrock composed of flatlying pillow basalt (?), sandstone, and shallow water limestone (546–388 m depth). The ROV was unable to sample the potential basalt layer, but pieces of float were collected, which consisted of shallow-water limestone and sandstone. The limestone was dark brown to yellow on oxidized surfaces, but was white on fresh surfaces. Based on subsequent analysis of seismic reflection data, the sedimentary rocks were interpreted as the lower part of the Aceh fore arc basin that had been uplifted along the fore arc high, potentially along the West Andaman fault system that was observed in multibeam data all along the southwestern side of the basin. Fresh faces on small scarps were observed in the vicinity of damaged or dead biota, raising the possibility that these faults were active as recently as December 26, 2004. However, a bamboo coral attached to one of these faces cast this interpretation in doubt. The observation of fresh limestone blocks on the slope, but oxidized limestone surfaces on the outcrop, raised the possibility that the fresh limestone debris on the slope was dislodged during the shaking on December 26. Above a depth of 500 m, there was little evidence of marine life, interpreted as due to strong bottom currents that may be related to the December 26, 2004 tsunami.

Biological Results

Dive 5 was in the region of the "Sweet Spot" and rose from ~800 m to 400 m water depth. At depths below 500 m there was a rich megafauna, similar to that observed

on Dive 4, but also containing echinoids, seastars, ophiuroids, and abundant shrimp. At ~500 m depth evidence of recent cracks in the seabed was observed; however, closer examination during the dive and subsequent still photography showed the crack faces were colonized by erect gorgonians as well as encrusting organisms.

Immediately upslope from this level there appeared to be damage to the erect megafauna; broken stems or gorgonians lying on their fans were observed. At depths shallower than 500 m there was no evidence of megafauna, although examination of still photographs showed a stunted fauna attached to rock surfaces. It is possible, but not proven, that the seabed shallower than 500 m was subject to direct impact of the tsunami wave, which at this depth would exert a current of ~30 cm/s. Such a current, especially as a shock, might be sufficient to damage or break off erect megafauna, leaving these depths bare of erect megafauna whilst having much less impact on the stunted or encrusting fauna of the rock surfaces.

On this dive there was also evidence of recent rock fractures and possible downslope transport. It was not possible to quantify this effect on the megafauna, although some gorgonians attached to small boulders appeared to have been disturbed and were lying on their fans. Much of the seabed along the dive route was rock face and boulders. Any sediment present was sandy and usually no more than a few centimeters deep. As a result, no cores were taken.

FOREARC BASIN SURVEY

En route from the Sweet Spot dive site to the next ROV location known as "Mosher's Mystery Tour," a geophysical survey (Figure 31) was conducted across the E-W extent of the Aceh (forearc) Basin (Profiles 20–24) and along its seaward margin to the north (Profiles 25–26). Profile 20 began at 2222z, May 21, 2005 and profile 26 ended at 0946z, May 23, 2005. Weather and sea states were excellent, resulting in extremely high data quality.

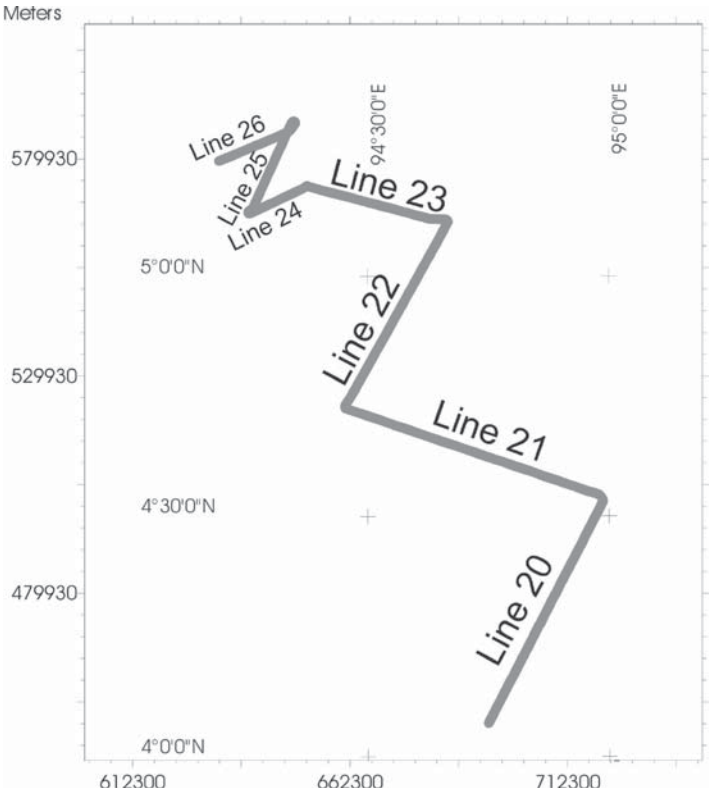

Figure 31. Track locations of seismic survey lines on the fore arc high.

Profile 20 crosses the Aceh Basin from SW to NE near its southern limit. Penetration reached ~1.3 s in basin fill. There is seismic evidence for debris flows and folds within the fill. This profile also crossed a topographic high (almost certainly a large, faulted fold) where penetration was limited. At the NE end of the profile there is a major deformed sediment pond, the SW side of which may be bounded by a large normal fault. Active movement along this fault is suggested by increasing rotation of fill sediments with depth. Possible liquefaction pockmarks were noted at the surface in this profile.

Profile 21 crosses the basin from SE to NW, once again crossing well-stratified thick forearc basin fill sediments. The most distinctive feature of this fill is a prominent intrabasinal angular unconformity at ~0.7 s sub-seafloor (Figure 32). Beneath the unconformity, fill is deformed; deformation appears to increase towards the NW. At the NW end of the profile, large folds reach the seafloor, separated at intervals by flat-lying sediment ponds of varying size. Several debris flow intervals were noted in this section as well.

Profile 22 crosses the basin obliquely from SSW to NNE. Imaged basin fill (penetration reached almost 1.5 s) is largely flat lying, although low-amplitude reflections near the bottom of the profile suggest folded strata at depth. Multiple debris flows are observed intercalated with parallel-continuous reflections within the fill (Figure 33). The thickness of these beds seems to increase with depth. The prominent angular unconformity observed on Profile 21, underlying the landward flank of the basin, was again observed on the NW part of this profile.

Profiles 23 and 24 together again cross the Aceh Basin, in this case approximating an E to W transect. Basin fill is flat lying, with virtually no disruption of the seafloor. There is folding at depth. Sub-seafloor penetration was generally 1.0–1.2 s. At ~0020z, May, 23, 2005 there was an acoustically transparent diapiric (fluid escape?) structure at ~0.4 s sub-seafloor that may result from an underlying debris flow. A possible interpretation is that a vertical fault associated with this structure

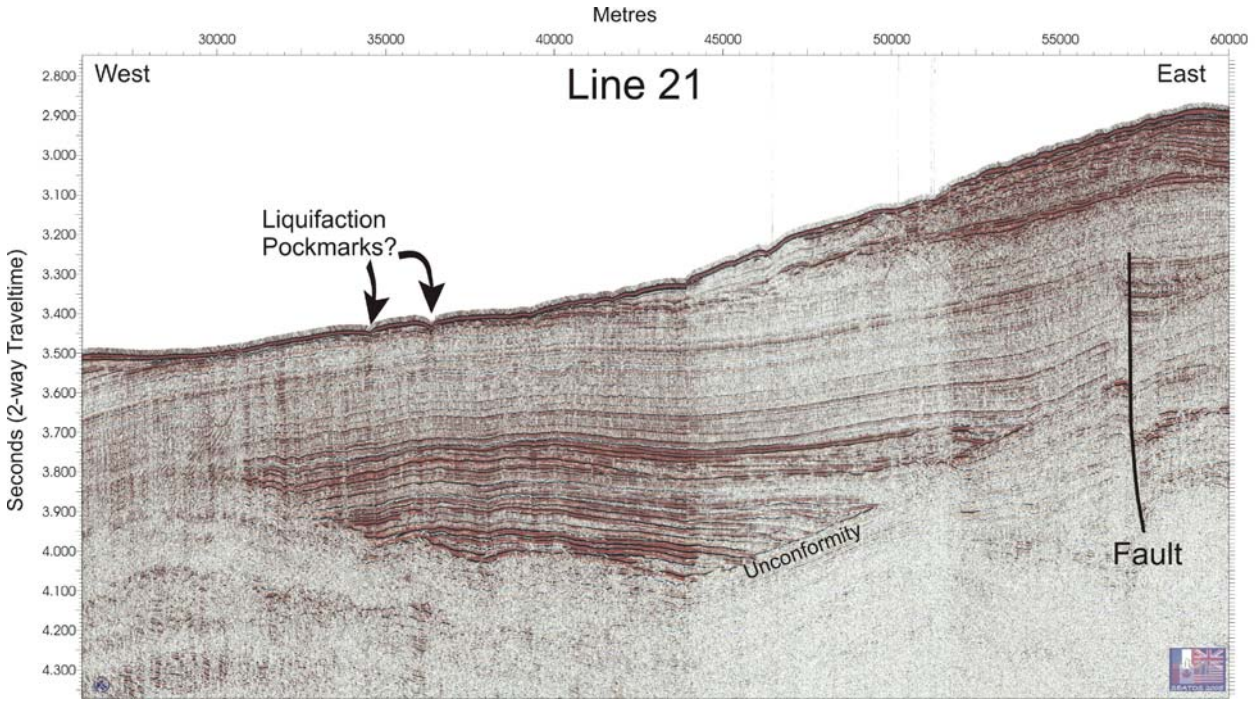

Figure 32. Airgun seismic profile along Line 21 on the fore arc high.

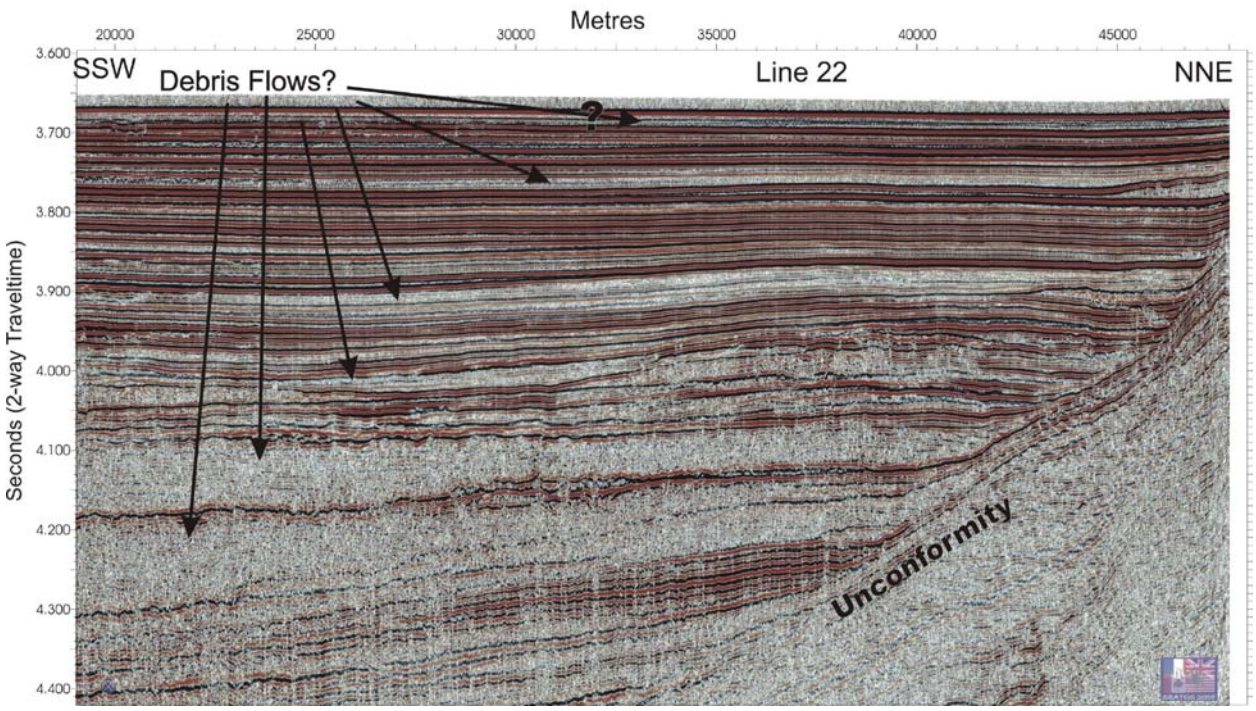

Figure 33. Airgun seismic profile along Line 22 on the fore arc high.

reaches the seafloor. The seaward end of Profile 24 is dominated by a series of folds, which get larger to the NE. The western boundary of the basin contacts these folds with sharp truncation of upturned reflectors, suggesting normal faulting (Figure 34). This site was one of the ROV dive sites (Mosher's Toe).

Profile 25 extends from the seaward end of the Aceh Basin NNE to approximately the middle of the basin. At the SSW end of the profile there are numerous faulted folds; the faults are normal, with downthrows towards the basin. The fill, ~1.0 s thick, is flat-lying above becoming slightly undulatory at depth. There is no disruption of the seafloor. A prominent angular unconformity forms the base of the fill. Penetration averaged ~1.0–1.2 s.

Profile 26 extends from the middle of the Aceh Basin back towards its seaward edge, trending ENE to WSW. Basin fill is flat-lying above to slightly undulatory at depth; the base of the fill is defined by the same angular unconformity imaged by seismic Profile 25. The seaward margin of the basin is dominated, as on Profile 25, by faulted folds. The normal faults are prominent, with downthrown sides towards the basin; offsets appear to be in the range of 0.1–0.2 s. Submarine landfall debris at the base of slope is apparent. The seaward end of the profile is characterized by a prominent topographic high (almost certainly a fold); penetration crossing this high is limited. This feature is 1,500 m high. At the top is a 70-m deep gouge zone that was the target of ROV Dive 7 (Figure 35).

Forearc Basin ROV Survey

Two ROV surveys were carried out on the western margin of the forearc basin (Figure 36). The goal of the first survey, Dive 6, at depths of 1200 to 1300 m, was to investigate a strike-slip fault imaged on the HMS *Scott* multibeam data to ascertain whether there was any evidence of recent strike slip movement. The second dive, located on the western margin of the planar floored forearc basin, was to investigate a fault imaged on the SCS and, again, to determine whether there had been any recent movement here.

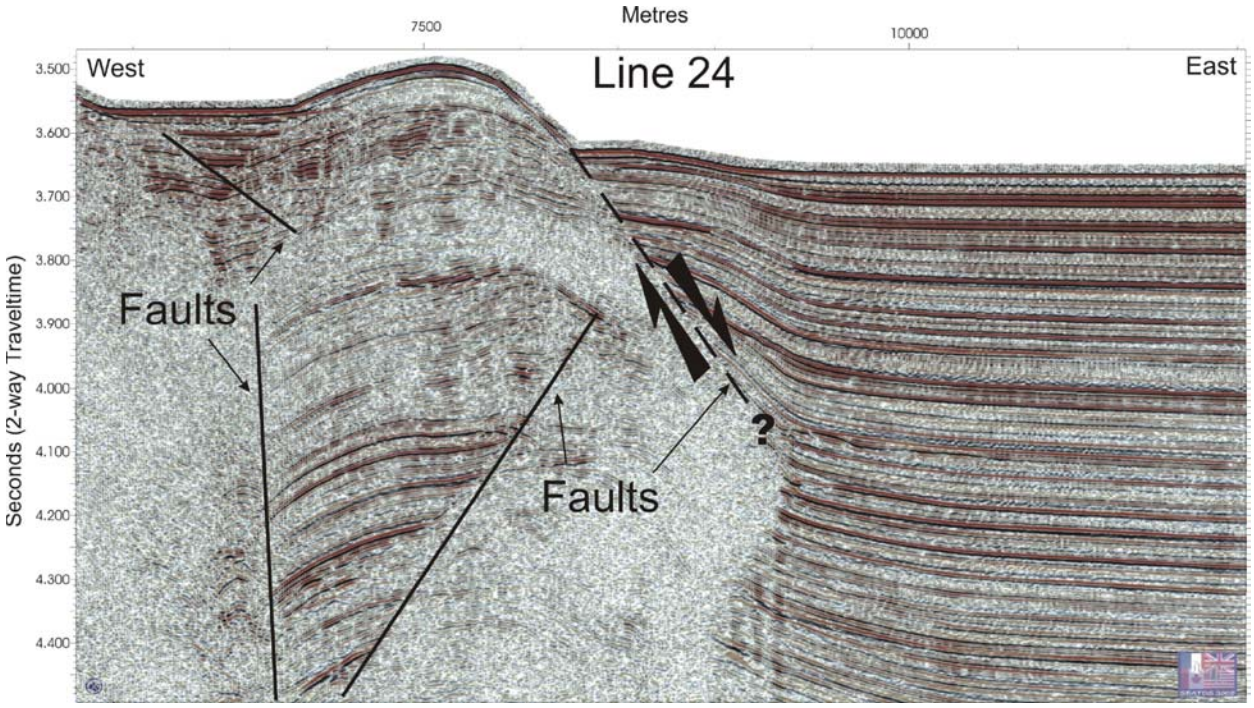

Figure 34. Airgun seismic profile along Line 24 on the fore arc high.

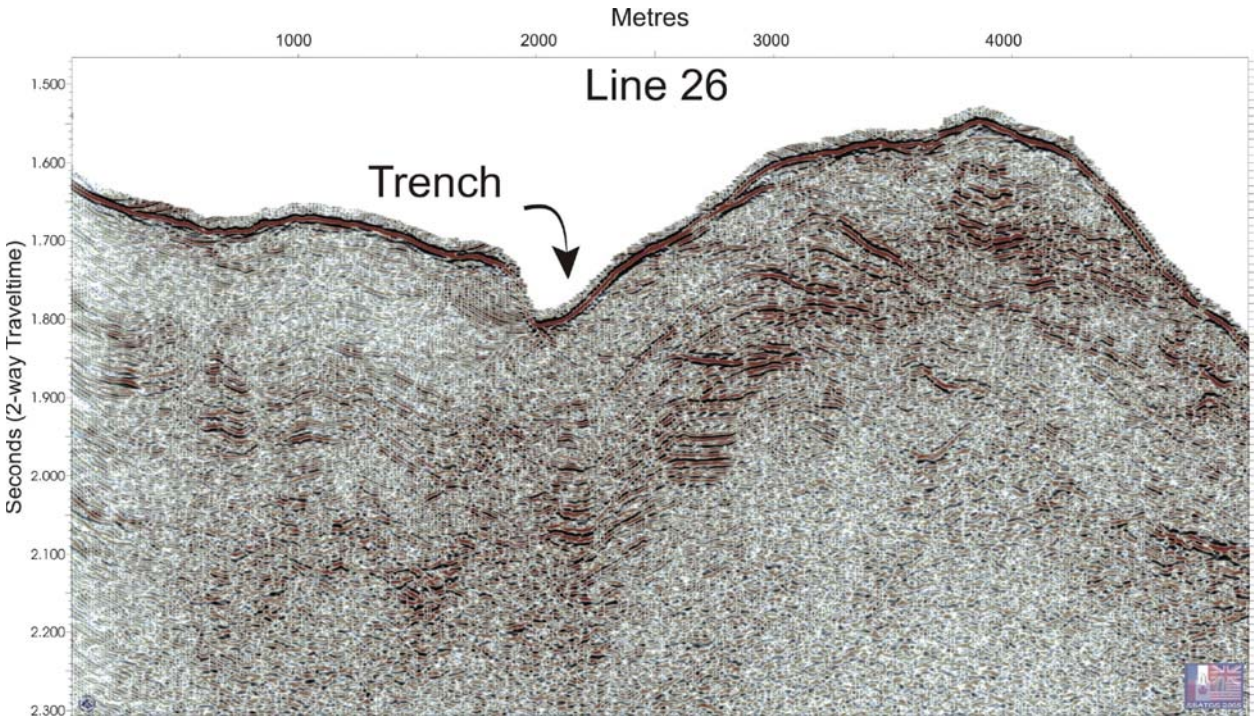

Figure 35. Airgun seismic profile along Line 26 on the fore arc high.

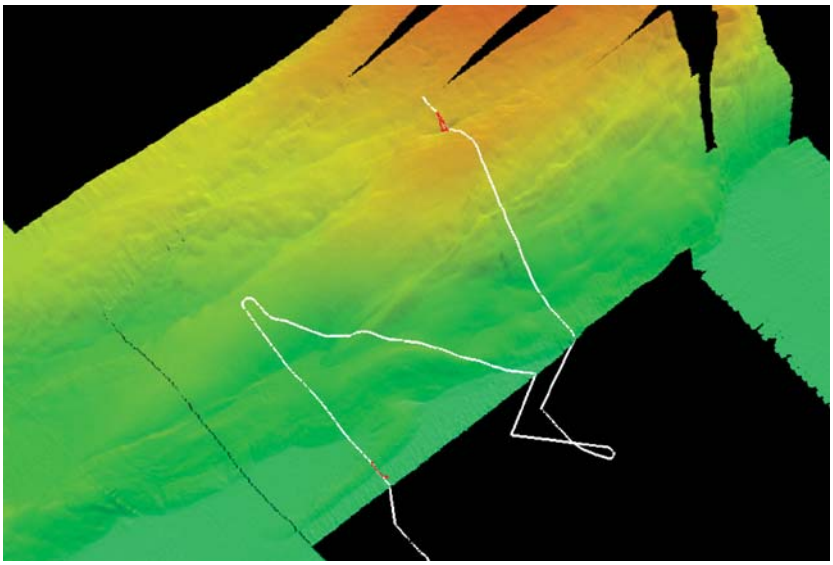

Figure 36. Overview of the dive sites on the western margin of the forearc basin from the multibeam data set. The Dive 6 track is in the north and Dive 7 is in the south; both are in red. White lines are the SCS transects. For details, see Figures 37 and 38

Site 6: Forearc Basin Survey ("Mosher's Mystery Tour")

Geotechnical ROV Results

Site 6 began on a high in the forearc and descended into a linear depression imaged on multibeam data, interpreted as a strike slip fault, that is the site of a fault along a crossing line on the SCS data (Figure 37). The seafloor on the high was at a depth of approximately 1,200 m and the depression was about 100 m deeper. At the top of the high there was rock pavement, with orthogonal joint sets oriented parallel and perpendicular to the margin. The systematic set was perpendicular to the margin or parallel to the dive heading, and the later, non-systematic set (parallel to the margin) showed abutting relationships with the earlier set. Rippled sand was in places nested within crack-bounded depressions, but the pavement was mostly devoid of loose sediment cover. Sampling of the pavement proved that it was a clayey, terrigenous sediment with foraminifera that was semi-consolidated and extensively bored by organisms. Downslope there was a series of ledges of similar pavement with increasing debris and a sandy rippled surface at the bottom of the slope. The absence of any scarps indicated that this fault did not rupture the surface on December 26, 2004. The heavily bored pavement at the top of the ridge was consistent with an erosion surface that was swept clean of sediment.

Biological Results

Dive 6 investigated the scarp of a possible fault identified from seismic data. The seabed below the scarp comprised a pavement of cemented mudstone, with occasional patches of rippled sand. Fauna were generally sparse. Dive 6 was terminated as a result of a hydraulic leak from the ROV's starboard manipulator. A second dive at the site followed a different transect, crossing terraces at 1,300 m occupied by brisingids, anemones, sponges and gorgonians. There was little evidence of seabed disturbance. No core samples or megafauna were collected.

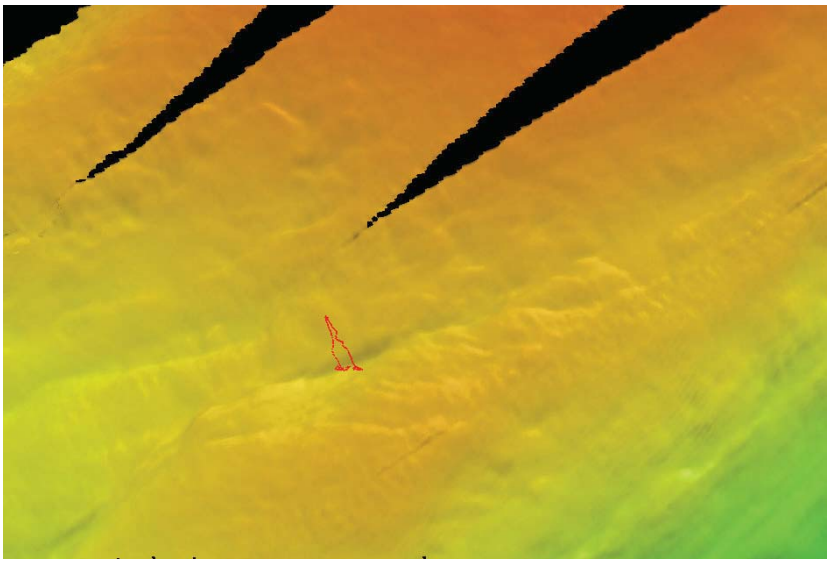

Figure 37. Close up image of Dive 6 (in red). Image is Mosher's Toe site from the multibeam data.

Site 7: Northern Forearc High ("Mosher's Toe")

Geotechnical ROV Results

At Site 7, the ROV surveyed the northeastern slope of a ridge along the edge of the Aceh Basin where a possible fault is imaged on a seismic reflection profile (Figure 38). The seabed was muddy and the surface was flat at the base becoming increasingly hummocky upslope. Observed crack features were identified as burrows produced by shrimp. There was no evidence of recent deformation.

Biological Results

Dive 7 examined the deeper slope between 2,689 m and 2,593 m in the same area as Dive 6. The seabed was sandy mud, with occasional cobbles. The fauna were dominated by hexactinellid sponges occupying, what may have been, the stems of dead gorgonians. An attempt was made to recover a specimen with the suction sampler, but the base of the stem was buried in sediment at least 4.5 cm deep. Gorgonian stems were also occupied by brisingids and flytrap anemones. Occasional linear burrows up to ~0.5 m long in the sediment appeared to be occupied by shrimp. Blade cores and push cores were collected at the start and end of the dive transect.

Site 8: Don's Volcano

Geotechnical ROV Results

The purpose of the dive was to investigate a small bathymetric conical shaped high surrounded by a relatively flat sedimentary basin (Figure 39). The morphology of the high suggested a submarine volcano. The conical structure had a total relief of about 200 m, a diameter of about 1 km at its base, and was located in a position aligned with the ship's course for the return trip to Phuket, Thailand. The ROV landed at 12:48 UTC several tens of meters to the southwest of the conical structure. The ocean floor was mudstone covered with a layer of silt. The ambient water column had a lot of suspended particles and visibility was poor. During the short trip to the flanks of the conical structure, the ROV revealed a

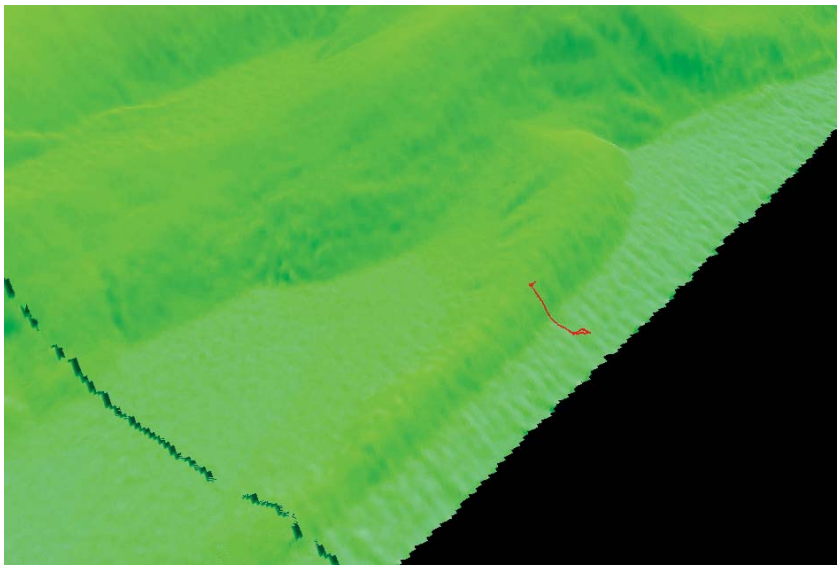

Figure 38. Close up image of Dive 7 (in red). Image is of Mosher's Mystery Tour site from multibeam data.

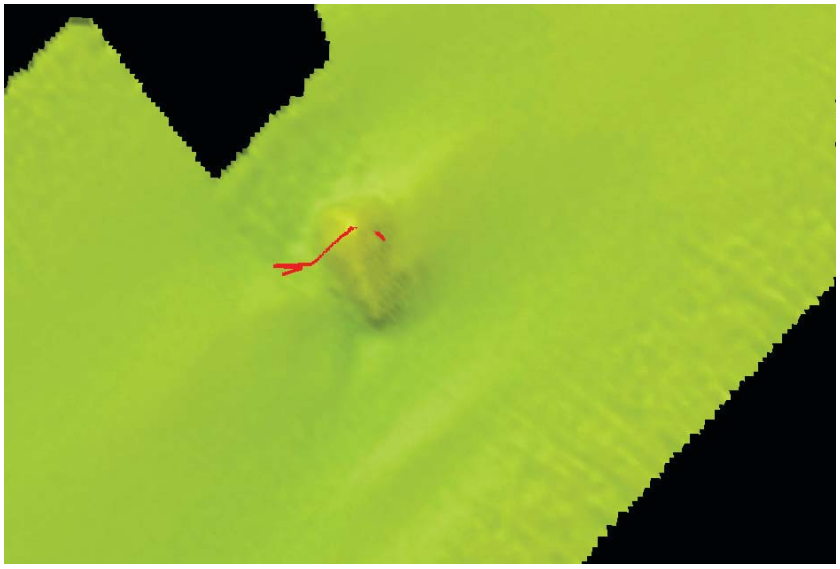

Figure 39. Close up image of Dive 8, Don's Volcano, from the multibeam data.

series of small ledges a few centimeters in height, as well as cobble fields. Samples of the rocks were broken-off and collected with the ROV manipulator.

The lower regions along the flank of the conical structure included boulder fields. The boulders became more common in the upslope direction. The surfaces of the boulders and *in situ* rocks had a fabric that suggested a cooling rind consistent with cooling basalt. A small depression at the top of the conical structure suggested a small caldera. The flanks of the conical structure were interspersed with small, flat areas covered with well-sorted and well-rounded cobbles. All rocks on the conical structure appeared to be black. Rock samples were collected regularly during the ascent to the summit of the conical structure. Many flat horizontal surfaces were covered with the remains of large coral that had died decades or centuries prior to our discovery. The ROV dive was terminated 18:01 UTC. Rock samples recovered, along with the *in situ* geologic structures, confirmed the conical structure is a small basaltic volcano. Outstanding questions include (1) When was the last eruption? (2) What is the origin of the cobble fields? and (3) What caused the coral to die?

Biological Results

Dive 8 was mainly to investigate for chemosynthetic communities. It specifically surveyed a 200-m-high mound interpreted as a volcanic feature from the HMS *Scott* multibeam data. The ROV climbed the steep sides of the mound, encountering beds of weathered fragments of gorgonians. Rock samples confirmed a volcanic origin of the mound. At the summit of the mound, large bryozoans, sponges, and gorgonians dominated the fauna. An aggregation of pennalids was also present in a crevice. A survey of the summit did not find any evidence of current or recent volcanic or hydrothermal activity. No core samples or megafauna were collected.

4. References

Ammon, C.J., J. Chen, H.-K. Thio, D. Robinson, S. Ni, V. Hjorleifsdottir, H. Kanamori, T. Lay, S. Das, D. Helmberger, G. Ichinose, J. Polet, and D. Wald. 2005. Rupture Process of the 2004 Sumatra-Andaman Earthquake. *Science* 308: 1133–1139.

Berryman, J.G., H.F. Wang. 2000. Elastic wave propagation and attenuation in a double-porosity dual-permeability medium. In: Neville Cook special issue. C.-F. Tsang and L. Myer, eds. *International Journal of Rock Mechanics and Mining Sciences* 1997:63–78.

Gower, J. 2005. Jason 1 detects the Dec. 26, 2004 tsunami. *Eos* 86(3).

Gusiakov, V.K. 2005. http://www.pmel.noaa.gov/tsunami/indo20041226/sibolga nias.htm

Harada, K. 2005. The December 26, 2004 Sumatra Earthquake Tsunami, Tsunami Field Survey around Phuket, Thailand. http://www.drs.dpri.kyoto-u.ac.jp/sumatra/thailand/phuket survey e.html, Research Center for Disaster Reduction Systems, Disaster Prevention Research Institute, Kyoto University, Japan.

Henstock, T., L. McNeill, and D. Tappin. In press. Seafloor morphology at the 26 December 2004 Indian ocean earthquake rupture zone. *Geology*.

Kulikov, E. 2005. Dispersion of the Sumatra tsunami waves in the Indian Ocean detected by satellite altimetry. Report from P.P. Shirshov Institute of Oceanology, Russian Academy of Sciences, Moscow

Lay, T., H. Kanamori, C.J. Ammon, M. Nettles, S. Ward, R. Aster, S.L. Beck, S.L. Bilek, M.R. Brudzinski, R. Butler, H.R. DeShon, G. Ekström, K. Satake, and S. Sipkin. 2005. The great Sumatra-Andaman earthquake of 26 December 2004. *Science* 308:1127–1133.

Masterlark, T. and H.F. Wang. 2002. Transient stress-coupling between the 1992 Landers and 1999 Hector Mine earthquakes. *Bulletin of the Seismological Society of America* 92:1470-1486.

Okada, Y. 1985. Surface deformation due to shear and tensile faults in a half-space. *Bulletin of the Seismological Society of America* 75(4):1135–1154.

Okada, Y 1992. Internal deformation due to shear and tensile faults in a half-space. *Bulletin of the Seismological Society of America* 82:1018–1040.

Stein, S. and Okal, E. 2005. Speed and size of the Sumatra earthquake. *Nature* 434:581–582.

Watts, P., M. Ioualalen, S.T. Grilli, F. Shi, and J.T. Kirby. 2005. Numerical Simulation of the December 26, 2004 Indian Ocean Tsunami using a Higher-order Boussinesq Model. In Proc. 5th Intl. Symp. on Ocean Wave Measurement and Analysis (WAVES 2005, Madrid, Spain, July 2005) ASCE Publication.

Yalciner A.C., D. Perincek, S. Ersoy, G. Presateya, R. Hidayat, and B. McAdoo. 2005. Report on December 26, 2004, Indian Ocean Tsunami, Field Survey on Jan 21-31 at North of Sumatra. By ITST of UNESCO IOC.

Appendix A:
Tsunami Wave Modeling Results

Numerical Simulation of the December 26, 2004 Indian Ocean Tsunami: SEATOS Cruise report (DRAFT)

Stéphan Grilli [1] (group leader),
Mansour Ioualalen[2], Frédéric Dias[3],Kate Collins[4]
Fengyan Shi[5] (shore-based), James T. Kirby[5] (shore-based),
and Philip Watts[6] (shore-based).

Abstract: There were two main objectives for the modeling group: (i) based on new information obtained during the cruise, to refine the tsunami source and perform increasingly accurate simulations of the 12/26/04 tsunami at the Indian Ocean Basin scale; (ii) to perform regional simulations on refined grids and better estimate coastal tsunami impact for selected areas (Ko Phi Phi, Banda Aceh,...). The latter can be referred to as case studies. The tsunami source used in the modeling is based on existing pre-cruise information, supplemented by seafloor morphology and other information about the earthquake obtained during the cruise and provided by the geophysics and seismology groups. The initial rupture model used in our pre-cruise work (Watts et al., 2005) is made of four separate segments, with different characteristics, along a 1200 km long rupture zone. Tsunami sources for these segments are obtained by using Okada's (1985) method. According to information from existing rupture models (de Groot-Hedlin, 2005; Ammon et al., 2005), we trigger these sources in a time sequence spanning 331 s, and perform a numerical simulation of the tsunami with a high-order Boussinesq model (i.e., a dispersive long wave model with full nonlinearity up to a certain order). The pre-cruise source already gave reasonable agreement between numerical results and a few observed runup values.

During the cruise, as more became known about the tsunami source, we iteratively conducted modeling studies aimed at better reproducing tide gage measurements, Jason I satellite observations, as well as runup data collected by a variety of international teams, at a number of selected locations. We also created the topographic and grid data for the regional studies and modeled those in order to perform the selected case studies.

[1]Department of Ocean Engineering, University of Rhode Island (URI), Narragansett, RI 02882, USA; grilli@oce.uri.edu
[2]Geosciences Azur, (CNRS-IRD), Villefranche-sur-Mer, France.
[3]Ecole Normale Supérieure, Cachan, France
[4]University of British Columbia, Dept. of Earth and Ocean Sciences, Vancouver, BC
[5]Center for Applied Coastal Research, University of Delaware, Newark, DE 19761, USA.
[6]Applied Fluids Engineering, Inc., 5710 E. 7th Street, Long Beach, CA 90803, USA.

INTRODUCTION

The December 26, 2004 tsunami is one of the most devastating tsunamis in recorded history. It was generated in the Indian Ocean off of Sumatra, at 0h 58'53" GMT, by one of the largest earthquakes ever recorded, with a moment magnitude $M_w = 9.1 - 9.3$ (Ammon et al., 2005; Lay et al., 2005; Stein and Okal, 2005). The number of fatalities caused by the tsunami is greater than 290,000 in more than 10 countries across the entire Indian Ocean, although the vast majority of these occurred on the Indonesian island of Sumatra near Banda Aceh. In addition to this disastrous human toll, the tsunami was clearly one of global impact and of global importance, with seismicity and wave action documented around the world for days afterwards. The widespread destruction caused one of the largest emergency relief efforts ever mounted by world powers and agencies. Scientists had been warning of the growing exposure of coastal residents to tsunami hazards for years, although the location and impact of this event was not anticipated by most. The lack of any effective tsunami education or tsunami warning system in the region exacerbated the number of fatalities, even if many victims on the island of Sumatra, closest to the epicenter, had little chance of escaping the killer waves.

There were direct instrument observations of the event in and around the Indian Ocean region, including seismometers, tide gages (Figs. 1,2), buoys, GPS stations, and at least one satellite overpass (Jason 1; Figs. 3,4; Gower, 2005; Kulikov, 2005). Some of the tide gage data was immediately processed in order to estimate the likely location and extension of the tsunami source area (e.g., Fig. 5). A similar analysis performed by Lay et al. (2005), using 9 additional arrival times around the western Indian Ocean basin, yields a tsunami source area for strong initial tsunami excitation apparently extending 600-800 km north of the epicenter. All of this data, after proper correction and interpretation represents invaluable records of what happened on 12/26/04, and will help us both understand the tsunami event better and calibrate and validate our numerical models.

Direct eyewitness observations of the December 26, 2004, tsunami event were numerous, and many of these observations were in the form of still pictures and movies, because the region is a popular tourist destination. These records display a wide variety of waveforms and wave activity that are distinct to each location. In addition, various media recorded numerous eyewitness accounts, and many of these were posted on the world wide web, with a great deal of detail being given about the size and timing of the tsunami waves (e.g., http://www.yachtaragorn.com/Thailand.htm). The quantity of such records, along with their unknown quality, makes the processing and collection of these observations a difficult and lengthy task. We devoted a lot of time during the cruise in analyzing some of these less traditional observations, in order to reconcile these with the other more absolute data discussed above and to be able to use these with some degree of confidence, when validating our models.

Soon after the tsunami, the international scientific community mounted a response to this event through multiple tsunami survey teams. These were largely coordinated by the International Tsunami Information Center, a United Nations agency. These teams of scientists documented damage, measured vertical runup and horizontal inundation, and assembled careful reconstructions of wave activity (e.g., Gusiakov, 2005; Harada, 2005; Yalciner et al., 2005; e.g., Fig. 6). Each team was restricted to a limited geographical region, given the length of damaged coastline and number of countries involved. The runup and inundation

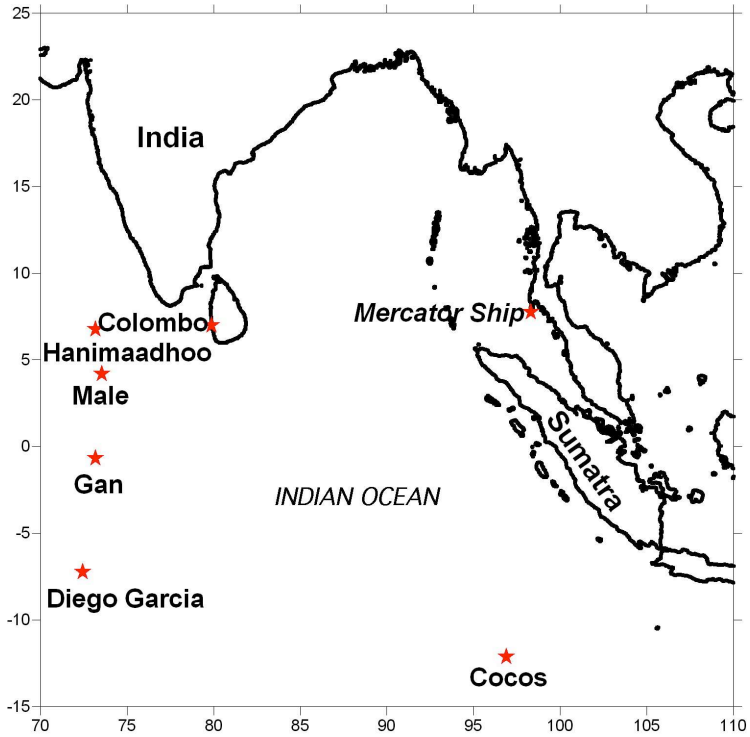

Fig. 1. Location of some tide gages in the Indian Ocean basin.

data are still becoming available through various publications and web sites, in a piecemeal fashion, region by region.

Prior to this cruise, we conducted initial modeling studies of the tsunami, using reasonable sources, based on available seismological and other information, and compared runup results with some of the available observations at a few locations (Watts et al., 2005). The agreement was found reasonable. More detailed analyses and comparisons were conducted during the cruise and additional comparisons with various field data were made. These however do not yet include a comprehensive comparison of modeling results with all of the available data and records. Such a lengthy analysis is still premature, pending confirmation of the selected characteristics of the tsunami source.

Thus, we focussed our efforts on constructing increasingly accurate tsunami sources and tsunami modeling grids (including ocean bathymetry and coastline topography), based on geophysical and seismological data, some of it newly acquired or analyzed during the cruise. Based on these sources, we performed tsunami simulations aimed at explaining the observed large scale features of tsunami propagation and inundation at the Indian Ocean Basin scale. We also performed regional numerical simulations, using refined grids, to better estimate coastal tsunami impact for selected areas (Ko Phi Phi, Banda Aceh,...). The latter are referred to as case studies.

GEOPHYSICAL AND SEISMIC CHARACTERIZATION

General considerations

Large faults form over time, presumably, through small slip events followed in time by larger slip events (Wells and Coppersmith, 1994). Consequently, large single-event displace-

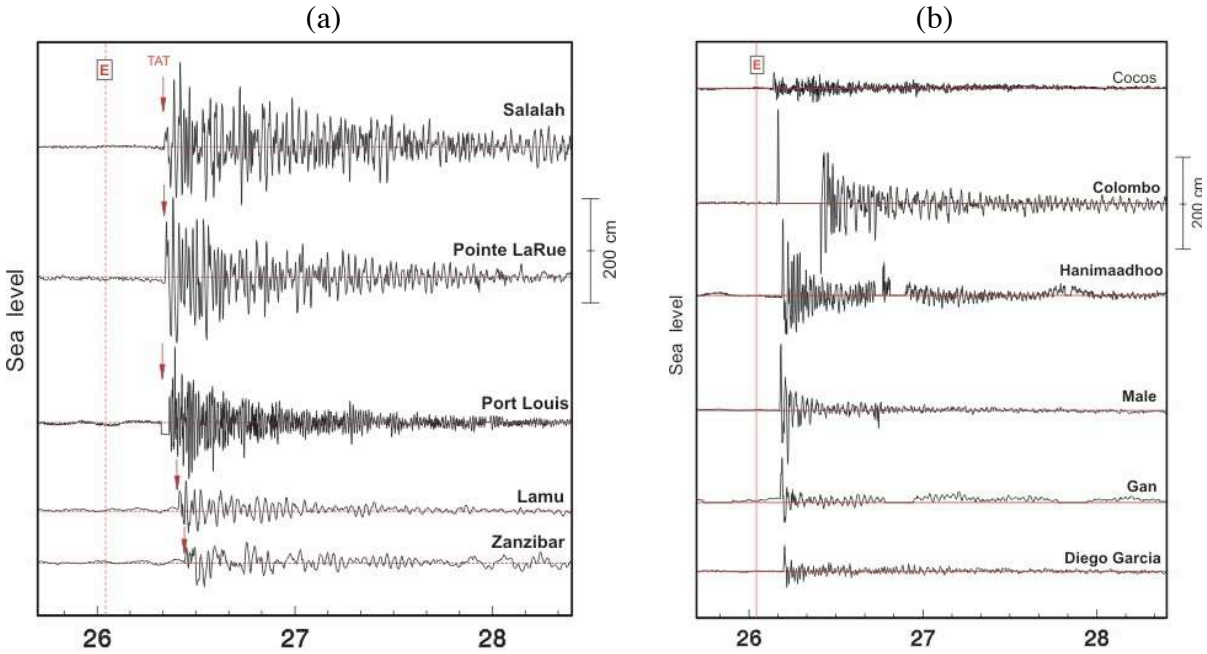

Fig. 2. Measurements at tide gages of Fig. 1 (source NOAA, 1/05): (a) Western Indian Ocean. (b) Eastern Indian Ocean.

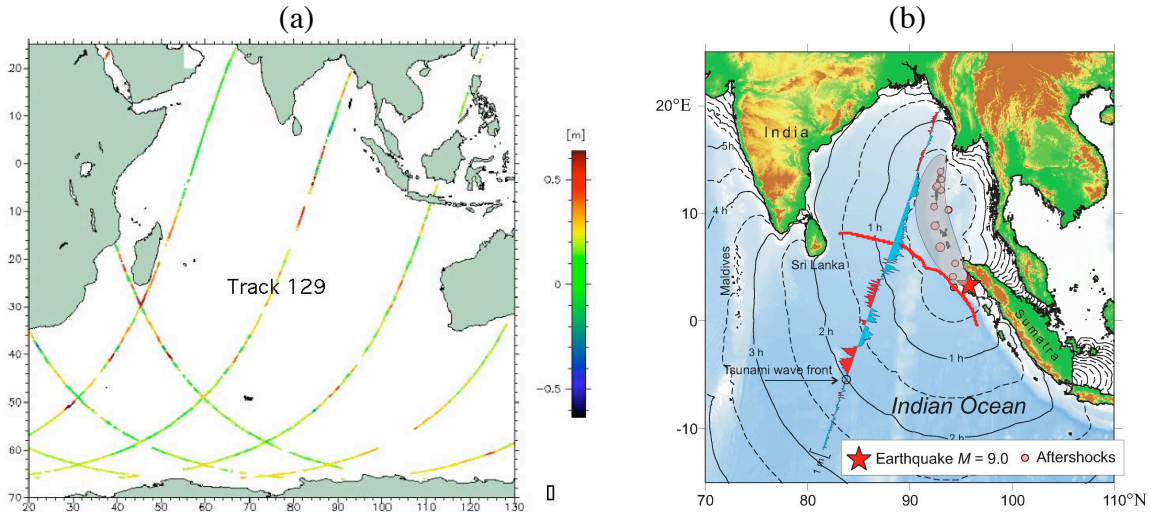

Fig. 3. Track and data for Jason 1 satellite on 12/26/04 : (a) Track 129 and altimetry (Gower, 2005). (b) Cycle 109 along track 129, with tsunami source and propagation time (Kulikov, 2005).

ments tend to occur on structures that have already accumulated large total displacements. Therefore, the tectonic structures responsible for the December 26, 2004, event should be evident in the offshore bathymetry, unless they are buried under loose sediment. These structures are generally described as the Indo-Australia (or downgoing) plate subducting beneath the Eurasian (or overriding) plate at 50-60 mm per year, with a largely East-West direction of convergence. The Bay of Bengal consists mostly of the Australia-Indian plate, with a sequence of islands running north-south along the eastern edge of the bay, denoting the plate boundaries and the edge of the subduction zone (see Fig. 9). In the Bay of Bengal, sediment from rivers contribute to a massive sediment fan that covers the entire downgoing plate from north to south, whose motion creates a large accretionary wedge east of the subduction zone

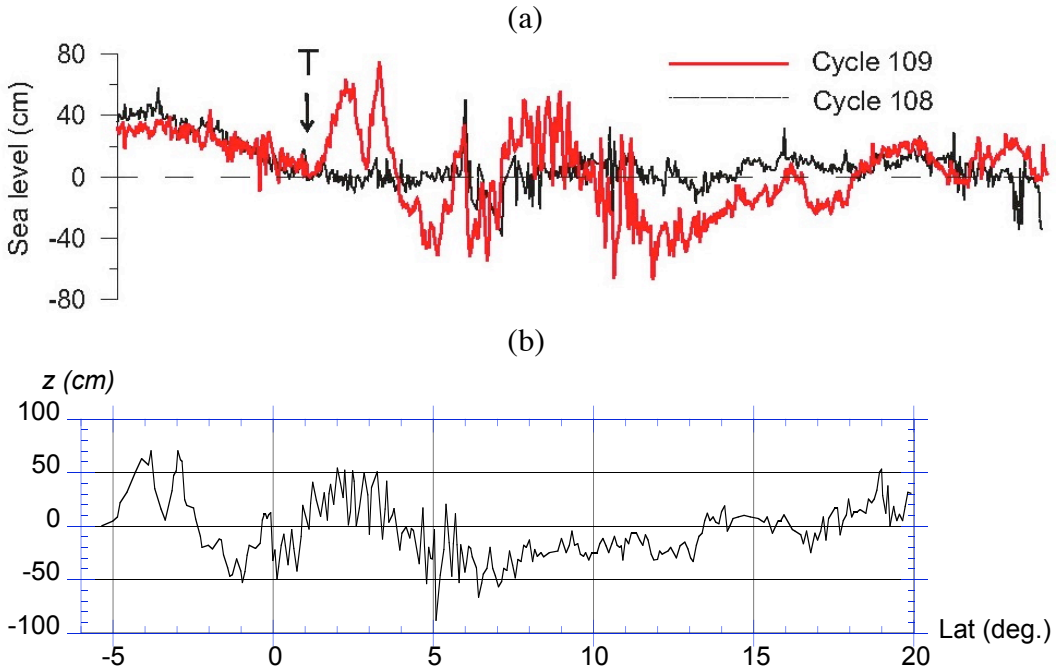

Fig. 4. (a) Jason 1 altimetry for cycles 108 and 109 along track 129 (Kulikov, 2005); (b) Tsunami signal: difference of cycles 109 and 108.

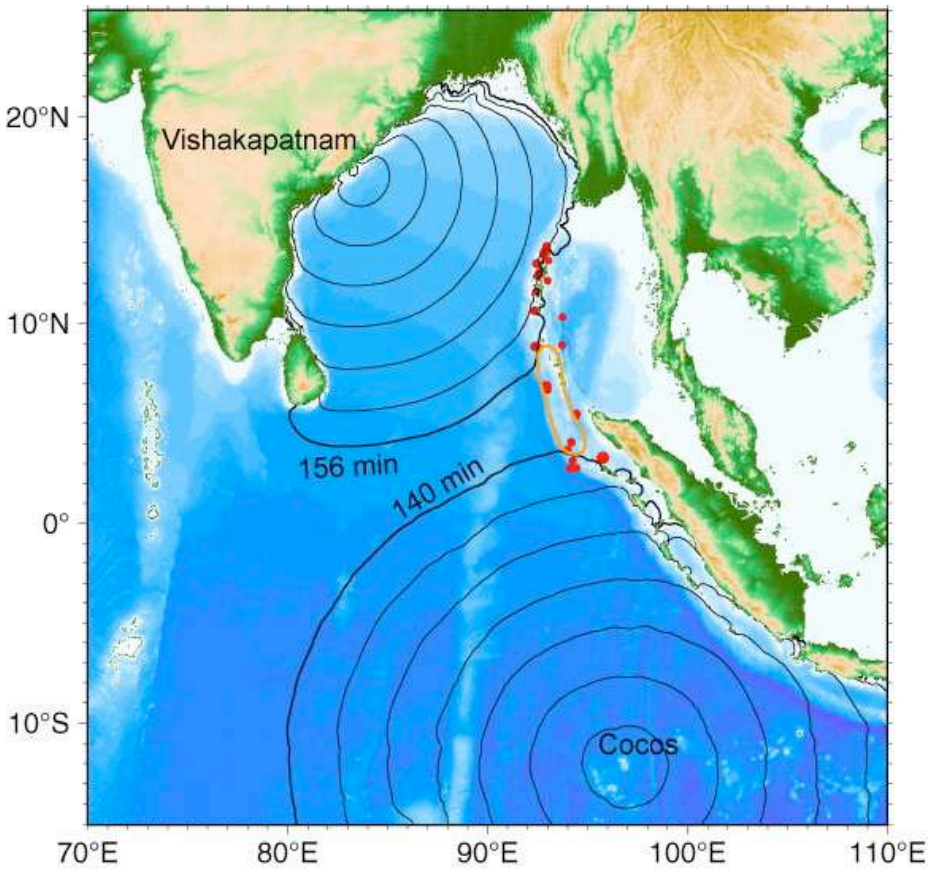

Fig. 5. Tsunami source area constraint based on arrival times at Cocos Island and Vishakapatnam tide gages (source NOAA; 1/05).

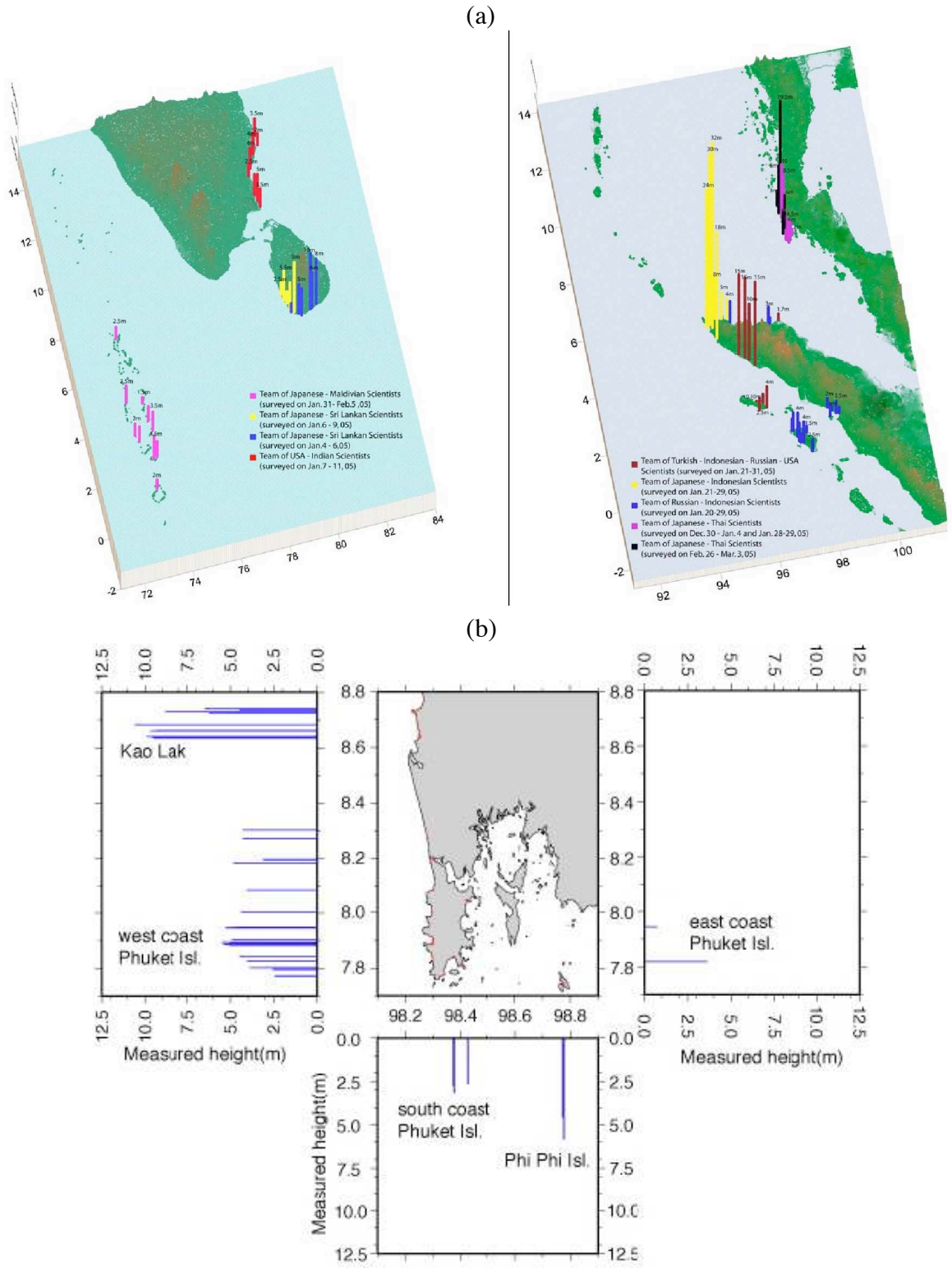

Fig. 6. ***Runup data*** **: (a) India, Sri Lanka and the Maldives, Northern Sumatra (Indonesia), Thailand (Yalciner et al., 2005); (b) Details of area around Phuket (Thailand) (Harada, 2005).**

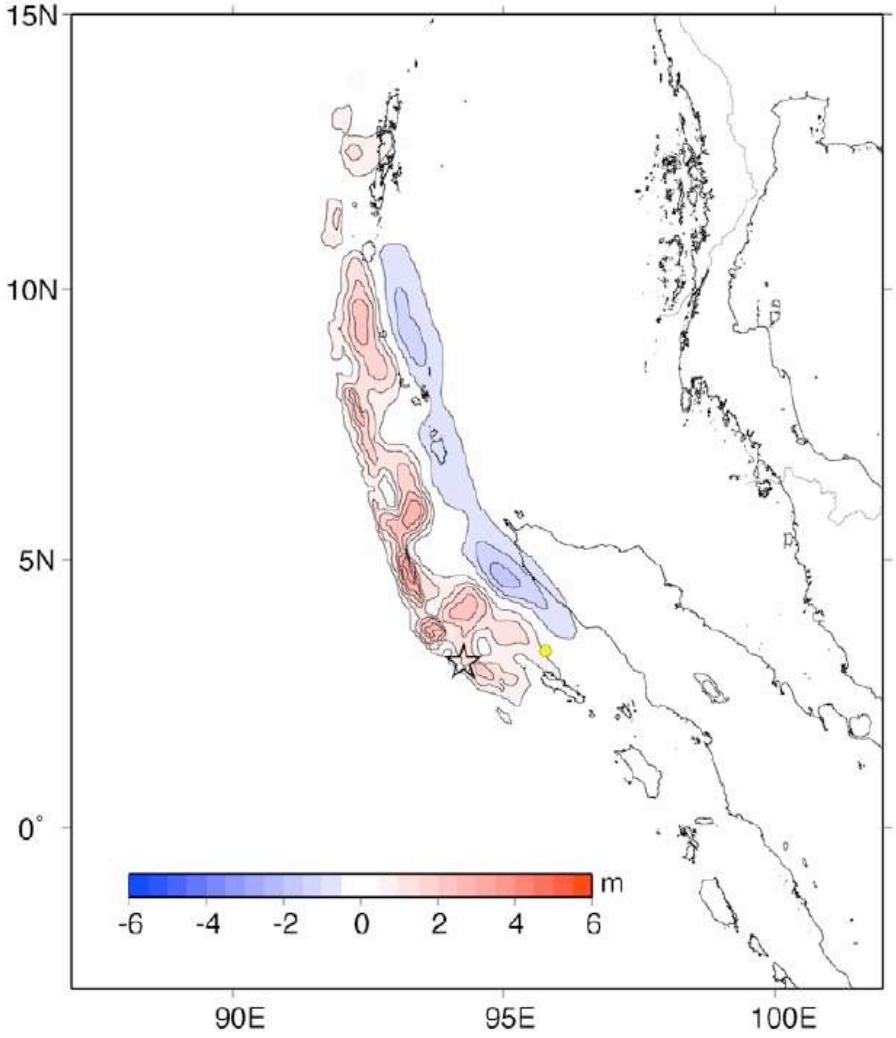

Fig. 7. Static uplift computed with spectral element method based on an inversion of seismological data (Ammon et al., 2005; Model III).

(a) (b)

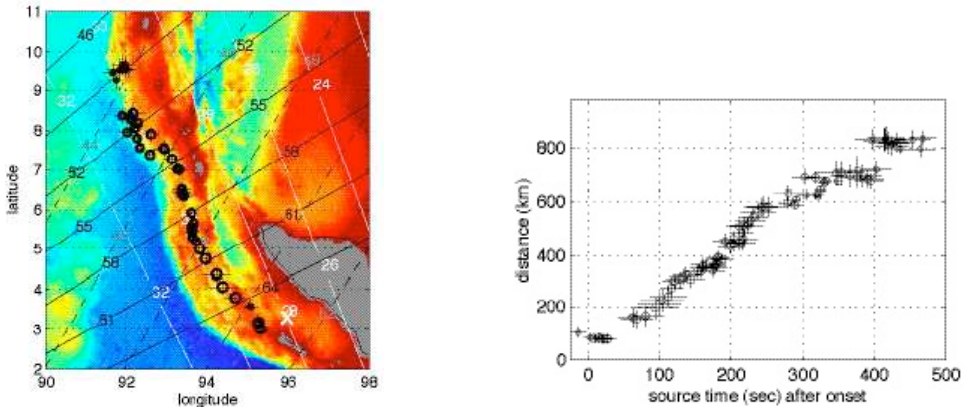

Fig. 8. Analysis of rupture propagation based on hydroacoustic data (de Groot-Hedlin, 2005): (a) Gradual motion to the Northwest of transverse (T)-wave source, from epicenter (X). (b) Distance between T-wave source and epicenter as a function of time.

(Davis et al., 1983). The subduction zone is thus visible along the entire rupture length, with deformation and erosion of the overriding plate in plain view.

In the case of the December 26, 2004, earthquake, to estimate a tsunami source prior to the cruise, we examined the bathymetry in the Bay of Bengal in order to describe the morphology of structures visible on the seafloor, which is an expression of the three-dimensional tectonic structures that exist, as well as the tectonic processes that are taking place at depth. During the cruise, a series of seismic profiles (using twin air guns) and direct video recording (using a Remotely Operated Vehicle-ROV) were made, whose detailed analysis, together with other seismological analyses that were analyzed, will help understanding and elucidating the tectonic motions that occurred during the 12/26/04 event. These in turn will be the basis for updating our definition of characteristics of tsunami sources used in model simulations and, hopefully, for an improvement of these simulations.

Analysis of the 12/26/04 rupture

The main shock of the December 26, 2004, earthquake occurred along the subduction zone between the downgoing Indo-Australian and overriding Eurasian plates, at a hypocentral depth of around 25-30 km from the surface (Ammon et al., 2005; Tanioka 2005). The main shock epicenter was located at 3.3° latitude N and 96° longitude E, as indicated by a star on Figs. 1 and 7. The rupture proceeded almost exclusively northwest from the epicenter (Ammon et al., 2005; Tanioka 2005). The total rupture length is around 1200-1300 km, requiring about 400-500 seconds for the rupture to propagate end to end, at an assumed shear wave speed of around 2.5-3 km/s. Along such a long rupture length, one expects significant slip nonuniformity. This is born out by various seismic inversion models, which suggest up to 15-20 m slip in the bottom two-third of the rupture zone and less in the North (Ammon et al., 2005; Tanioka 2005). Aftershocks occurred along the entire length of the rupture zone. A significant slow slip component may have occurred in the Northern 400-500 km of the rupture zone, on a time scale beyond the seismic band, contributing to an additional 50% in released energy, bringing the total released energy to $M_o \sim 1.0\,10^{23}$ J or a $M_w = 9.3$ magnitude earthquake (Stein and Okal, 2005).

Fig. 7 gives an example of static uplift resulting from the earthquake, calculated using a seismic inversion model (Ammon et al., 2005); it clearly shows that vertical uplift of up to 6 m occurred on the west side while subsidence down to -6 m occurred on the east side of the rupture region. The arched rupture zone also shows 3-4 separate sub-zones, or segments, which also correspond to the time progression of the rupture along the fault. Based on the inversion of hydroacoustic measurements from arrays located at 2,800 to 7,000 km from the epicenter, de Groot-Hedlin (2005) showed that the rupture proceeded in two distinct phases; initially it progressed northwest along the Sunda trench with a velocity of approximately 2.4 km/s. At 600km from the epicenter the rupture slowed to approximately 1.5 km/s, as it continued to propagate to the Northwest (Fig. 8).

We point out here that there can be many faults that experienced rupture along the subduction zone, and especially along secondary structures running from the subduction zone up to the surface. These secondary structures are evident in the 3 km high face of stepped (or *echelon*) thrust faults rising above the subduction trench in the Southern part, and in the rough tapestry (or fabric) of the sea floor on the overriding plate over the whole rupture zone. It is along these secondary faults that coseismic displacement from the main shock is accom-

modated, with many local variations about the coseismic displacements that we calculate below.

The epicenter for the main shock is near a transition point along the subduction zone. This transition point has the appearance of the letter "S", where there are two sharp bends and a turning point in the curvature. The entire subduction zone has a gentle curvature similar to those found along almost all major subduction zones. The transition point just off of Sumatra is a remarkable feature, possibly related to the initiation of rupture. North of the transition point, we interpret the decrease in sharp relief and increase in rupture width to an increase in downgoing plate dip, which tends to lower the friction of colliding plates, because the downgoing plate is being pulled towards the earths core by phase change. We hypothesize that the dip is lowest in the southern part of the rupture zone, corresponding to higher friction and locking of the two plates. South of the transition point, we expect the dip angle to increase and the friction to decrease. This hypothesis may help explain the location of the epicenter and large slip patches off of Sumatra. The rapid changes in subduction zone curvature may be due to rapid changes in flexure of the downgoing plate. The rise of dip angle produces one sharp curvature, whereas the fall of dip angle produces the other sharp curvature.

TSUNAMI SOURCES

Initial analyses

Fig. 9 summarizes our initial pre-cruise morphological analyses. Based on geophysical and seismological analyses (Tanioka, 2005), we identified four segments with different morphologies along the ruptured subduction zone. These four segments are defined by individual locations, shape, orientations, and slip (Table 1). Let us consider each structure in turn:

1. Segment 1 covers the Southern arc of the ruptured subduction zone, facing in a general southwest direction perpendicular to rupture. The faulting trends north along two relatively sharp bends, one to the north and one to the south of the segment. Here, the overriding plate is at its steepest, and the water depth is largest along the ruptured subduction zone, at around 5,100 m in the deepest part of the Java trench.

2. Segment 2 presents a long and relatively straight section of the subduction zone that trends almost North-South along rupture. The most notable feature of this segment is the nearly uniform profile of the overriding plate, with a steep rise from the subduction trench to a shallow ridge, followed by a descent into a deeper basin further East.

3. Segment 3 features a change in orientation and shape, notably a widening of the distance between the subduction zone and the basin to the east. The basin is narrower here, more in the form of a trench. The ridge is shallow enough to form a number of small islands.

4. Segment 4 undergoes a change in orientation, as well as a change in structure, which is more complex and broken than before. A significant number of larger islands are formed on the overriding plate.

Given the different shapes and orientations of the subduction zone described above, we consider each segment as a distinct tsunami source generated by bottom uplift/subsidence

Parameters	Segment 1	Segment 2	Segment 3	Segment 4
x_o (longitude)	1091550	917000	830000	867300
y_o (latitude)	370600	665000	1075100	1439300
d (km)	25	25	25	25
φ (degrees)	300	350	0	10
λ (degrees)	90	90	90	90
δ (degrees)	11	13	15	11
Δ (m)	30	30	30	25
L (km)	220	410	300	350
W (km)	90	90	150	150
μ (Pa)	$4.0\,10^{10}$	$4.0\,10^{10}$	$4.0\,10^{10}$	$4.0\,10^{10}$
M_o (J)	$1.8\,10^{22}$	$3.4\,10^{22}$	$4.0\,10^{22}$	$4.0\,10^{22}$
λ_o (km)	90	90	150	150
η_o (m)	-9.2	-9.5	-7.6	-7.4
t_o (s)	0	105	223	331

Table 1. ***Initial analysis*** **Parameters used to generate "fast slip" motion with Okada's (1985) method, and define tsunami sources in model (see, Fig. 10).**

caused by seismic activity (Fig. 10a). Each tsunami source has unique and different earthquake parameters that capture the morphology of its own segment. This means that the single rupture event will be represented by a sum of four smaller rupture segments with distinct sea floor morphology.

More specifically the earthquake tsunami sources for vertical coseismic displacement are based in our work on the half-plane solution of an elastic dislocation problem (Okada, 1985). A planar fault of length L and width W is discretized into many small trapezoids and the point source solution of Okada (1985) is used to sum the contributions made by each trapezoid to vertical coseismic displacement, based on the actual depth of the trapezoid. The shear modulus μ can be specified based on the depth d of the earthquake centroid, at latitude-longitude (x_o, y_o), as well as other seismic and geological descriptors. This source was implemented in a software tool, the "Tsunami Open and Progressive Initial Conditions System" (TOPICS, Version 1.2), which provides as outputs, a characteristic tsunami wavelength λ_o that is the smaller of the fault dimensions L or W, and a characteristic initial tsunami amplitude η_o that is the minimum depression found from the coseismic displacement. The seismic moment M_o is proportional to, but slightly less than, $\mu LW\Delta$, because a Gaussian slip distribution is assumed about the centroid, where Δ is the maximum slip. TOPICS allows for the superposition of multiple fault planes, which can be assembled into complex fault structures or slip distributions.

Tsunami source parameters in initial analyses

Consistent with the four segments identified in Fig. 9 and discussed above, we define four separate tsunami sources that we trigger in a time sequence in our model, following the observed time propagation of the rupture (Fig. 8).

The earthquake parameters for each tsunami source are given in Table 1. The total seismic

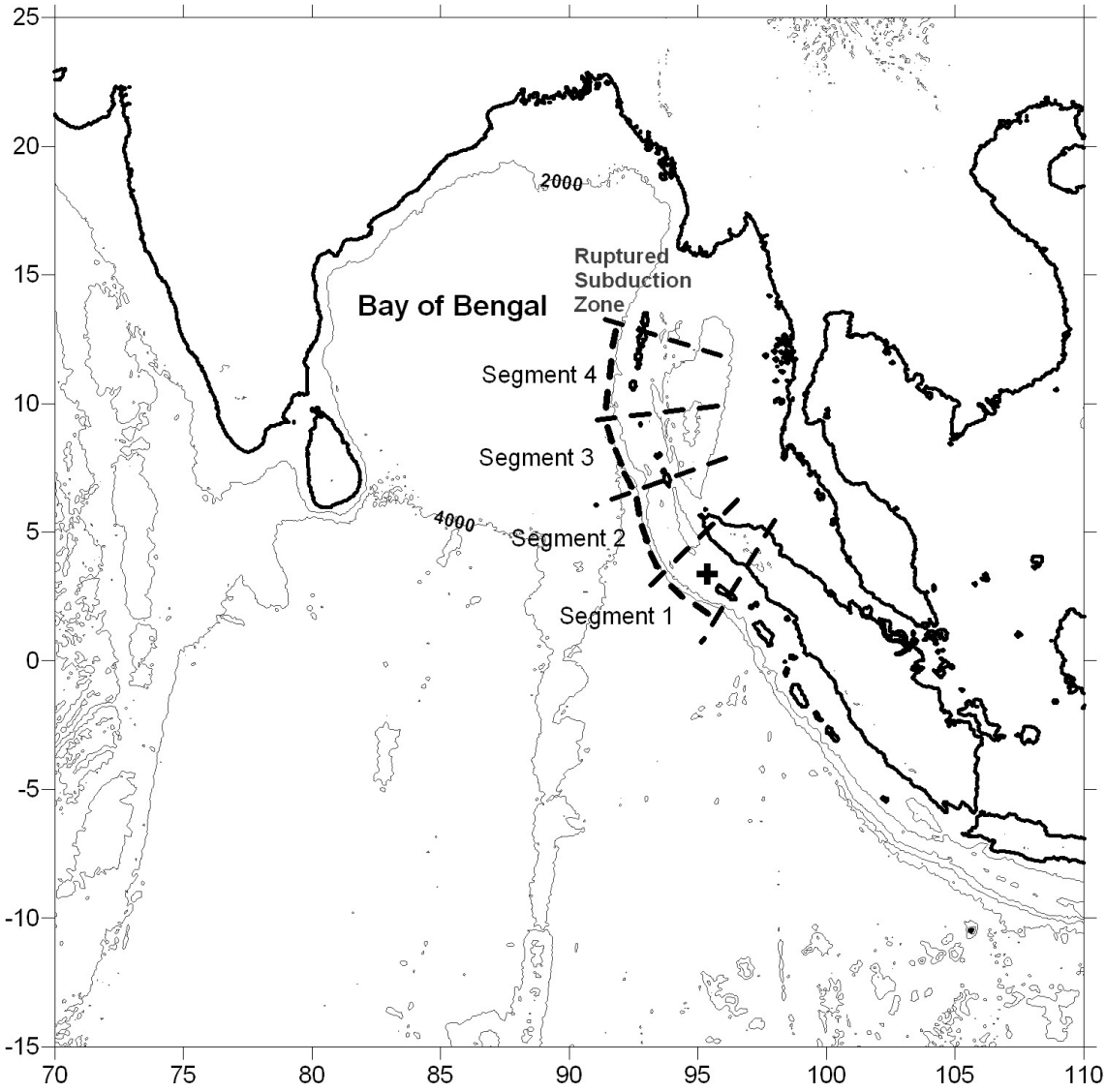

Fig. 9. ***Initial analysis*** **Tsunami simulation grid designed for the Bay of Bengal using ETOPO 2 bathymetry and topography, with location of 4 independent rupture segments (Table 1). (+) Location of the $\mathrm{M_o} = 9.3$ earthquake epicenter.**

moment released is $M_o = 1.3\,10^{23}$ J, equivalent to $M_w = 9.4$. Most of the tsunami source parameters are similar if not identical along each segment. The location (x_o, y_o), strike φ, length L, and width W of each segment follow directly from Fig. 9. The rake λ and depth d are fixed in the present work, something that we intend to refine further in future work when more accurate geophysical and geological interpretation of the event become available, in particular, based on new data acquired and other material reviewed and discussed with the seismological and geophysical groups during this cruise. The dip δ varies in such a way as to reproduce the correct distances between sea floor features. The slip Δ captures the seismic inversion results mentioned above; thus maximum vertical uplift/subsidence would be approximately given by $\eta_o \propto \Delta \sin\delta$, i.e., about 7.4-9.5 m for the data in Table 1, which is consistent with the range of values estimated by the seismic inversion models. [In Okada's model, maximum subsidence is somewhat larger than maximum uplift.]

As in other modeling studies, such as that of Lay et al. (2005), the effects of slow slip

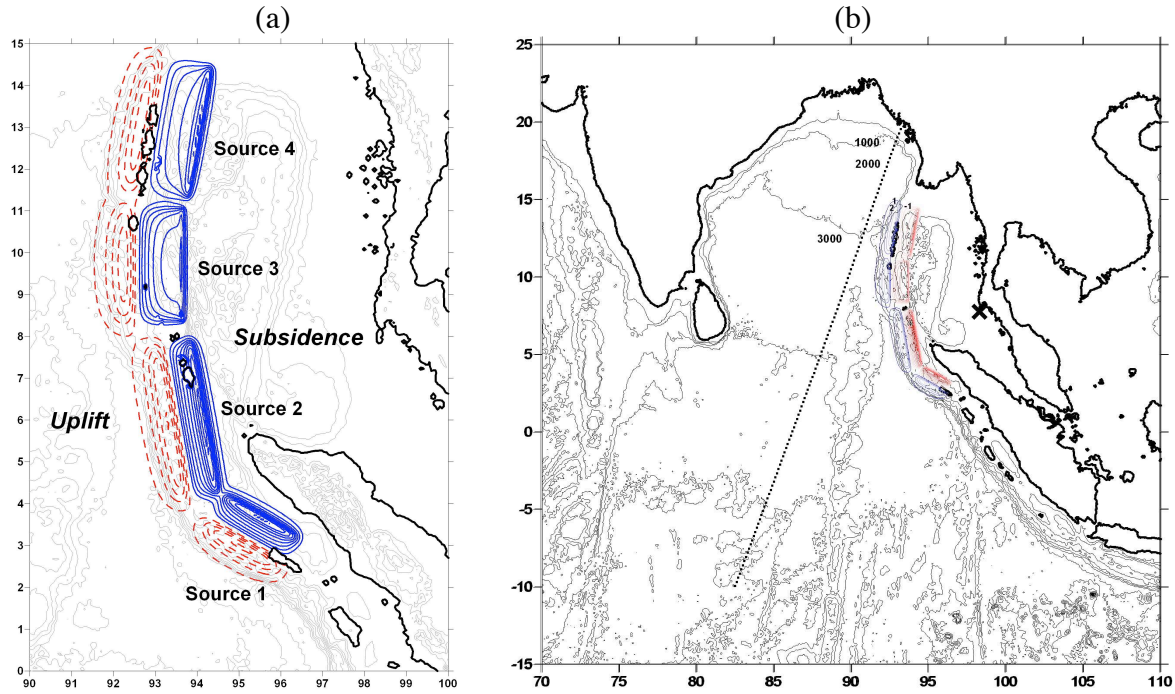

Fig. 10. ***Initial analysis*** **: (a) Earthquake tsunami sources modeled along the rupture zone based on Okada's (1985) method using parameters in Table 1. (b) Same sources located in larger grid used in tsunami simulations (coordinates are lat.-long.): (. . . .) track of Jason 1 satellite; (X) location of yatch Mercator.**

observed in the northern segment (4th segment) had to be included in the source, in order for computations to reproduce some of the observed features of the tsunami (in particular along the satellite altimetry track in Figs. 3 and 4). In our initial analyses, rather than attempting to model slow slip occurring over time scales of more than 1000 s, we simply increased the value of the maximum "slow" slip parameter Δ for the 4th segment. Inclusion of actual slow slip components in the source will be done in future studies.

The coseismic displacement obtained for each tsunami source using the data in Table 1 is depicted in Fig. 10a, with uplift and subsidence contours at a ± 1 meter spacing. We note right away the similarity of our sources with the uplift-subsidence contours inferred from seismic inversion models and plotted in Fig. 7. As expected, our source for the 4th segment shows significant larger uplift/subsidence than in the seismic model, because of the inclusion of slow slip. We note that the four tsunami sources do not merge perfectly with one another, as a result of the division of the source in discrete segments, although this fact disappears from the wave front in model simulations, within a few minutes of tsunami propagation.

We also note that each segment has a different shape of coseismic displacement. These differences arise largely out of the variations in width and dip between each segment, and are intended to mimic sea floor bathymetry. Specifically, segment 1 experiences concentrated local uplift along its steep fault scarp. Segment 2 is similarly steep where uplift occurs, and produces a more prominent subsided region where the elongated basin is located. Segment 3 has broader uplift and milder slopes, as well as concentrated subsidence where an abrupt trench exists in the bathymetry. Segment 4 produces uplift in the vicinity of existing islands, whereas the trench is less prominent in both the subsidence and the bathymetry. Not all

seafloor features match our calculations perfectly, and there is room to improve all of the tsunami source parameters selected at this stage. For example, the location, strike, depth, and rake of all tsunami sources can be modified in future simulations. However, we have reasonable confidence in our current tsunami sources, because they capture major characteristics of the sea floor morphology and, as we will see, the generated tsunami provides reasonable agreement with observed data.

The first tsunami source, from Segment 1, is triggered at the start of the numerical simulation. In this initial analysis, we calculate the delay between the triggering of subsequent tsunami sources from the distance between epicentral locations along the rupture path, assuming an average shear wave speed of 3 km/s. Segment 2 thus ruptures $t_o = 105$ s into the simulation, Segment 3 ruptures 223 s into the simulation, and Segment 4 ruptures 331 s into the simulation. We expect to refine those times further in future computations, based on information acquired and analyzed during the cruise regarding the speed of propagation of the rupture (Fig. 8).

TSUNAMI SIMULATIONS

Construction of model grids

Tsunami simulations for the December 26, 2004 event were performed at the Indian Ocean basin scale on a 2' x 2' grid and, later, at a smaller regional scale, on a finer grid, to study tsunami propagation and impact around the islands of Phuket and Phi Phi.

We simulated the tsunami in the Bay of Bengal (Fig. 9) using ETOPO 2 bathymetry and topography data to construct our numerical simulation grid at the ocean basin scale. Additionally, for the regional grid near Phuket and Ko Phi Phi, we complemented this data with information obtained from local maritime charts (see later for detail). For use in the model, we converted the decimal degree data into a Universal Transverse Mercator (UTM) projection, with arbitrary origin fixed at 90° long. E. We regridded the data using linear interpolation, to produce the uniform grid with 3.4x3.4 km cells, which roughly corresponds to a 2 minute arc grid spacing. In Fig 10a, the topographic contours are plotted every 500 m, while the bathymetric contours are plotted every 1000 m. In order to have results for the tide gages shown in Fig. 1, east of 72° long. E, we located the western boundary of our computational grid at 70° long. E and the southern boundary at 15° lat. S (Fig. 10b).

Methodology

The earthquake tsunami sources for vertical coseismic displacement are simulated in TOPICS based on parameters given in Table 1 for each segment shown in Fig. 9 (see above). The 4 sources are given in Fig. 10a.

We simulate tsunami propagation and inundation with FUNWAVE, a public domain higher-order Boussinesq wave model developed over the last ten years at the University of Delaware (Wei and Kirby, 1995; Wei et al., 1995; Chen et al., 2000; Kennedy et al., 2000). FUNWAVE is a fully nonlinear Boussinesq model retaining information to $O\{(kh)^2\}$ in frequency dispersion and to all orders in nonlinearity a/h, where k denotes the wavenumber scale, a denotes wave amplitude, and h denotes water depth. Wei et al. (1995) showed that the retention of nonlinear effects beyond the usual order in standard weakly nonlinear Boussinesq models is crucial to the correct modeling of shoaling solitary wave crests, and thus in the present

case is important in the modeling of shoreline inundation. The presence of frequency dispersion in the model is important for the case of shorter wave propagation into relatively deep water, and allows for the mechanism of wave crest splitting during wave propagation over shallow bathymetry. Kulikov (2005) conducted a dispersion analysis for the December 26, 2004 tsunami based on the satellite altimetry data shown in Figs 3,4. By analyzing the distribution of waves of various frequency in the tsunami transect captured by the satellite, he showed that there were significant dispersive effects in the wavetrain and concluded that a long wave model including dispersion (such as FUNWAVE) should be used to model this event. FUNWAVE also includes dissipation from breaking waves, and model predictions of shoreline runup have been well tested in the case of wave shoaling and breaking.

We combine TOPICS and FUNWAVE into a single model referred to as Geowave, in which the tsunami sources predicted by TOPICS are transferred as an initial condition into FUNWAVE. Geowave can simulate multiple tsunami sources with different generation mechanisms, occurring at different times. [The application of this methodology to landslide tsunamis can be found, e.g., in Watts et al. (2003).] Additional benefits of a Boussinesq wave propagation model over traditional nonlinear shallow water wave models are that the horizontal velocity profile over depth is no longer constrained to have a constant value, and vertical accelerations (i.e., non-hydrostatic pressures) are no longer neglected. During propagation and inundation, non-uniform velocity profiles over depth are most often encountered when water waves propagate in deep water, when water waves runup onto a shoreline of intermediate slope, or when water waves become significantly nonlinear. Dispersive effects are both necessary and manifested during propagation of deep water waves, during propagation of an undular bore in shallow water, and during propagation of edge waves along the coastline (Liu et al., 1998).

Tsunami simulations at the Indian Ocean basin scale

We perform a numerical simulation of the December 26, 2004, tsunami in the Bay of Bengal by combining the four tsunami sources in Fig. 10a, triggered at appropriate times, as discussed before. We do not perform simulations where we run each tsunami source separately, because the near field impact and far field propagation are almost uniquely defined from one or another of the tsunami sources. Thus, there should be little confusion as to the origin of the water waves in most impacted regions, because of the long rupture length and directional nature of tsunami propagation. In the configuration of Fig. 9 and 10, the model is discretized with 1289 x 1294 cells, with a 5.9 s time step.

The maximum tsunami elevations above sea level simulated for the Indian Ocean are depicted in Figs. 11 through 13. The tsunami radiation patterns in Fig. 11 show some dependence on various features of the sea floor. To the West, tsunami propagation depends on the sediment fan that covers most of the Bay of Bengal. To the East, a much more complex pattern emerges due to interference and interactions of multiple wave fronts propagating to and among various shorelines.

Runup As should be expected from Fig. 6 and what is known about the major destruction caused by this event, large runups can be seen near Banda Aceh in Fig. 12, around the Andaman islands in Fig. 13a, and on the eastern side of India and Sri Lanka in Fig. 13b. Large runup values are also observed in Fig. 11, on the West Coast of Phuket, and these are detailed in the regional study below. One should keep in mind, however, that these

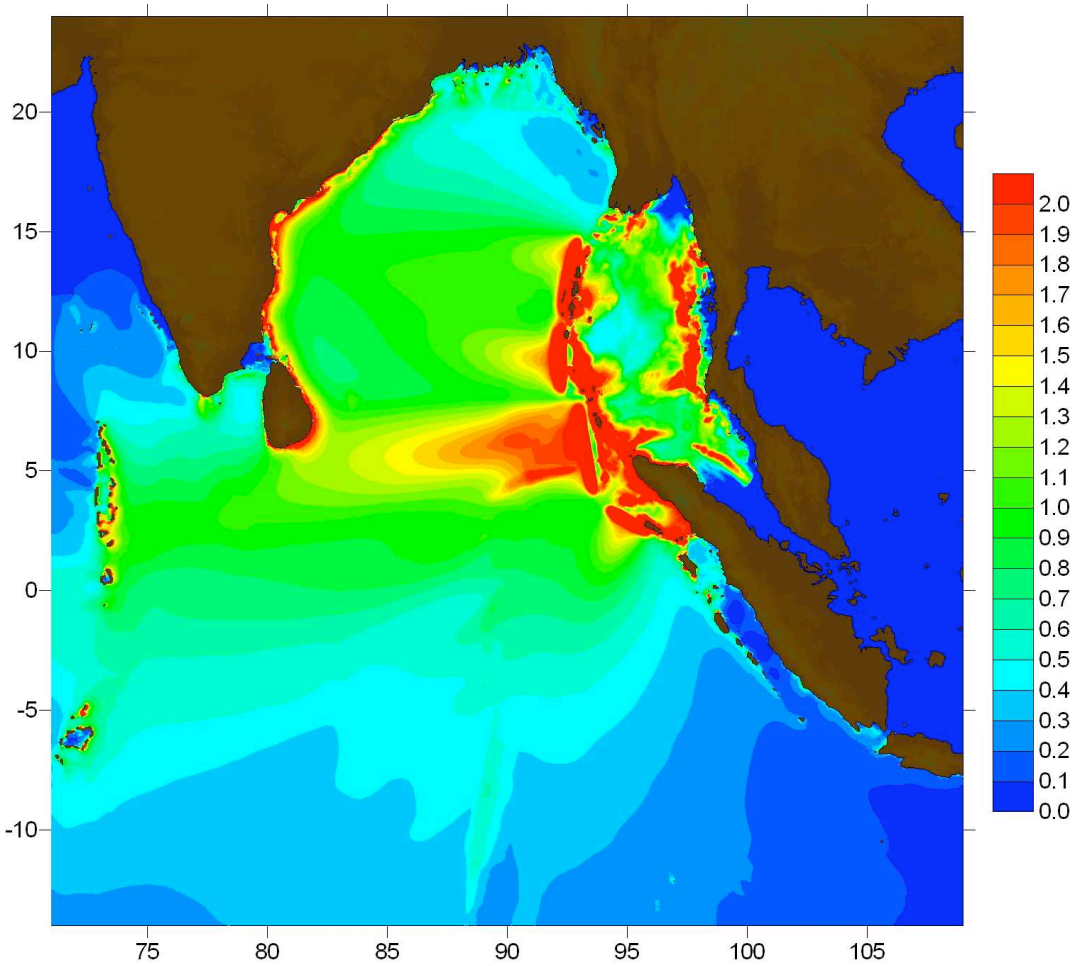

Fig. 11. ***Initial analysis*** **Maximum simulated tsunami amplitudes in Bay of Bengal.**

results are computed on a fairly coarse grid and with little detail of the nearshore bathymetry and coastline topography. Hence, they lack sensitivity to local features of the topography that could further focus tsunami waves and enhance runup. Thus, more work is needed to accurately calculate detailed runup values and distributions in the most impacted areas. In the regional study near Phuket that follows, we use both accurate nearshore data and a finer grid size, and hence we expect that predicted runup values should accordingly be better simulated and, in particular, be more site specific.

In Table 2, we provide maximum runup values for several locations within the simulation domain of Fig. 9. The simulated maximum elevations in Figs. 11-13 and the runup values listed in Table 2 compare favorably with observations available from a variety of sources (Gusiakov 2005; Harada 2005; Yalciner et al. 2005; see Fig. 6).

Satellite track In Fig. 14, we compare model results along the satellite track shown in Fig. 10b with processed satellite data from Fig. 4b. Each dot in Fig. 10b in fact represents a numerical gage whose time series is simulated in the model. The actual motion of the satellite over time given in Gower (2005) is then used to select the relevant data for each numerical gage along the track. Although there is a small space shift, we see that the crest to trough difference (i.e., the wave height) of the initial front and following depression in

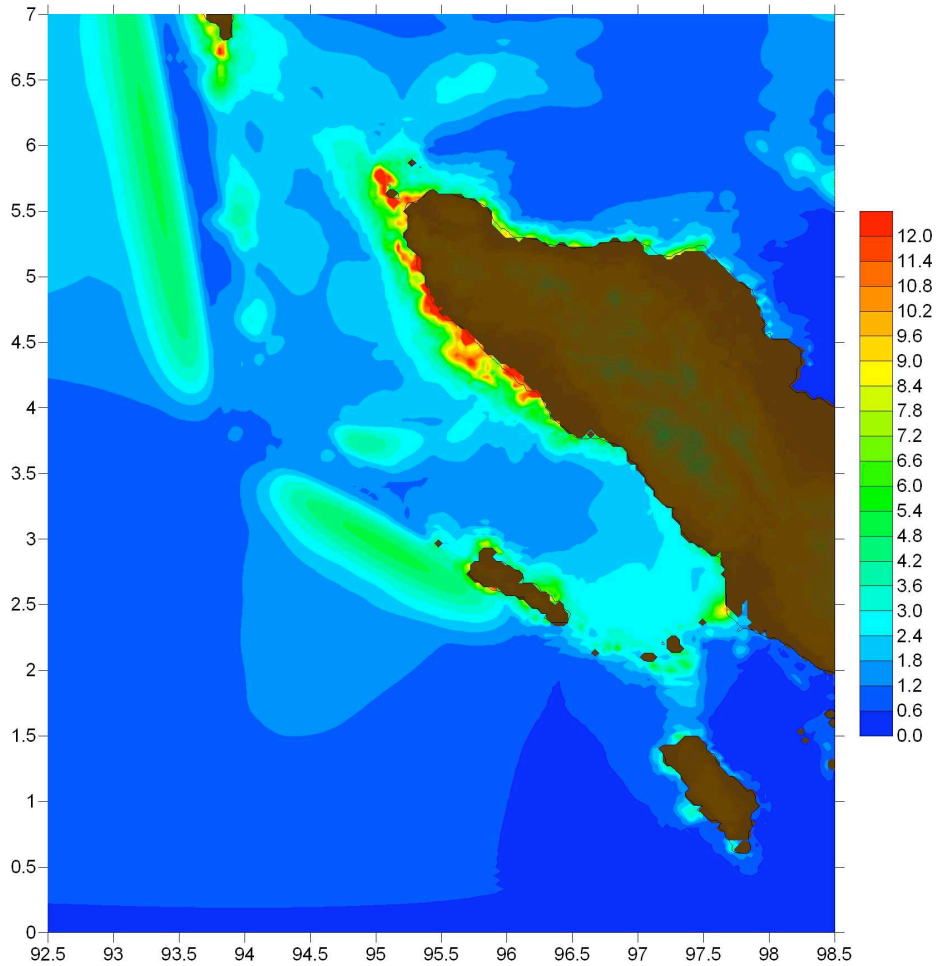

Fig. 12. ***Initial analysis*** **Details of maximum simulated tsunami amplitudes near northern Sumatra (Banda Aceh).**

the tsunami, around 3-5 deg. lat. S, is well predicted at about 1.25 m. This is encouraging, considering the uncertainties in the location of the MWL in the satellite data. The second crest predicted in Fig. 14 does not seem to occur in the data (although some crest splitting is also seen in the satellite data), but the rest of the wave train, from 0-18 deg. lat. N. is quite well reproduced in the model.

Tide gages Table 3 lists 6 tide gage locations (4th-9th lines) where time series of surface elevations were measured during the event. In addition, we list Mercator, a Belgian Yatch that was anchored 1 mile off Nai Harn Bay (South-West of Phuket; www.knmi.nl/onderzk/seismo/seismoreindex.html; Fig. 2b), in about 12m of water at the time of the event and had its depth echo-sounder on. We finally list Patong beach and Ko Phi Phi, where we calculated time series of surface elevation in the model and where arrival times were known from eyewitnesses, since these are important locations in the regional study that follows.

Fig. 15 shows both measured and computed time series in our initial model grid for Mercator and the 6 tide gages. The actual data points are marked by circles and we see that the time resolution varies between time gages, from 1' up to 8'. In the latter case, this introduces a significant filtering of the tsunami signal. Note in Fig. 15d that the tide gage

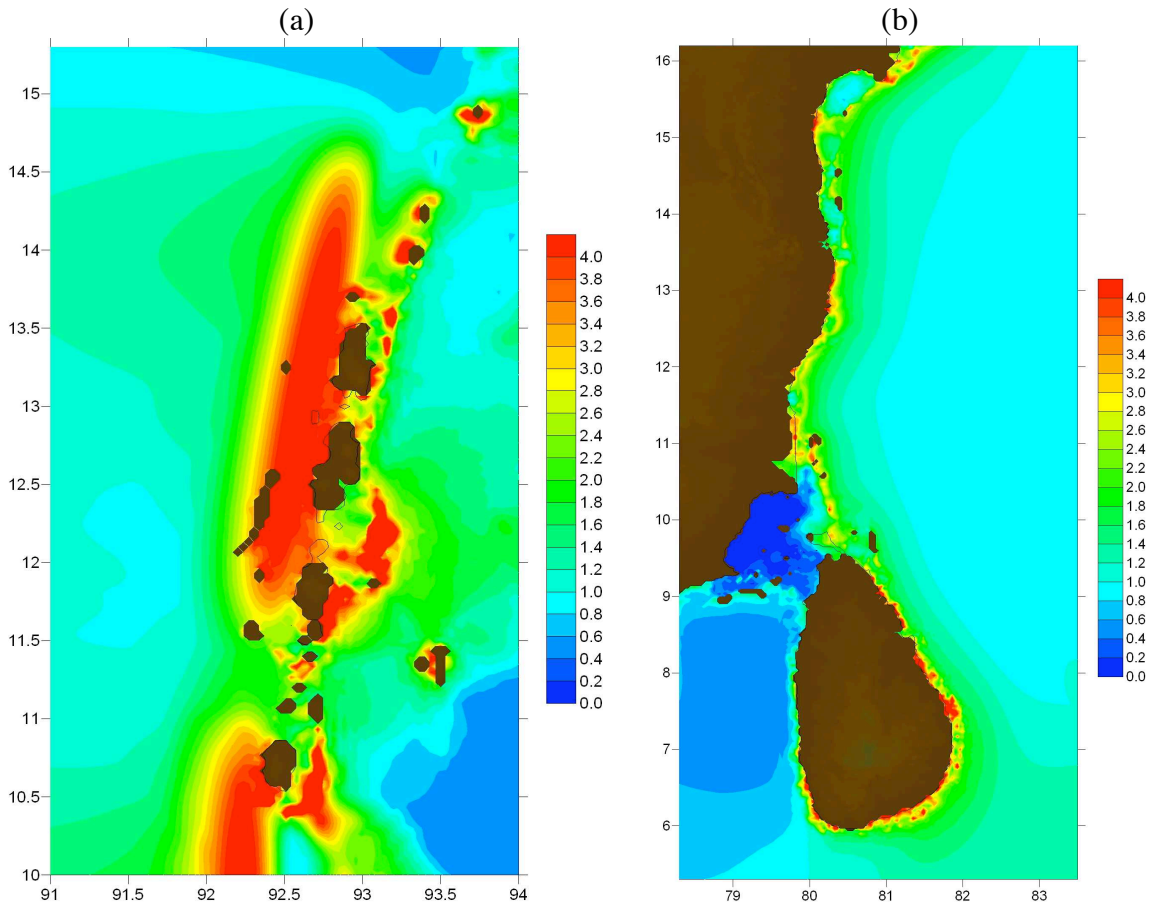

Fig. 13. ***Initial analysis*** **Details of maximum simulated tsunami amplitudes near : (a) Andaman islands; (b) Sri Lanka and southeast India (Madras area).**

Locations	Model runup	Model (long. E, lat. N)	Field runup
Northern tip, Aceh, Indonesia	11.8 m	(95.248,5.573)	20-28 m
Upper NW, Aceh, Indonesia	10.9 m	(95.284,5.559)	12.2 m
Upper NW, Aceh, Indonesia	10.2 m	(95.307,5.567)	9.8-10.3 m
Upper NW, Aceh, Indonesia	10.2 m	(95.323,5.570)	10-11 m
Upper NW Aceh, Indonesia	23.6 m	(95.341,5.067)	5-35 m
Colombo, Sri Lanka	1.9 m	(79.883,6.812)	2.1 m (t. gage)
Galle, Sri Lanka	2.4 m	(80.475,5.974)	2-3 m
SE coast, Sri Lanka	5.5 m	(81.816,7.427)	5-10 m
Chennai, India	3.2 m	(80.285,13.552)	2.9 m
Nagappaattinam, India	2.4 m	(79.740,10.865)	2-3.5 m
Port Blair, India	5.6 m	(92.000,11.702)	5.0 m
Rangoon, Burma	1.3 m	(96.966,17.309)	NA
Kamala Bch., Phuket, Thailand	4.9 m	(98.275,7.973)	4.5-5.3 m
Patong Bch., Phuket, Thailand	4.1 m	(98.276,7.900)	4.8-5.5 m
Ko Phi Phi, Thailand	2.8 m	(98.777,7.739)	4.6-5.8 m

Table 2. ***Initial analysis*** **Simulation results at the shore and runup from field surveys (Gusiakov 2005; Harada 2005; Yalciner et al. 2005; Fig. 6) at a few key locations.**

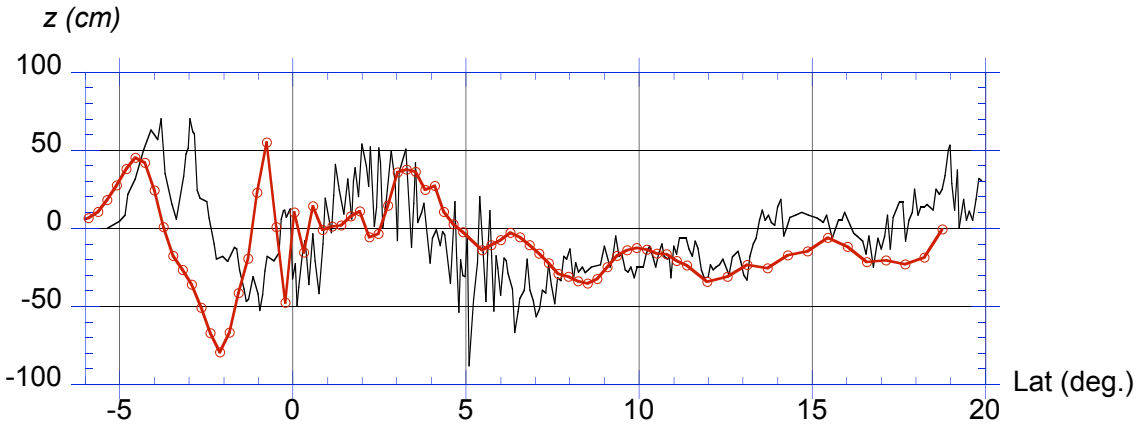

Fig. 14. ***Initial analysis*** **Comparison of tsunami measured with satellite altimetry by Jason 1 (Fig. 3) (——) and results of initial model analysis with a 2' grid (—○—).**

Locations	Coord. (Lat., Long.)	Model arrival time	Data arrival time	Depth h_1 (m)	K_s
Mercator, Phuket	(7.760,98.298)	1h45'	1h48'	12	1.25
Patong Bch., Thailand	(7.900,98.276)	1h49'	1h51'	9.4	1.20
Ko Phi Phi, Thailand	(7.739,98.777)	2h41'	2h45'	2.8	1.00
Cocos Island	(-12.117,96.88)	2h12'	2h27	5	4.64
Diego Garcia	(-7.233,72.433)	3h44'	3h54'	5	2.19
Columbo, Sri Lanka	(6.983, 79.850)	2h50'	2h59'	5	4.53
Gan, Maldive	(-0.683,73.150)	3h24'	3h32'	5	2.13
Male, Maldive	(4.183,73.517)	3h18'	3h25'	5	3.20
Hanimaadhoo, Maldives	(6.767,73.167)	3h33'	3h40'	5	1.00

Table 3. ***Initial analysis*** **Comparison of simulation and data at tide gages (4th-9th lines) (Fig. 1). Mercator is a Belgian yatch that was anchored 1 mile off Nai Harn Bay (South-West of Phuket) during the event. Patong and Phi Phi are two points of interest where arrival time is known. Arrival times list the time of the maximum of the first depression or elevation wave, whichever comes first. Depth is estimated at 5 m for all the tide gage.** K_s **is theoretical shoaling coefficient from last model grid point to the tide gage.**

seems to have failed in Columbo right after the arrival of the first tsunami crest. The location and depth of each gage is given in the table as well as computed and observed arrival times of the tsunami, corresponding to the time of the maximum of the first depression or elevation wave, whichever comes first.

Due to the coarse 3.4km grid size used in the model, the depth h_o of the boundary grid cell where the tide gage is located does not typically match the actual tide gage depth h_1 and, in general, is quite a bit larger. This means that part of the slowing-down effects of the tsunami, proportional to $\sqrt{gh}$ (where g is gravity and h is depth) in shallow water are not correctly modeled. This can be somewhat corrected by assuming a plane slope between the

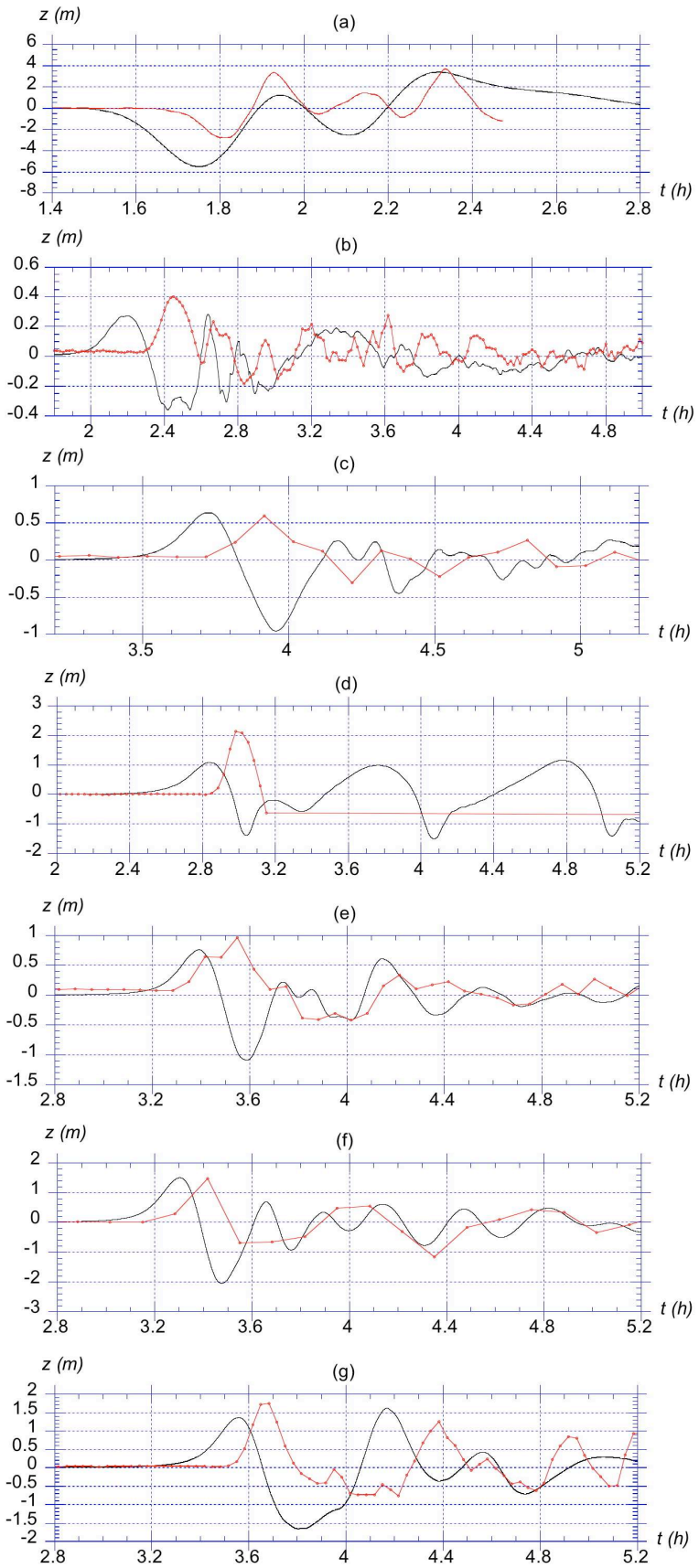

Fig. 15. ***Initial analysis*** **Comparison of numerical (——) and (—o—) tide gage data for (Fig. 1; Table 3): (a) mercator yatch; (b) Cocos; (c) Diego Garcia; (d) Columbo; (e) Gan; (f) Male; (g) Hanimaadhoo.**

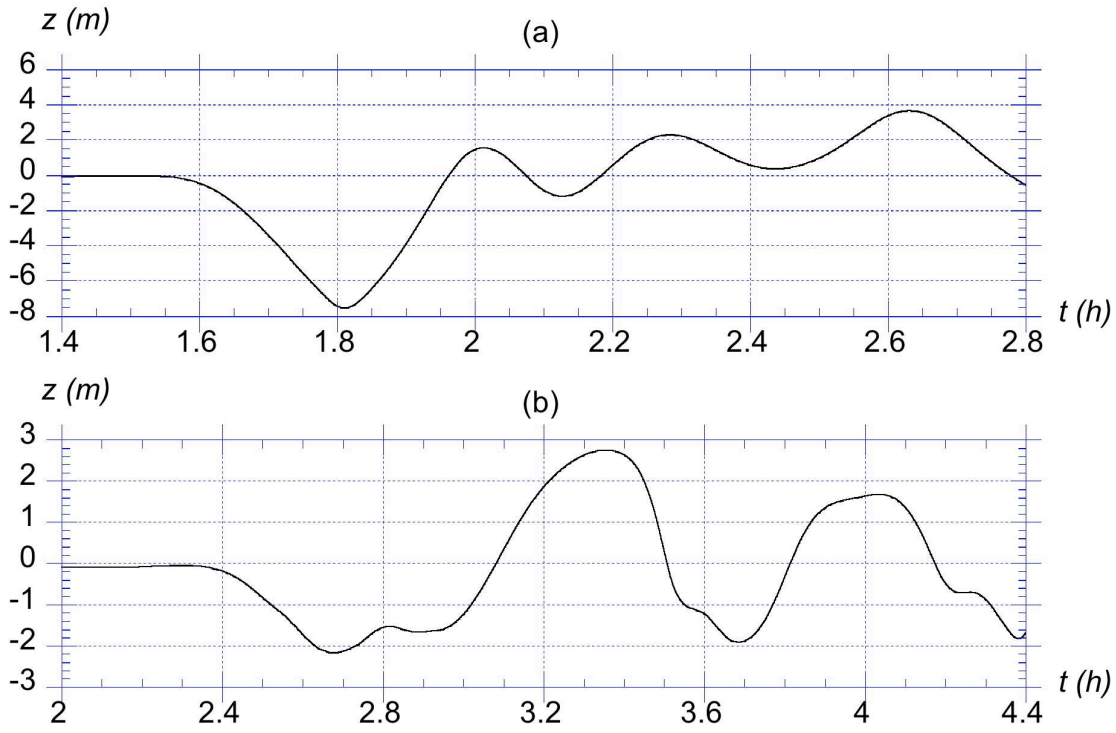

Fig. 16. ***Initial analysis*** **Numerical results (——) for (Table 3): (a) Patong Beach; (b) Ko Phi Phi.**

last grid cell and the location of the tide gage and calculating the time lag this creates as,

$$\Delta t = \frac{2\Delta x_o}{\sqrt{g}} \left(\frac{\sqrt{h_o} - \sqrt{h_1}}{h_o - h_1} \right)$$

where Δx_o is the distance between the grid cell center and the tide gage. Corrections Δt were computed for each gage in Table 3 (varied from 0 to 114 s) and model results were shifted in time by this amount. Due to the reduction in depth, tsunami amplitude shoaling is also expected from the last computed depth in the model to the tide gage. Although no such correction has been applied in Fig. 15, as an indication of shoaling effects, we give in Table 3 the value of the shoaling coefficient $K_s = \sqrt{h_o/h_1}$ computed with Green's law, based on the assumed depth $h_1 = 5$ m listed in the table for the tide gages, for lack of better information at this stage. Such shoaling effects, not included in the model because of grid coarseness, would increase the height of the tsunami before it reaches the breaking point (in about 0.8 times the local depth) and might have affected values at the tide gages.

In Fig. 15a, we see that the yatch Mercator experienced an initial depression wave, followed by three waves of elevation, with a maximum trough-to-peak height of 5.6 m. The depression wave in the model arrives 1h45' after the earthquake, about 3' before that measured by the yatch, and times for the first and third elevation waves are also in good agreement. The first elevation waves is too small and the second elevation wave is not reproduced in the model. The height of the third elevation wave is well predicted. Trough to peak heights of each wave are in good agreement.

Figs. 15b-g show results at the 6 tide gages. Arrival times for the gages in the model are 7'-15' ahead of those measured at the gages (Table 3), with an average of 9.3'. Many of

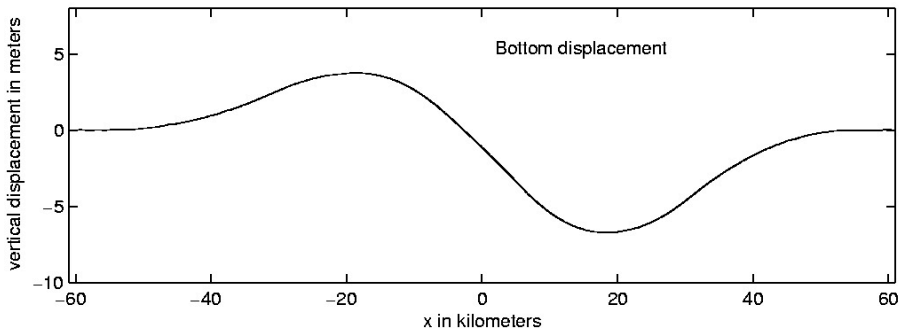

Fig. 17. ***Fast vs. Slow slip*** **1D-analytical long wave model: Typical shape of specified bottom deformation.**

the gages, however are located in shallow and protected areas and, as discussed above, one might expect the tsunami to shoal up further and slow down somewhat more than predicted by Δt before it reaches these tide gages. Regarding wave elevations, the model shows good agreement with observations for the last three gages (e-g), which correspond to a fairly direct path, orthogonal to the tsunami source axes (Fig. 10). Except for the larger time lag, the model results in Cocos are also in good agreement with the tide gages. The tide gage in Cocos, however, is located inside a lagoon in shallow water and part of this larger time lag can be explained by slowing-down effects poorly represented in the model. Also, one would expect more shoaling of the tsunami than modeled.

Fig. 16 shows the time series computed in the model for Patong Beach and Ko Phi Phi. Although no data was available, runups (Table 2) and arrival times were known. Also, the arrival of a leading depression wave followed by a few waves of elevations is well documented, as well as the fact that the largest elevation waves was the 2nd or 3rd one depending on location. These features can be seen in the time series shown in the figure.

As a final remark, all of the tide gage data, both modeled and observed, for gages that are located on the western side of the Bay of Bengal, i.e., on the side of the uplift in the tsunami source show leading waves of elevations whereas the record for the yatch Mercator on the eastern side near Phuket, close to the source area where subsidence occurred, show a leading depression wave. This agrees with all of the eyewitness observations, pictures and movies that show that the ocean retreated on the eastern side, in Thailand, before the tsunami arrived, but did not do so on the western side. This is also consistent with first-order dispersive long wave theory, based on which one can show that a bottom subsidence will create a leading depression wave followed by a tail of oscillations and a bottom uplift will create a series of soliton-like waves of elevations, followed by a tail of smaller oscillations (Hammack, 1973; Hammack and Segur, 1974, 1978).

Discussion of initial results

Based on the above comparison of model results and field data, we believe that our initial numerical simulations at the Indian Ocean basin scale, although still quite preliminary as far as the selection of the source, have captured many of the tsunami features of the actual event.

It is difficult as of now to attribute any differences between observed and simulated runup values to something specific in our numerical simulation. We have noted before that the tsunami sources can be improved and we hope to do so in the near future based on results

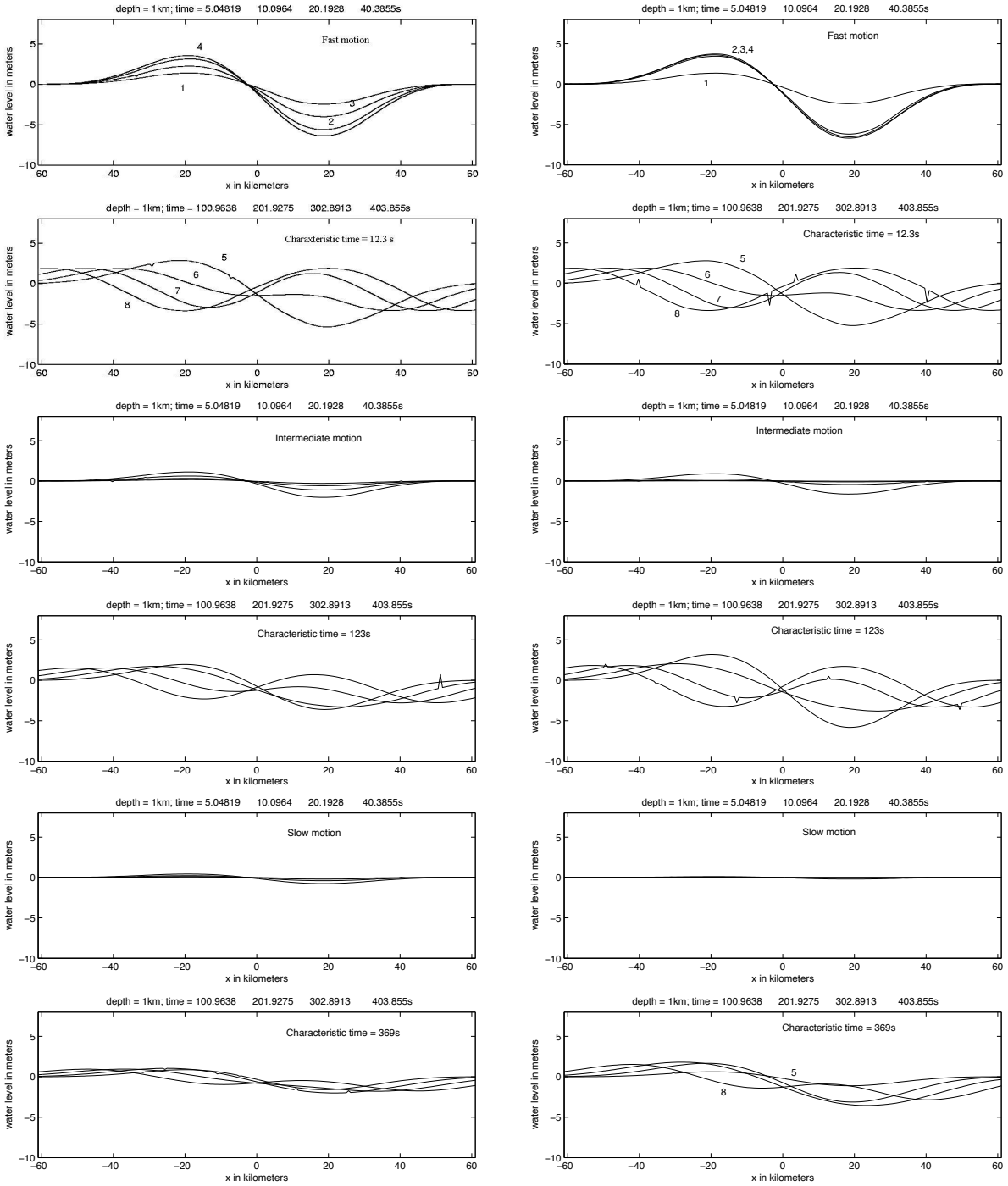

Fig. 18. ***Fast vs. Slow slip*** **1D-analytical long wave model: 6 cases of long wave generation for the bottom deformation of Fig. 17. Left: exponential growth f_1; Right: sine growth f_2.**

obtained during this cruise. Moreover, the simulation grid is still not refined enough near certain coastlines to capture the runup process in detail. This will be improved in the following case study for the area around Phuket (Thailand) and should be also improved in the future for other severely impacted areas such as near Banda Aceh. Likewise, the shallow water bathymetry and coastline details are not available in this work for most of the Bay of Bengal. This information was included in our model during the cruise, only for conducting the following case study around Phuket and preparing data for a second case study to be conducted near Banda Aceh. These are common problems in regional simulations of tsunamis, and therefore suggest a quantum leap in simulation techniques, including unstructured grids. Regardless, the Boussinesq model does a good job of reproducing wave action despite these shortcomings. We are therefore motivated to perform a more detailed study of this event based on our successes to date, using more accurate and detailed field data, as it becomes available.

Effect of fast slip versus slow slip Ammon et al. (2005) indicated that a significant slow slip component may have occurred in the Northern 400-500 km of the rupture zone, on a time scale beyond the seismic band. Here, this effect was included in the simulations by increasing slip in the 4th segment of the tsunami source (Table 1). To estimate the tsunamigenic potential of slow versus fast slip ruptures, following Hammack (1973) who studied waves generated by step motions on the bottom, we developed an analytical one-dimensional linear long wave model and simulated the generation of surface waves due to a bottom deformation having a double Gaussian shape, with specified maximum uplift and subsidence (Fig. 17). We specified this deformation to grow from 0 to its maximum value as a function of time, following either an exponential function $f_1(t) = (1 - \exp -\alpha\, t)$ or a sine function $f_2(t) = \frac{1}{2}(1 - \cos \pi\, t/T)\, H(T - t) + H(t - T)$, where H denotes the Heaviside function. We then selected fast, intermediate and slow deformation characteristic times, defined as $t_c = 1.11/\alpha$ or T, for each type of function, respectively. This yields 6 different cases shown in Fig. 18. For these computations, we used a depth $h_o = 1$ km. Maximum uplift was 3.74 m and subsidence -6.73 m.

This analysis shows, first, that for each type of time function, fast and intermediate slip motions create significantly larger tsunamis than slow slip motion. Second, for intermediate and slow motion cases, function f_2 creates slightly larger tsunamis than function f_1. Finally, despite its less efficient tsunami generation, slow slip nevertheless creates sizeable tsunamis, for long times.

Effects of sphericity A spherical Boussinesq model was developed, based on the same type of equations as used in FUNWAVE (Kirby et al., 2004), and implemented in a curvilinear coordinate system allowing the definition of boundary fitted grids with variable mesh size. In addition to spherical corrections, this new model includes effects of the Coriolis force (f parameter modeling). We are planning to use this model next for the basin scale simulations of the 12/26/04 event, to provide better long range modeling of the tsunami. We believe spherical effects could help explain some of the differences in arrival time observed at time gages since our simulated tsunami arrives too early at all of the western tide gages and it takes a longer time to travel along an arc than a chord or a tangent to a great circle. Also using a boundary fitted non-uniform grid will allow for a more accurate and better resolved discretization of coastal areas in the model, without unnecessarily increasing the mesh size in deeper water regions and correlatively the model computational time.

KO PHI PHI CASE STUDY

Overview

Although larger casualties and more destruction in absolute terms occurred, as a result of the 12/26/04 tsunami, in other areas of the Sea of Bengal, particularly near Banda Aceh (Indonesia), we selected the island of Ko Phi Phi to conduct a tsunami modeling case study, first, because the relative impact of the tsunami in terms of both casualties and destruction of buildings, as compared to the situation before the tsunami hit, was well above 50%. Second, the well documented arrival and impact of the tsunami and the unusually complex local bathymetry and topography, make modeling the event at Phi Phi quite a challenge, from which we may learn valuable lessons regarding tsunami impact on island communities in general.

The island of Ko Phi Phi (also known as Phi Phi Don) is located at 7 deg. 45' lat. N and 98 deg. 47' long. E, approximately 50 km East of the southern tip of the island of Phuket (Fig. 19a). The island has a butterfly shape with two high ground areas, on the eastern and western sides (with a maximum elevation of 185 m), connected by a narrow strip of sand, about 1.2 km long and 200-300 m wide, running west-east (Figs. 19a and 20a). Prior to the tsunami event, due to the topography of the island, most of the population and tourism infrastructures (hotels, resorts, guest houses, restaurant, shops,...) were located on the sand strip, which was densely built. Both supplies and visitors are transported to Ko Phi Phi by a ferry, which regularly sails from Phuket and docks in a small harbor on the southern side of the sand strip.

Ko Phi Phi typically had a population of 2-3,000 people, during peak holiday periods, half of these being tourists. On the morning of 12/26/04, because this was Sunday and weekly rentals expired, many tourists had already left the island on an earlier ferry, whereas tourists coming for a weekly New Year vacation had not yet arrived. Many tourists, however were still packing in hotels and, particularly, in the large resort located on the western side of the sand strip, facing north (large buildings above the center of Fig. 20b).

Tsunami mechanism from visual evidence

Two sequences of still pictures (Figs. 21, 22 and 23) are discussed in the following, that show both the arrival and initial impact of the tsunami on Ko Phi Phi, from about 10h45' (GMT + 7h) local time, i.e., about 2h46' after the earthquake started. Based on direct reports from eyewitnesses, people were largely unaware there had been an earthquake. A few inhabitants we interviewed reported having felt some vibrations but none had any clue a tsunami was coming. Most people on the island were having their normal activities, which took place mostly on the sand strip. Hence, the tsunami toll on the island was particularly heavy in proportion of the population, with 1,200 to 1,500 report dead or missing after the tsunami hit. As can be seen on Fig. 20b, destruction was almost total in the middle part of the sand strip and on the western side, except for the solidly built resort above the ground floor. On the north side of the middle part area of the sand strip, in particular, we were told that there were about 300 well built wood cottages. None of these are left standing, not even their foundation.

Pictures from the hilltop The first set of pictures was taken by Das Ehepaar J.T. and Caroline Malatesta, looking down and westward, likely from the highest point (viewpoint) on the

(a)

(b)

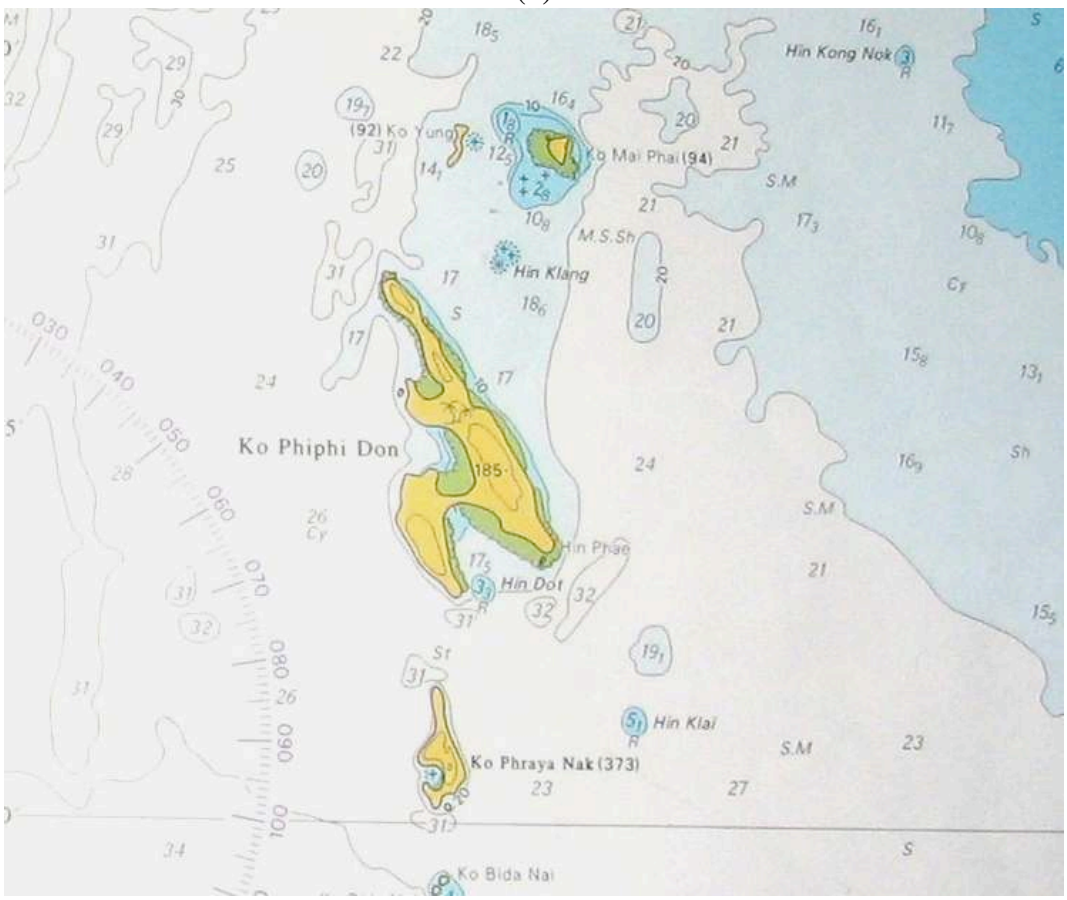

Fig. 19. ***Ko Phi Phi case study*** **Maritime charts of Thailand West Coast (Mu Ko Similan to Ko Lanta Yai), at 1:200,000 scale, at lat 4 deg. (North is up): (a) Overall area of Phuket and Ko Phi Phi; (b) Close up of Ko Phi Phi.**

(a)

(b)

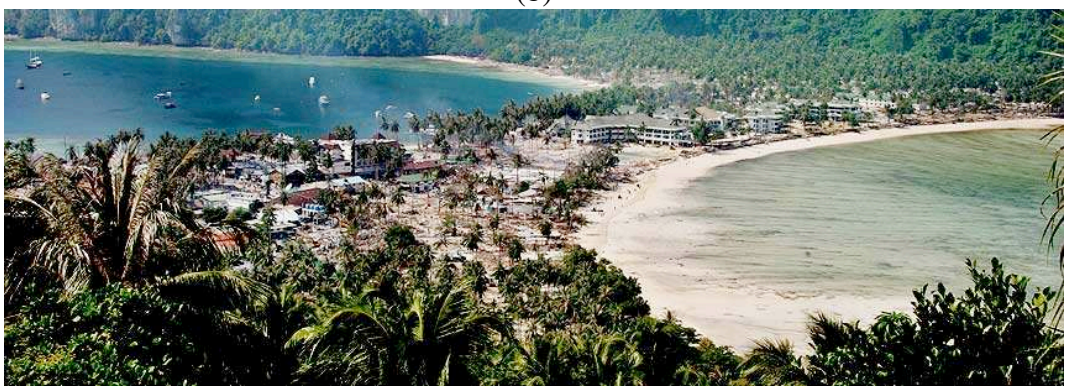

Fig. 20. ***Ko Phi Phi case study*** **Undated pictures of Ko Phi Phi looking west: (a) before the tsunami event; (b) Destruction in the sand strip area after the tsunami hit.**

eastern side of the island (marked by 185 on the map in Fig. 19). They had left for a hike earlier in the morning and first observed unusual wave activity in the northern bay of the island [A full account of their fateful morning can be found at http://www.magazine.wlu.edu/web/page/print/386.html] :

- "…Caroline pointed out to me that the water was changing color and withdrawing to the sea.", "…we noticed that the bay started receding, almost like a bathtub being drained. At first we thought it was low tide and were fascinated at how quickly the tide went out. But then it kept on going and going until the sea floor and coral reefs were exposed." "We were amazed that we could see rocks and coral reef exposed nearly 100 yards from the shore.", "We knew that low tide had generally been around noon so we found it odd that the water level was going down so early in the day…". They were apparently witnessing the arrival of a depression wave in the northern bay of the island (Fig. 21a).
- "About five minutes later, we saw a wave the length of the bay coming towards the

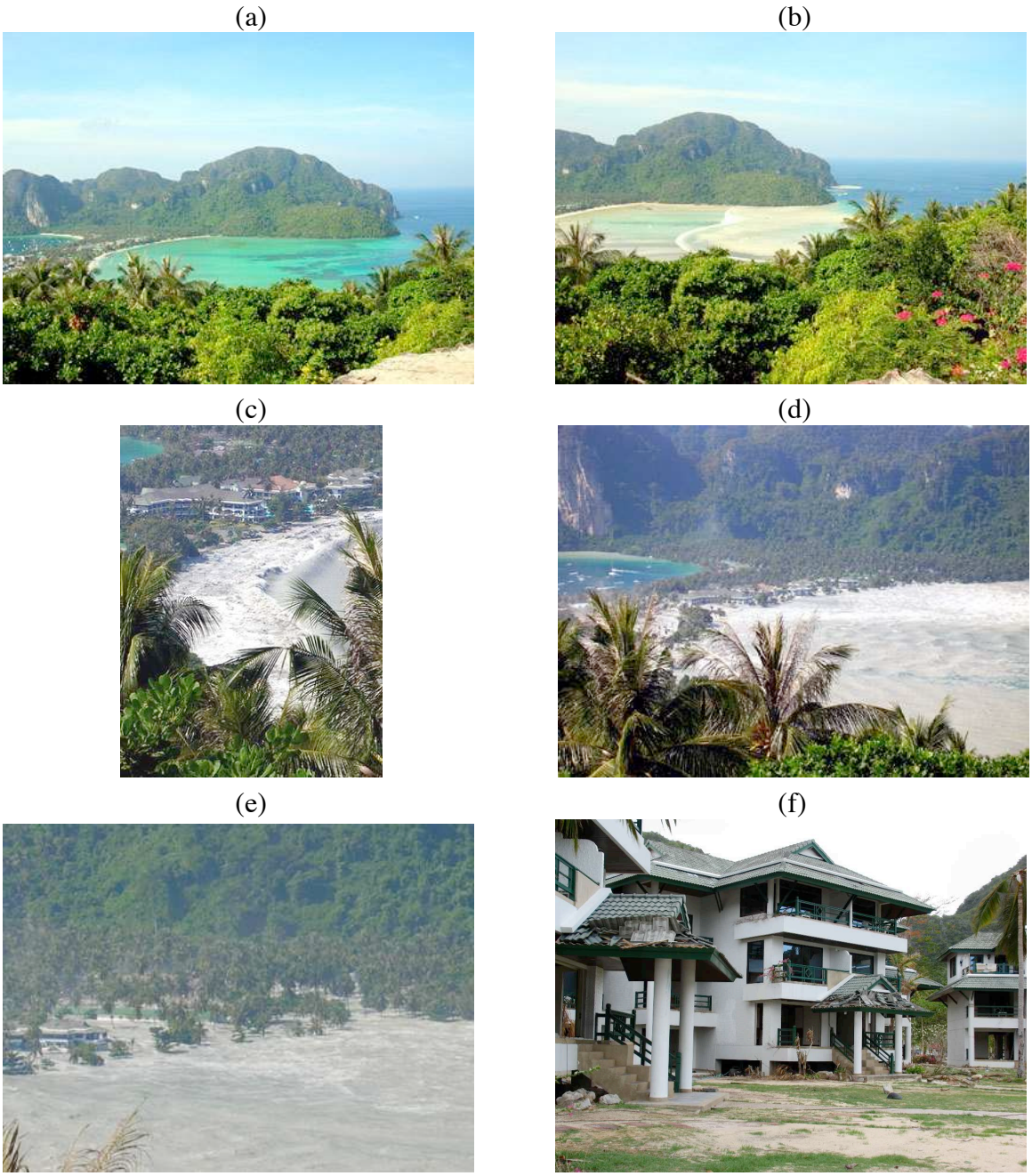

Fig. 21. ***Ko Phi Phi case study*** **Arrival of 12/26/04 tsunami on Ko Phi Phi, at approximately 10h45' local time (GMT + 7h) on the North shore. [Pictures a-e taken by Das Ehepaar J.T. and Caroline Malatesta]: (a) Arrival of depression wave on the North shore; (b) Arrival of large elevation wave on the North shore; (c) Elevation wave runup on North-East beach; (d) Elevation wave reflects off North-East beach and moves westward as an edge wave. (e) Maximum runup on North-West beach. (f) Telltale of maximum runup on 5/9/05.**

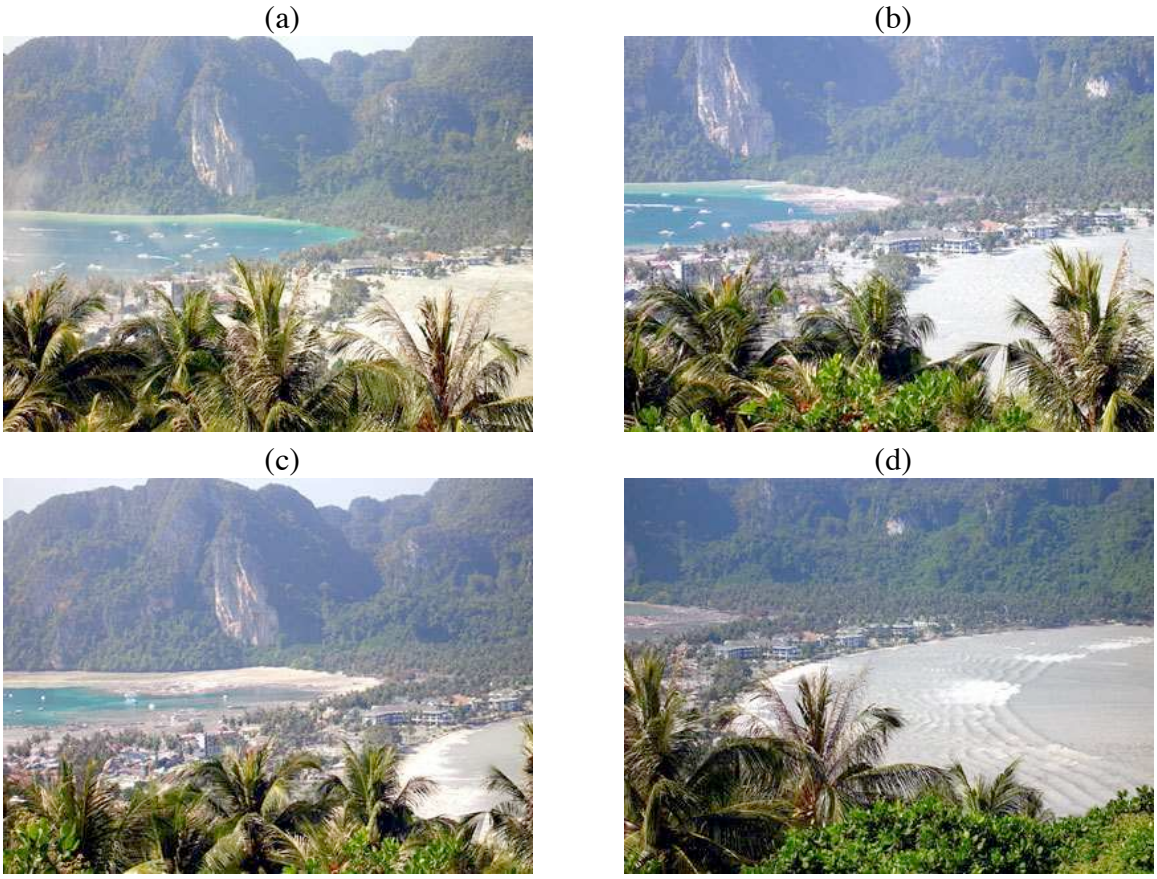

Fig. 22. ***Ko Phi Phi case study*** **Continued from Fig. 21: (a) West of North beach is flooded by large elevation wave up to second floor of buildings, arrival of tsunami at South beach harbor; (b) Flood caused by elevation wave flows through island narrow sand strip, North-South into harbor, carrying debris; (c) Accumulation of debris in the harbor; (d) Undular bore moving northward on North shore.**

shore." "We realized that it was big when we saw it pick up a speedboat as if it were a feather and just carry it all the way inland." This was the arrival of the first large elevation wave in the tsunami wavetrain (Fig. 21b,c).

- "The water crashed into the shore and completely flooded the island. Palm trees were falling and people were screaming." This was the wave impacting the northeast side of the bay, reflecting as an edge wave, and heavily flooding the northwest side of the sand strip (Fig. 21c,d,e).

Looking more closely at these pictures, we clearly see in Fig. 21a and b, to the left, many rocks and shallows being exposed then, in Fig. 21b, a wave as wide as the northern bay propagating as a breaking bore in a general southeast direction. In Fig. 21c, this wave both floods and reflects off the eastern side, then causes maximum runup on the western side (Figs. 21d,e). The "Belgian waffle" wave pattern seen in the lower part of Fig. 21d is indicative of two intersecting (incident and reflected) wave trains. In Fig. 21d,e, the tsunami floods the middle part of the sand strip and the resort area on its western side, and behind it, up to the second floor level.

More pictures were taken after the arrival of the largest tsunami wave in the northern Bay. Figs. 22a,b show the beginning of the arrival of a tsunami wave in the southern bay (light green color in the water on the western shore). These pictures also show how the flood water accumulated on the north shore starts flowing over the sand strip into the southern bay, carrying a lot of debris (brown water). In Fig. 22a we clearly see that both the middle part and western side of the sand strip were completed flooded. Destruction was almost complete in the middle and eastern part of the sand strip (Figs. 24a-c and 25) In Fig. 22b,c, we see that the larger hydraulic head on the northern shore creates a strong debris flow into the southern bay, starting from the western side and moving down to the middle of the sandstrip. Damage surveys confirm these observations; in Fig. 24c, upper parts of cottages from the northern shore are piled up on the southern shore; in Fig. 24d, a large amount of debris can be seen covering the harbor in the southern bay. The arrival of tsunami waves from the south and the simultaneous flow North-South through the sand strip of water accumulated on the north shore by the initial tsunami were both confirmed by eyewitnesses reports taken during our visit of Phi Phi. In fact, many small boats and people were transported from the northern bay to the southern bay. The tsunami that occurred in the southern bay and caused additional destruction by moving eastward, likely as an edge wave, along the south beach is not documented in the sequence of pictures. Except perhaps in Fig. 22d, which shows an undular bore apparently moving out of the northern bay. This bore could be due to the combination of depression wave arriving in the northern bay and a wave of elevation providing an additional hydraulic head on the southern shore.

Pictures from the Gaultine III yatch This sequence of pictures was taken from a yatch anchored near the east side of the northern bay, about 1 km from shore (Fig. 23). The sequence covers 5 min. from the time the water reached a minimum due to the initial depression wave and, hence, covers the arrival of the largest wave of elevation previously seen in Figs. 21b-d. The sequence is consistent with our earlier discussion but provides an interesting viewpoint, horizontally from about 3.3 m above sea level on the deck of the Gaultine III. A full account of these observations can be found at http://www.yachtaragorn.com/Thailand.htm.

- In Fig. 23a "...GAULTINE III and ARAGORN are spun in a counterclockwise eddy of the ebb coming off the beach...". Taken also during the first minute, Fig. 23b shows the scene facing south, to the right of Fig. 23a, with the beginning of the sand strip to the right of this picture. In both figures, one clearly see the reefs is emerged and many rocks are showing.
- Figs. 23c-g follow each other along the eastern side. Figs. 23c-f, taken during the third minute show a large breaking wave (bore whose backside we see) moving in a southeast direction, reflecting off the shore and starting to break backwards. The wave appears to be 4-5 m high in the last two pictures: "By this time, the wave must be 15 feet tall behind the cat...". In Fig. 23f, we see the leaning mast of one of the boats caught between the wave and the eastern shore.
- In 23g, taken in the fourth minute, we see the same boat as in Fig. 23f, behind the catamaran, leaning the other way. Behind, the main wave gets taller and clearly moves to the right. This is the beginning of the edge wave seen in Figs. 21c,d. In Fig. 23h, to the right of 23g, we are looking directly south at the sand strip (the cell phone tower to the east of the sand strip is visible on the left of the picture) and we see a large wave is directly about to impact the beach: "...the wave is higher than the

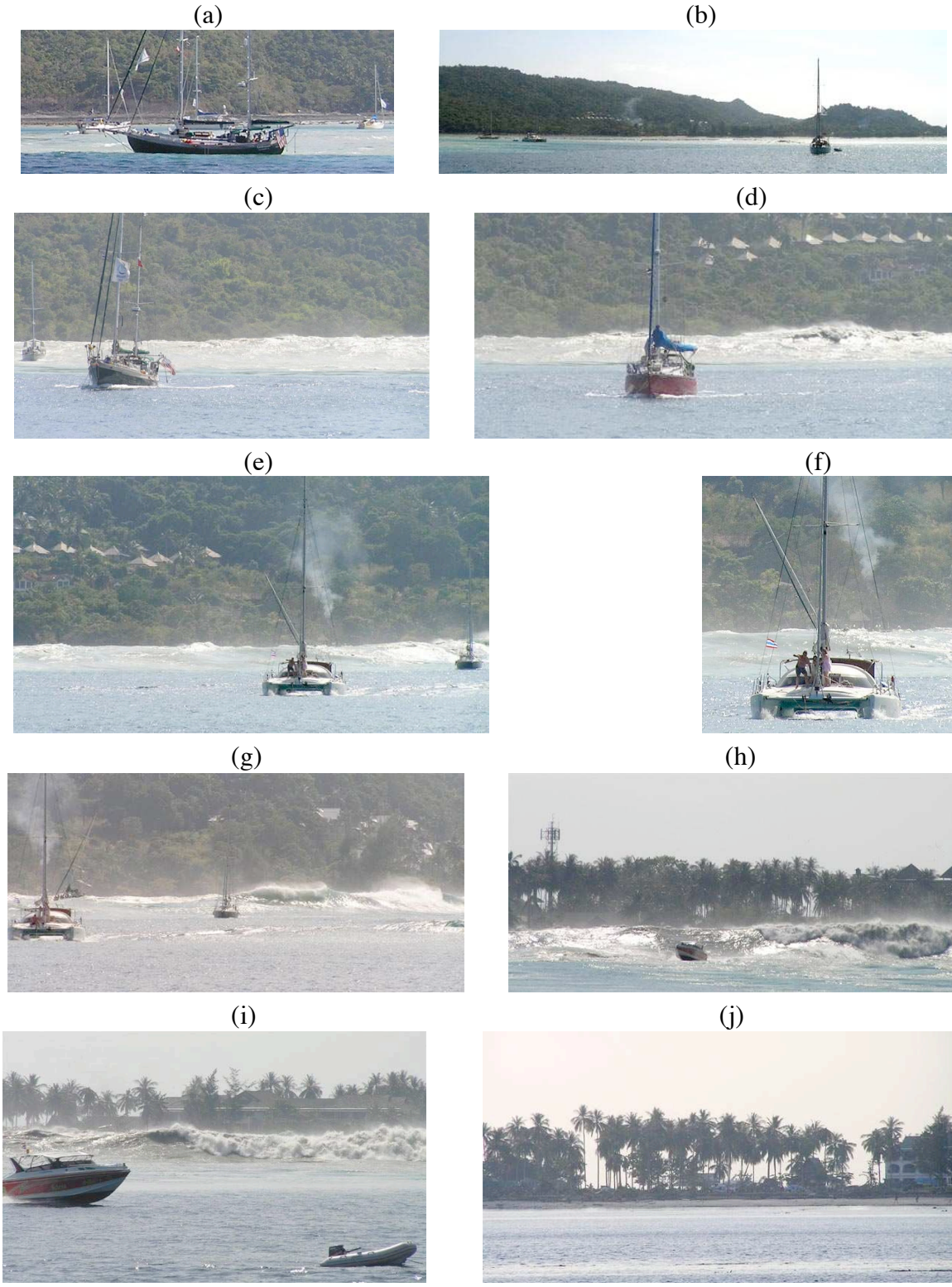

Fig. 23. ***Ko Phi Phi case study*** **Pictures taken on North shore on 12/26/04, starting soon after 10h45' local time, from yatch Gaultine III (Lou Evans), and covering 5 min. from (a) to (i): (a)(b) Facing East, depression wave arrives and exposes reef; (c)(d)(e) Main wave moves south-east and reflects off the eastern cliff; (f) closeup of (e); (g) reflected wave moves down the shore and breaks; (h) Breaking edge wave is moving westward down the sand spit; (i) wave attacks resort on west side; (j) the morning after.**

spit of land, as only first-story roofs are visible behind the wave. The motorboat in the foreground was able to escape…". Numerous roofs of one story buildings, likely the north shore cottages mentioned before, are barely visible above the wave. This stage approximately corresponds to Fig. 21c.

- Fig. 23i was taken during the fifth minute and "…shows the wave crest at its highest, covering your view of the second story windows in the hotel (resort) in back. The speedboat is getting out of there, and you can see by the lack of a wake on the dink that the water is about to turn to ebb again." This stage approximately corresponds to just before the stage of Fig. 21d.
- Fig. 23j, taken the morning after, looks south to the east of the resort. One can see the elevation of the sand strip above MWL.

Runup data

Fig. 21f was taken during our own survey of Phi Phi and we see how high the water reached, i.e., at mid-height of the little roofs covering the entrance porches; the tip of one of these roofs emerging from the water can be seen on the left of Fig. 21e. Although we did not have accurate measuring equipment, we estimated the mid-point of these roofs to be at 5.5-6 m above see level. In Fig. 21e, we see runup might even have been larger behind the resort, due to the presence of the hill.

A Japanese survey team (Harada, 2005) in fact reported two maximum runup measurements on the northern shore of the sand strip of Phi Phi. One measurement of 5.32 m, 62 m from shore at the westward extremity, referred to as "second floor of hotel", is consistent with our own observation at the resort hotel (Fig. 21f). The other measurement of 6.89 m, 242 m from shore at the eastward extremity is a trace on a house wall in town, in the area first hit by the largest elevation wave (lower part of Fig 21c). The survey team suggests to correct these raw measurements by subtracting the tide levels in Phuket, which was maximum at 10 am local time on 12/26/04, at around 0.75-0.8 m above MWL.

Tsunami modeling

The area modeled in the regional grid we defined for this study is shown in Fig. 26. The grid extends from 90° to 100° long. E and from 2° to 15° lat. N. The tsunami sources used are identical to those previously used for the basin scale model, whose parameters are listed in Table 1.

Grid definition For the simulation, to both increase the mesh resolution and save on the number of grid cells, we initially tried to use a 500m x 500m cell, and to only include the part of the source most directly affecting Phuket (segments 2 and 3), from 4.8° to 10° lat. N. This, however, led to problems in the model boundary conditions near the source borders, likely due to instabilities in the sponge layer areas aimed at absorbing outgoing waves. Pending the resolution of these numerical problems, we elected to use the wider grid shown in Fig. 26, with a slightly larger 910m x 910m mesh size (or about 1/2'). This grids includes all the source segments and has a total of 1214 x 1560 cells and uses a 5 s time step. This fairly large time step, assuming a Courant number of 0.5, corresponds to the speed of propagation of the tsunami in a shallower depth of 825m (i.e., near the shelf break at 500 m), rather than in the deeper water of 3000-4000m depth on the western side of the grid of Fig. 26. We selected this time step to save on the computational time In this configuration, computations

(a) (b)

(c) (d)

Fig. 24. ***Ko Phi Phi case study*** **Widespread destruction on Ko Phi Phi, on 12/29/04 : (a) Middle section of the island, looking North; (b) Eastern side of the middle section, near cell phone tower looking East; (c) Cottage roofs from the North shore middle section transported on the South beach; (d) Southern harbor covered with debris, looking southwest.**

(a) (b)

Fig. 25. ***Ko Phi Phi case study*** **Situation on Ko Phi Phi, 2/05, after initial cleanup efforts.**

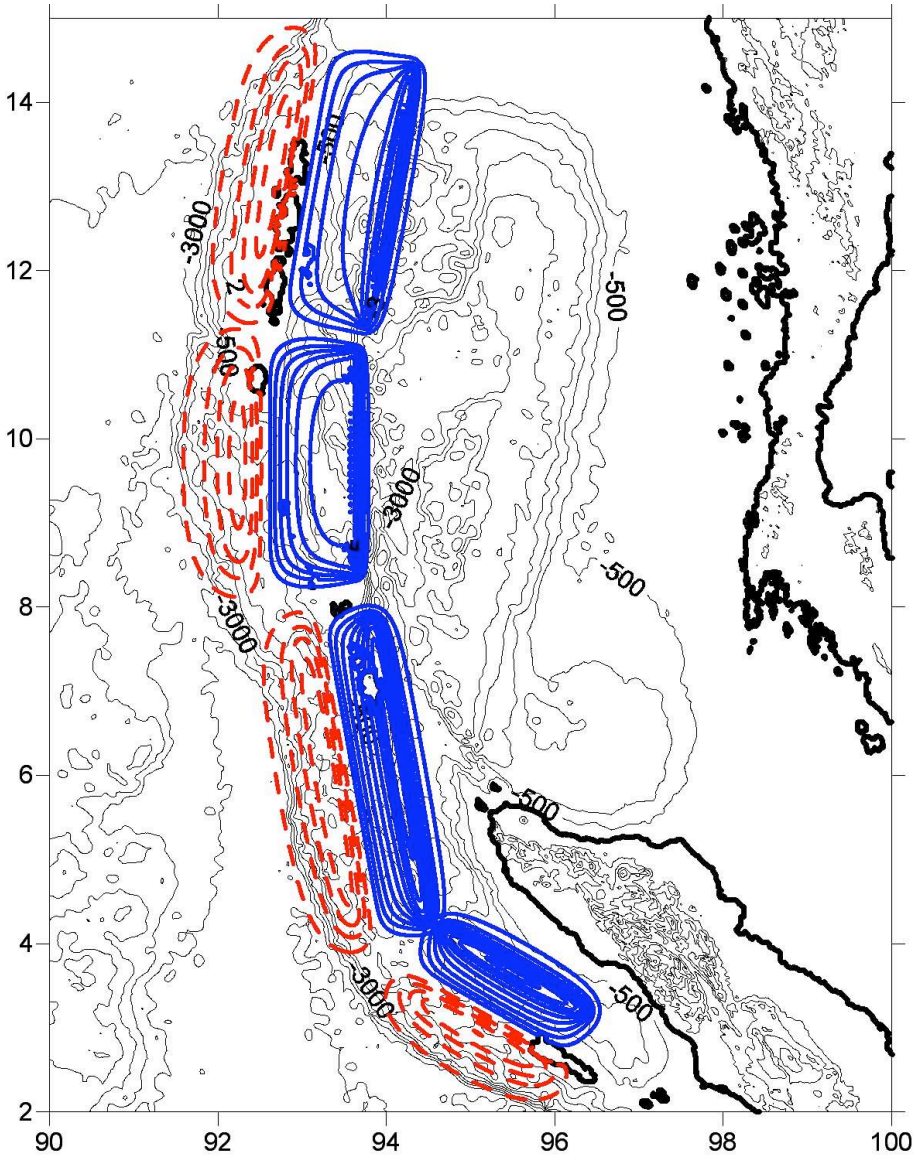

Fig. 26. ***Ko Phi Phi case study*** **Area and tsunami source modeled in Geowave for Phi Phi's regional grid, from 90° to 100° long. E and from 2° to 15° lat. N. Contour lines for the sources are plotted every 1 meter (red: uplift; blue: subsidence).**

on a 4 node Opteron cluster take 3'30" per time step.

As discussed before, the grid bathymetry and coastline topography were defined by digitizing data from the maritime charts of Fig. 19. Fig. 27 shows the level of detail this corresponds to for the selected regional grid. Comparing Figs. 19 and 27, we see that all the main features of both the topography and the coastline are well resolved, particularly in the shallower water around Phi Phi.

Results As of the end cruise, the computation with the regional model grid had reached 2h11' (or 1570 time steps) since the start of the earthquake. Wave breaking, however, that could not be absorbed by the dissipation terms in the model started causing instabilities, which ended computations. Preliminary results show arrival times at the location of the Mercator yatch very close to those obtained in the basin scale grid, as well as amplitudes of the leading

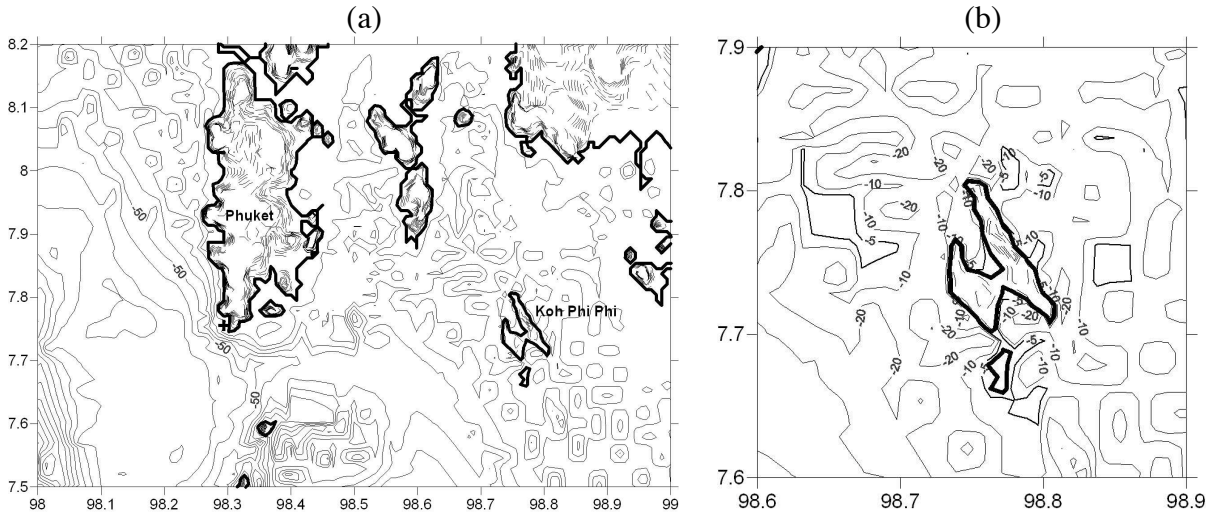

Fig. 27. ***Ko Phi Phi case study*** **Details of area modeled in Geowave regional grid (910 x 910 m) around Phuket (a) and Phi Phi (a,b). Bathymetry and coastline topography were obtained from maritime charts of Fig. 19.**

depression and first elevation waves. The depression wave in both the large and regional grid is too large, which may indicate that the maximum subsidence predicted for tsunami sources 2 and 3 is too large (Table 1). We are planning to restart computations with a slightly smaller subsidence specified at these sources. This might eliminate the instability problem observed here.

Also, we would like to use an even finer grid size around Phi Phi, such as the 500 x 500 m grid we initially tested. Fig 28 shows this grid resolution around Phi Phi and we can see by comparing it to Fig 27b that it is much better than in the current grid.

CONCLUSIONS

We develop four separate sources for the December 26, 2004 tsunami, resulting from a single earthquake occurring along a 1200 km long rupture zone. We relate differences in tsunami source parameters to differences in seafloor morphology.

We use these tsunami sources to perform a numerical simulation of the tsunami in the Bay of Bengal, at the ocean basin scale, with a higher-order Boussinesq model, and find reasonable agreement with observed runup values, time series at tide gages, measurements at one yatch, and a satellite altimetry track across the Bay of Bengal. Our simulation grid is quite fine, although we expect to refine it further in the near future, and exploits the significant capabilities of our Boussinesq wave propagation and inundation model. We are prepared to conduct a more detailed study that takes GPS data and gravity anomaly data into account, as well as the geophysical data acquired during this cruise, and that will be aimed at reproducing even better, measurements available for multiple tide gauges, as well as numerous detailed runup data that is being collected by a variety of international teams of scientists in the Indian Ocean area.

We did a preliminary analytic study of the tsunamigenic potential of slow versus fast slip uplift/subsidence. We are planning to better account for slow slip effects in future simulations.

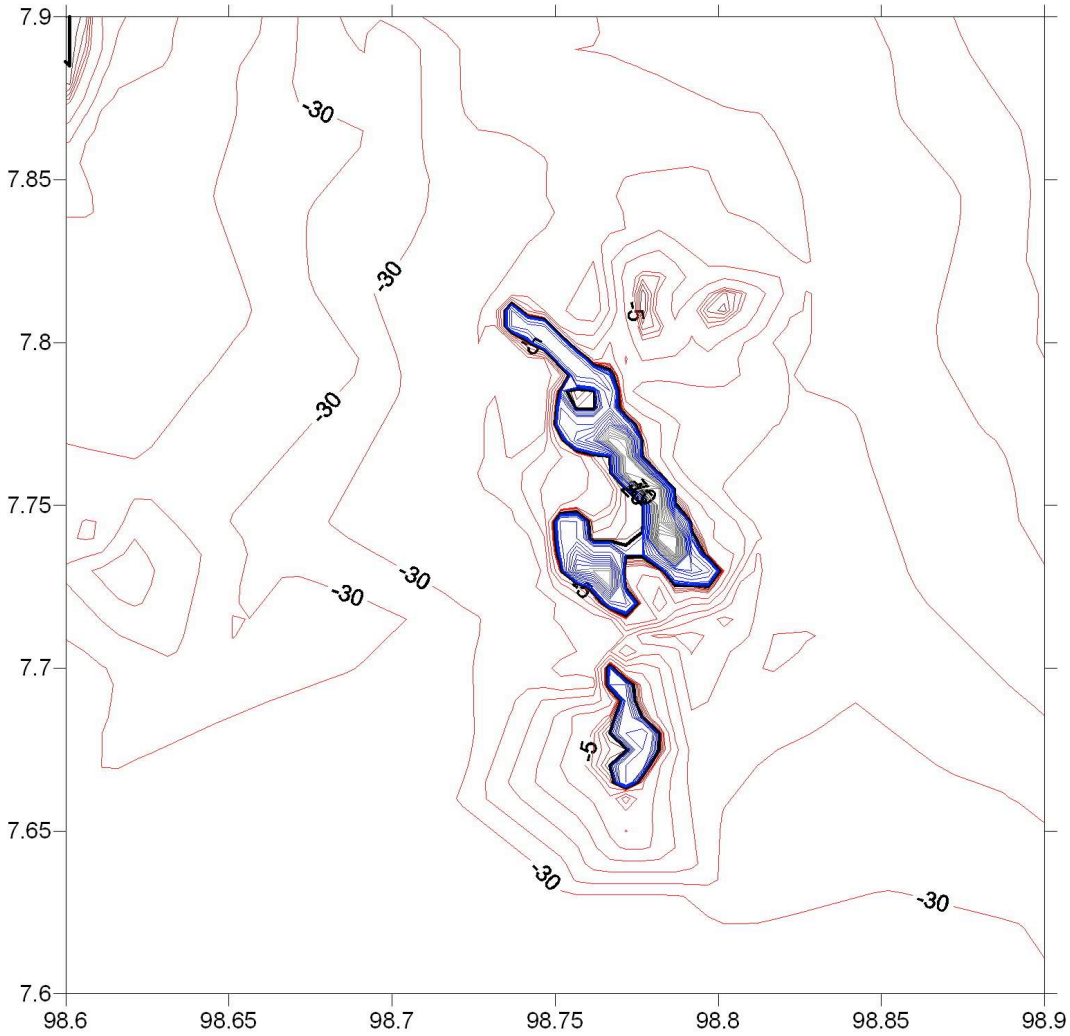

Fig. 28. ***Ko Phi Phi case study*** **Details of area modeled in Geowave regional grid (500 x 500 m) around Phi Phi. Bathymetry and coastline topography were obtained from maritime charts of Fig. 19.**

We conducted a case study for the area of Phuket and Ko Phi Phi, using a finer regional grid with topography obtained from maritime charts. We collected detailed information for the arrival of the tsunami at Ko Phi Phi, from a variety of sources (both reports with pictures and eyewitness interviews). Although this is work in progress, results obtained so far are promising.

ACKNOWLEDGEMENTS

In addition to the funding provided by the BBC and Discovery channel to support ship time, partial support for the modeling efforts during this cruise was provided from a US National Science Foundation teacher Armada program grant. Partial funding was also provided by the University of Rhode Island (USA), the University of Delaware (USA), the Commissariat à l'énergie atomique (France), and Institut de Recherche pour le Développement (Géoscience Azur, France). Mention of trade names is for identification purposes only and does not constitute endorsement.

REFERENCES

Ammon, C.J., Chen, J., Thio, H.-K., Robinson, D., Ni, S., Hjorleifsdottir, V., Kanamori, H., Lay, T., Das, S., Helmberger, D., Ichinose, G.Polet, J. and Wald, D. (2005). "Rupture Process of the 2004 Sumatra-Andaman Earthquake." *Science* (in press).

Chen, Q., Kirby, J. T., Dalrymple, R. A., Kennedy, A. B., and Chawla, A. (2000). "Boussinesq modeling of wave transformation, breaking, and runup. II: 2D." *J. Waterway, Port, Coast, and Ocean Engng.*, 126(1), 48-56.

Davis, D., Suppe, J., and Dahlen, F.A. (1983). "Mechanics of fold-and-thrust belts and accretionary wedges." *J. Geophys. Res.*, **88**, 1153 - 1172.

Gower, J. (2005). "Jason 1 detects the Dec. 26, 2004 tsunami." *EOS*, 86(3).

de Groot-Hedlin, C.D. (2005). "Estimation of the rupture length and velocity of the Great Sumatra earthquake of Dec. 26, 2004 using hydroacoustic signals." *Scripps Institution of Oceanography*, La Jolla, CA.

Gusiakov, V.K. (2005). http://www.pmel.noaa.gov/tsunami/indo20041226/sibolga_nias.htm

Hammack, J.T. (1973). "A note on tsunamis: their generation and propagation in an ocean of uniform depth." *J. Fluid Mech.*, 60(4), 769-799.

Hammack, J.T. and Segur, H. (1974). "The Korteweg-de Vries Equation and Water Waves. Part 2. Comparison with Experiments." *J. Fluid Mech.*, **65**(2), 289-314.

Hammack, J.T. and Segur, H. (1978). "The Korteweg-de Vries Equation and Water Waves. Part 3. Oscillatory Waves." *J. Fluid Mech.*, **84**(2), 337-358.

Harada, K. (2005). "The December 26, 2004 Sumatra Earthquake Tsunami, Tsunami Field Survey around Phuket, Thailand." http://www.drs.dpri.kyoto-u.ac.jp/sumatra/thailand/phuket_survey_e.html, Research Center for Disaster Reduction Systems, Disaster Prevention Research Institute, Kyoto University, Japan.

Kirby, J.T., Fengyan, S., Watts, P, and Grilli, S. (2004) "Propagation of Short Dispersive Tsunami Waves in Ocean Basins." *AGU Fall Meeting*, 12/04.

Lay, T., Kanamori, H., Ammon, C.J., Nettles, M., Ward, S., Aster, R., Beck, S.L., Bilek, S.L., Brudzinski, M.R., Butler, R., DeShon, H.R., Ekström, G., Satake, K. and Sipkin, S. (2005). "The great Sumatra-Andaman earthquake of 26 December 2004." *Science* (in press).

Kennedy, A. B., Chen, Q., Kirby, J. T., and Dalrymple, R. A. (2000). "Boussinesq modeling of wave transformation, breaking, and runup. I: 1D." *J. Waterway, Port, Coast, and Ocean Engineering*, 126(1), 39-47.

Kulikov, E. (2005). "Dispersion of the Sumatra tsunami waves in the Indian Ocean detected by satellite altimetry." Report from *P.P. Shirshov Institute of Oceanology*, Russian Academy of Sciences, Moscow.

Liu, P. L.-F., Yeh, H., Lin, P., Chang, K.-T., and Cho, Y.-S. (1998). "Generation and evolution of edge wave packets." *Phys. Fluids*, 10(7), 1635-1657.

Okada, Y. (1985). "Surface deformation due to shear and tensile faults in a half-space." *Bull. Seis. Soc. Am.*, 75(4), 1135-1154.

Tanioka, Y. (2005). Personal Communication, April 2, 2005.

Stein, S. and Okal, E. (2005). "Speed and size of the Sumatra earthquake." *Nature*, 434, 581-582.

Watts, P., Grilli, S. T., Kirby, J. T., Fryer, G. J., and Tappin, D. R. (2003). "Landslide tsunami case studies using a Boussinesq model and a fully nonlinear tsunami generation model." *Nat. Hazards and Earth Sci. Systems*, 3(5), 391-402.

Watts, P., Ioualalen, M., Grilli, S.T., , Shi, F. and Kirby, J. T. (2005). "Numerical Simulation of the December 26, 2004 Indian Ocean Tsunami using a Higher-order Boussinesq Model." In *Proc. 5th Intl. Symp. on Ocean Wave Measurement and Analysis* (WAVES 2005, Madrid, Spain, July 2005) ASCE Publication (in press).

Wei, G., and Kirby, J. T. (1995). "Time-dependent numerical code for extended Boussinesq equations." *J. Waterway, Port, Coast, and Ocean Engng*., 121(5), 251-261.

Wei, G., Kirby, J. T., Grilli, S. T., and Subramanya, R. (1995). "A fully nonlinear Boussinesq model for free surface waves. Part 1: Highly nonlinear unsteady waves" *J. Fluid Mech*., 294, 71-92.

Wells, D.L., and Coppersmith, K.J. (1994). "New empirical relationships among magnitude, rupture length, rupture width, rupture area, and surface displacement." *Bull. Seismological Soc. of America*, 84, 974-1002.

Yalciner A.C., Perincek D., Ersoy S., Presateya G., Hidayat R., McAdoo B., (2005). "Report on December 26, 2004, Indian Ocean Tsunami, Field Survey on Jan 21-31 at North of Sumatra", by ITST of UNESCO IOC.

Appendix B:

SEATOS Data Logs

Day (yearday)	Time (UTC) (unless noted))	Water Depth (m)	Description
			"The Landslide Site"
132	0535	4369	Bottom sediment kicked up muds soft sediment - ROV pulled off bottom - moving along bottom.
132	0540		Fresh burrows. Ripple marks on bottom.
132	0546		Focus in on tube worms.
132	0548		Strong curren 2-3/10 knot.
132	0552		Test of visuals - adjustment of cameras
132	0555		Tube burrows - stick up 1 cm from bottom. Current coming from behind sub kicking up mud. Plan to zig zag to site
132	0610		Fixing problem with camera
132	0649		Fish ~ 20 cm long begin moving
132	0654		Subtle ripple marks aligned ~050°
132	0658	4301	4301 m depth
132	0700		Track ~ 10cm wide, ~50°, both deges are raised up a little. Heading 060
132	0712		Crack strick 60° ~ 1cm displacement left up, right down.
132	0723	4291	Depth check
132	0739		Disturbance of biotracks
132	0758	4289	Cracks - tension Loose block stike. Opening ~ few cm
Time is now noted as local			
132	1600		Large block with bedding dip ~90°
132	1615		Slump block with bedding dip 50° (or ridge) strike 113°
132	1651		Strike 060° scarp 10's of cm long in down dip direction
132	1708		Ripples aligned 070°
132	1715	4257	
132	1720		Ripples ~ 070°
132	1721		Scarp/vertical face strike 060°
132	1728		3 parallel cracks strike 040°. Several meters long, opening a few cm. Numerous cracks - metres long - 50-57 cm

132	1800	4229	Umbellula on seabed Age?
132	1825		Unknown debris looks like a log
132	1833		Fracture thrust? Age? (Same feature as last entry) Strike ~080°
132	1845		Heading 060°
132	1849		Apparently a block, only top few cm exposed.
132	1855		Block partially exposed by a few cm. Age unknown, rounded edges.
132	1910		Lines from seafloor to surface?
132	1920	4208	Exposed rock face ~2m long
132	1925	4183	Boulder ~4 m across
132	1930	4191	Vertical rock face 2m long 1m high.
132	1934		2 cracks strike 080° meters long open a few cm
132	1937	4184	Several blocks - size few 10's of cm
132	1945	4176	Cracks meters long , cms opening
132	1959	4168	Vertical rock face 2meters long tens of cm high
132	2001	4164	Blocks, rubble 10-20 cm exposed rock surface, vertical, meters long, ~cm's tall.
132	2023		Cracks ~meter long cm wide
132	2047		Small, parallel cracks 10's of cm long, ~1cm opening.
132	2052	4107	Cracks/collapse structure heading 060, strike 060° (hand drawing included on sheet)
132	2149	4180	Block/boulder ~1meter
132	2212	4105	Small ridges and rocks (10's of cm)
132	2215	4104	Ridges ~1meter high
132	2220	4105	Blocks ~2meters
132	2225	4103	Scarp ~1meter tall
132	2350	4043	Large block, probably clay
133	0000	4039	Large block at the base of a steep slope, angular edges; vertical slope. Encountered - traversed up the scarp from 4041-4012
133	1210	4015	Crack
133	1220	3974	Small berm - horizontal features, perhaps closed cracks? Or bedding.
133	1225	3956	~2m high berm, buried the vacuum tube, so sediment is soft
133	1230	3938	rough edged fine grained seafloor
133	1230	3942	Scarp base
133	1230	3938	Talys - small blocks, angular
133	1231		soft clay 1/4 - 1/2 m wide scarp top.
133	1234	3933	Boulder @ top >2m wide angular blocks - very soft. Boulder has sharp deges with angular features

133		above 3933	Block of exposed seabed or a large block with horizontal bedding? The ROV made a 'mark' in the block so it is very soft clay
133		3931	top of scarp - block was at the base
133	1241	3923	Another small scarp
133	1244	3914	Tension cracks
133		3910	Block - perhaps tilted (away from the ROV)
133	1246	3910-3890	Small exposed ridge faces ~1/2m
133	1250	3870	Seafloor "dropped away" ~5m (pilot comment) and the seafloor is flat. Starting to see evidence of bioturbation
133	1255	3868	Still very flat.
133	1256	3866	Fresh scarp surface ~1-2 m high
133	1258	3868	Surface is "corrugated" - suggesting recent surface.
133		3854	Cracks or sediment textrue variations - horizontally contiguous.
133		3846	Small slides - small exposed faces
133	0100	3844	horizontal, multiple cracks
133		3839	small exposed failure faces nonstomizing cracks
133	0105	3834	flattening out. Changing tape
133	0109	3818	Still fairly flat
133	0110	3815	Horizontal "failure" scars - shown as different sediment texture
133	0112	3812	Block of sediment with "ubes" sticking out the side. We're not sure what the biology
133		3807	7m high hole that we climbed
133	0115	3797	encountered another face. Climbing it.
133		3789	Exposed face 1/2m high. Sharp edges
133		3785	Top of ridge - worm castes are @ the top of the ridge.
133		3771	Very rogh surface that looks like slickensides. Slickensides again. Scalloped clay-type features that could be fresh failed surfaces
133		3755	Worm castes? - Set down to try to capture image but too much cloudiness in the water. Setting down made an indentation on the seafloor - very soft clay - penetrated the seafloor with 100 lbs downward force.
133		3742	Smooth seafloor from stet to here with small holes poking up & worm casts or debris from above littering the smooth surface.
133	0143	3736	Biological tracks
133		3731	One of the "worm castes" looked like it slid in a track downslope. Slide marks on the seafloor vertical downslope sometimes with "worm castes" in them
133	0145	3717	Still climbing. Smooth slope more vertical "chutes" some branching
133	0155	3698	Smooth slope.
133	0212	3637	Smooth slope, with subtel evidence of downslpe lineations

133	0225	3588	Maintaining smooth slope
133	0238	3544	Sonar looks like ROV is moving between small downslope-oriented walls. Taking snapshot of multibeam.
133	0241	3533	Lineations (downslope) on the seafloor.
133	0251	3509	Setting down for bio inspection/photos
133	0252	3508	photo of perhaps a feeding worm and holes in the seafloor.
133	0255		Restarting transit upslope
133	0300	3493	Rough seafloor @ a small scarp. Slide surface with sediment @ base. Slip surface clay surface is 'rough'
133		3490	Reached the top of the scarp
133		3482	Scarp with rubble at the bottom.
133	0305	3483	Continuing up smooth slope
133	0309	3477	Fish ~ 20 cm long begin moving
133	0310		Seafloor dropped away from the ROV ~ 6-7 m based on pilot comments
133		3473	Scarp with downslope channels disturbed seafloor at the face. Vertical striations on a rough surface. Blotchy sediment with darker colors. Scalloped surface of the scarp. Slipsurface "giant" normal faults. Steeper slope as we go up
133	0320	3462	"sharp" fresh edges throughout scarp. 3462 reached the top o the scarp.3462 reached the top of the scarp.
133	0325	3442	Corrugated surface. Smooth with biological debris.
133	0327	3432	Smooth with biological debris.
133	0335	3421	Ledge with scree in front of scalloped at top - sharper at top with vertical rough surface - 1 ft high
133	0337	3418	Smooth bio debris
133	0346	3389	Gently lumpy surface with elongated lumps
133		3386	Lineated surface in downslope direction
133	0349	3383	Darker material in troughs - subtle relief
133	0356	3364	8 m high steep slope. Spotchly light and dark sediment. Smoother than last scarp.
133	0359	3357	On top of ledge
133	0403	3347	Steeper slope 13 m high splotchy surface rough downslope striations. Hummocky fine striations with larger scale corrugations scalloped.
133	0405	3343	At top - whoops, not yet!
133	0406	3335	Still going up. Highly oriented downslope. Rough surface - splotchy.
133	0407	3339	Nice striations
133	0409	3333	Chutes oriented downslope
133	0410	3328	Cracks parallel to strike of slope with dark material - multiple breakaways.

133	0411	3323	More cracks parallel to strike splotches elongate downslope. Whole series of cracks oriented parallel to slope.
133	0413	3317	Another crack
133		3320	Another crack
133	0411	3318	On top - total height 26 m. Note: Kate took vehicle depths.
133	0417	3299	Ridge parallel to slope small depressions behind it. Ridges - several in a row parallel to each other.
133	0420	3295	Chute downslope
133	0425	3294	Pockmarked surface
133		3297	Big cracks - rope on bottom. Open down to strike of slope.
133	0427	3295	Little graben - lots of cracks.
133	0430	3298	Pockmarked surface
133	0437	3327	Going downslope
133	0438	3331	END OF DIVE
			Landslide Site- "The Block"
136	1947	4431	N-S trending tracks or ripples amplitued ~ cm's
136	1949	4433	cracks
136	2000	4433	Steep Face ~1m high Age - Old? ROV collision caused vertical face, active erosion. Material cannot sustain high angle face. Requested still image of bio.
136	2032	4429	Mechanic arm picked up box L3, collected surface sediment @ (4.1145°, 93.1167°)
136	2130	4431	Images of sea anemone.
136	2140	4431	Animal sucked in.
136	2150	4413	Still image of a "glass" sponge (Golf ball on a tee).
	Jamie - Aaron on watch		
136	2211		Setting down - small crack?
136	2216		Rugose topography (small scale)
136	2223	4437-4454	Beginning to go downhill; far side of block; visibility poor.
136	2237		another "glass" sponge.
136	2241		Uneven, small-scale topography, somewhat lineated (ripples?)
136	2246	4483	Stopping to collect blade cores and a push corer. Far side of block, @ end of dive waypoint
136	2259		Not clearing. Moving a few meters to do that.
136	2307		Topography at set-down point characterized by small blocks. Some appear to have moved, leaving tracks. On inspection, this is ROV disturbance.
136	2329	4489	Taking first blade corer in new spot ~ 3m away from disturbed area.

136	2340		L5 in the bottom.
137	0005		Still trying to close core L5
137	0008		Lifting core
137	0015		L5 in basket
137	0022		Lifting L4
137	0025		ROV moving away from disturbed area
137	0026		Animal track
137	0031		Pishing in L4 - pushed in very straight
137	0044		Lifting L4 “really nice core” - Paul
137	0053		L4 in basket
137	0058		Lifting 3rd push core
137	0101		Pushing in core
137	0104		In basket
137	0106		END DIVE
137	0109		On the way up
			“The Ditch”
137	10:00		Dive 3 - the Ditch - started heading in a zig-zig pattern going from NW to SE
137	10:49	4473	On the seafloor; turbid; in the “ditch”; sonar shows walls ahead on both sides (more prominent to the right)
137	10:54	4474	blocks on the seafloor; < 0.5 m; lightly covered with muc
137	10:57		another set of small boulders; debris, diameters various; lightly dusted; largest up to ~1m
137	11:00		near “ditch” wall; broken material; ridge-like; debris field
137	11:02		smaller diameter broken material; all dust-covered; some ridges - “cottage cheese”
137	11:12	4488	~0.75 m cast, cobble-size debris; cracked, angular
137	11:13		overhanging clasts - slope?
137	11:15		multiple cobbles/debris
137	11:17		ripples - assymetric, 25 cm, bifurcating
137	11:18		more cobble-size clastts, heavily sedimented; degraded ripples
137	11:19		possible fractures?
137	11:21		heading for a drop-off
137	11:23		sedimented clasts. Debris field; dropping off
137	11:27		ripples, well formed; more sediment-covered clasts, scalloped-shape rippples. (ambient current ~0.1 knots from the south
137	11:30		small cobbles

137	11:38		stopping for a geotechical core. Flowwing material downslope: ROV is right in a slope; middle core #2 taken at stratified sediment on the walls of the depression made by ?
137	11:50		pushed the core into the area that looked sedimented and it flowed out completely as if it was liquefiable; we'll take another pusch core as an experiment, then take a blade core
137	12:25		ripples trending NW/SE suggests flow SW perpendicular into the ditch
137	12:29		slipsurfaces - soft sediment ~cm vertical no biology
137	12:38		slipface ~10 cm trending parallel to the ditch
137	12:42		current downslope, vertical face ~ less than 1/2 m looks fresh - asking for a core vertically
137	12:56		crack (possible) parallel to trench
137	13:00		blade corer L7 used horizontally right spring closed when pulled out - some sample on opposite side of deployed spring -closed other side to save sample
137	13:40		getting a round core @same site core #3
137	14:13		adjust atlas camera to better pictures of seabed
137	14:26	4493	image of scarps, blocks (still image) heading 117 degrees; position 3.623 N, 93.475E; ~1.5 m displacement (visual); scarps trending SE; ditch "thrust"; crack trending 116 degrees; additional images with suction tube as a scale
137	15:06	4494	a scarp picture #114
137	15:48	4497	scatters in sonar showing a structure parallel to the trench
137	16:09	4493	(re-interpretation) slippage features noted at 137, 12:29 are ripples caused by substantial downslope current
137	16:15		small ditch perpendicular to big ditch; small ditch ~ 1m across appears that color darkens uphill; small ditch 10s of cm deep; "traverse gully" trend 60 degrees upslope
137	16:29	4487	transverse gully diverges; gully depth 0.5 m (note: handwritten log shows picture of a bifurcated gully with flow moving in the direction from the bifurcation into a single gully)
137	16:41		small amphitheatre gully continues about 10 m wide
137	16:45	4451	following a gully upslope; may not be same as original; 40 m from ditch numberous gullies
137	17:00	4456	moving downslope. Gullies to the east ~ subparallel to ROV track
137	17:23		moving through small-scale blocks, "lumpy" terrain, possibly associated with sonar bright spots
137	17:25	4488	stopping for stills/video at slip blocks; 10-20 cm blocks; "4488" waypoint. Picture 146
137	17:35	4494	40-50 cm tall vertical face trending 45 degrees upslope scarp#3
137	18:24	4493	moving again

137	18:27		3 blocks, stacked. 30 cm each. Large vertical face, boulders at base, 50 cm high?
137	18:42	4490	moving again
137	18:52	4476	rocky bottom - chunks & fragments on seafloor
137	19:05	4486	taking sediment samples - core
137	20:17	4483	rubble
137	20:21	4476	rubble; attempt imaging - imaged angular, cracked blocks - size ~ 1ft.
137	20:47	4470	2 m vertical face. Fresh conchoidal texture on surface (note: hand-writting log shows a sketch of a crossection of one side of the ditch with a 2.5 m high vertical wall facing SW and rubble on the floor of the ditch). Bedding planes - thicknesses ~ cms; still images taken; cracks parallel to bedding, aperture ~ cm (note: handwritting log shows sketch of bedding with cracks)
137	21:05	4484	tried to take core - went in ~1.5" - retrieved, stowing and moving on
137	21:35	4484	still @ site - mud on lens of PAL/SECAM ; see blocks behind basket as ROV sits
137	22:06	4476	moving. Blocks scattering. Rocky talus
137	22:09	4472	at the wall - looking NW - way pt.
137	22:10	4469	rubble @ base of wall
137	22:15	4471	same feature/different area - bench w/ rubble on the top. Making mosaic top to bottom. 2 m high to top
137	22:27	4467	heading NW
137	22:32	4470	anther face/extension of same face
137	22:40	4470	blocks broken off from bench ~ 2m further
137	22:45	4470	slip (irregular) face - multiple benches
137	22:50	4472	multiple benches - rounded. Talus
137	23:54	4472	sharp edge - top of wall (Austin)
137	23:57	4475	overhangs - near top of wall
138	0:00	4475	sharp edge - top of wall
138	0:01	4475	chutes - talus on top, scalloped
138	0:04	4475	a jagged edge - top of wall
138	0:07	4481	recent failures; downward directed scallops
138	0:11	4485	stopped - talus slope, sedimented. Some evidence for gravitational creep
138	0:22	4489	moving north talus slope
138	0:26	4489	large talus slope, ~1 m across
138	0:28	4489	more blosk, plumose face (hackles); cracks; scalloped faces
138	0:30	4489	very large fractured block; some ripples (pop up, edges on both sides)
138	0:33	4485	some ripples; scalloped terrain

138	0:35	4485	stopping, bottom of large talus face (scarp?) - above, gentle face, overlying; - ~ 1foot vertical face, fresh fractures (conchoidal?); - below, small avalanche failures
138	0:45	4486	(tape ROV 051) taking stills of the scarp
138	1:00	4486	hitting the top of the face with the suction pipe - enough consolidation to lift the vehicle
138	1:06	4486	moving again; moving ~ north again
138	1:08	4486	bedforms - downslope creep. Changing heading to 090 degrees to pick up sonar target (landward side of the "ditch")
138	1:17	4485	scarp, w/ striations, scaly fabric. Multiple failure surfaces. Scale: 1- 3 ft. (stopped for pictures)
138	1:28	4485	moving w - to look at the seaward side
138	1:44	4491	ripples - paralleling the crests, very regularly spaced
138	1:45	4494	small, angular talus blocks, w/ current scour. Stopped near prominent sonar target (seaward wall)
138	1:58	4484	large clay (overconsolidated, then released?) talus block , > 0.5 m. broken along joints, rubble. (two orientations).
138	2:13	4484	same face. Slickenlines & tension cracks. Hackles on rough surfaces/slicked smooth surfaces - coarser striationss where pebbles have scraped along slicked surface
138	2:17		on the move
138	2:21		more talus edge of wall, more sediment or talus, angular blocks to 1/2 m max.
138	2:23		skid marks, multiple steps, sharp top to ridge
138	2:25		steps with near horizontal bedding
138	2:26		rough surface at top, smoother below, orthogonal vertical fractures
138	2:27		talus slope topped by finer scree
138	2:28		sedimented talus slope - older face? Heavily sedimented
138	2:31:50		sharp face, orthogaleal, vertical fractures, sedimented talus
138	2:32		wall is 6 m wide - nice plumose features on joint surface - stepped wall - more rubble
138	2:38		end of dive
			"Mosher's Mystery Tour"
144	1208	1293	ROV on bottom. Ledges, bedrock, friable mudstone? Undulating erosion of surface trend 340 degrees
144	1218	1302	heading 205 degrees Over a series of steps and highly eroded steps, trend 320 degrees. Current heading from 348-base of ledge, sandy, ripple marks trending 250 degrees- spacing between ripples ~10 cm.
144	1228	1312	Small basin coarse sand blade sample L7. Hydraulic leak in mechanical arm- dive is aborted
144	1229	0	(ROV repaired and dive restarted)

144	1558		ROV on bottom. Grooved erosional surface, orange starfish, very small amount of sandy sediment filling sub-parallel grooves. 3 or 4 photos taken up to #30. Starfish is "Freyella".
144	1621		Off the bottom and moving.
144	1624		Crossing small crack perpendicular to our path. Crack is ~20 cm across and 5-8 cm high, both edge surfaces are darker than host rock. Small brachiopod on crack surface. Stylastereme coral growing in center of crack. Baban thinks coral is leaning slightly as if anchor point has rotated. Photos up to #45.
144	1634		Arm is used to "grab" seafloor surface at crack; surface is firm but not solid. Claylike.
144	1638		Sucking up sediment, seafloor material, coral. Crack is filled with soft sediment. If material is very light colored on fresh surface.
144	1645		On the move again. Heading 070. Photos taken on the fly.
144	1646		Stopping at small crack orrientated 350 degrees strike.
144	1647		On the move.
144	1649		Several small overhanging ledges.
144	1650	1211	Cobbles that appear freashly broken. Photo #81
144	1651	1211	Nice anemine. Photo 88. Sharp ledge. Seafloor is rough and pocked with many small ridges and cracks.
144	1655	1213	Several ravines orientated roughly parallel to our heading (downslope).
144	1657	1213	Intersection of orthoganal cracks. Stopping. Photo #109. Cracks are not coated with dark manganese. Photo #119.
144	1703	1212	Numerous small orthoganl cracks. Seafloor has a "crust" ~20-30 cm thick that is broken and weathered.
144	1706	1216	Stopping at 90 degrees jointing with upside- down sponge-like creature.
144	1709	1213	Debris on surface. Stopping to take cobble sample of pavement. Covered with biology.
144	1722	1213	Sample on the coring tray.
144	1724	1217	u/w - 067 degrees. Sand waves, in lows.
144	1728	1217	Stopping to photograph crinoid. More cracks, filled with sediment. Intersecting joint sets, but no indication of recent offsets.
144	1729	1219	More relief <1m. Most cracks parallel to heading (041 degree) perpendicular to pop-up trend. Photos to #166
144	1732	1219	Dead palm frond, presumably from the tsunami. Photo to #174. Stopping to collect.
144	1740	1220	u/w - 045 degree. Exhumed cracks . Small normal faults? Pronounced ripples in lows. Photos to #191.
144	1746	1220	067 degrees Heavily jointed terrane. Photos to #213.

144	1752	1225	Ledges, loose boulders. Heavily jointed.
144	1756	1229	Some black pebbles in cracks.
144	1804	1236	Continued jointed terrane. Heavily cracked. Photos to #248.
144	1809	1237	Plywood fragment. Photos to #262.
144	1811	1235	Orthoganal joint sets. Steeper slope, sepped.
144	1816	1235	Photos to #288
144	1817	1235	More debris- corrugated tin? U/w - 067 degrees.
144	1818	1235	Tree branch.
144	1820	1241	Photos to #320. Eel-like fsh.
144	1821	1241	Rounded cobbles, atop jointed terrane. Photos to #319.
144	1825	1243	U/W - 067 degrees.
144	1827	1242	U/W - 040 degrees.
144	1833	1242	Debris field. Photos to #336.
144	1835	1242	Rougher terrane; steeper slope.
144	1838	1243	U/W 045 derees Currents.
144	1840	1247	Less debris. Moving downslope.
144	1844	1250	Photos to #365
144	1848	1254	Moving downslope. Exhumed cracks, heavily jointed.
144	1853	1264	Debris field
144	1855	1272	Stepped slope. Heavily craked and jointed.
144	1857	1283	Stepped slope. Much debris.
144	1900	1290	Large Boulders. Near the bottom of the ditch.
144	1905	1307	Lots of smaller cobbles, not as poorly sorted.
144	1907	1300	Beginning up the northeastern slope.
144	1910	1307	Outcrop-heavily cracked. Photos to #422.
144	1912	1309	Stopped- bottom of ditch, near base of slope.
144	1920	1309	U/W - 040 degrees.
144	1922		Pavement outcrop, jointed, cracked. Climbing slope.
144	1924		Steeper bedding dips (?) Rippled sand.
144	1926		Photos through #443
144	1931		Ledge (current erosion, not breaking).
144	1933		Photos to #461.
144	1935	1300	Another Ledge. Photos to #472.
144	1939	1290	Ending Dive. All stopped.
			“Mosher’s Toe”

145	1	2686	On the bottom. Muddy. Sponge. Taking (L7) blade and push coe. Photos through #11. Trend of dive -200 degrees Survey Line - 244 degrees
145	37		U/W
145	39		Small hillocks. Another sponge. 233 degrees.
145	41	2686	Crack on the seafloor, 1-1.5 m. Temperature 5.5 degrees C (warm for this depth). Photos through #15.
145	46		Coconut on the sea floor.
145	47		Temperature 5 degrees C.
145	52		Heading 220 degrees. Resting traces, muddy seafloor. Speed 0.2-0.3 kts.
145	103		Long track, muddy, mostly flat seafloor.
145	105	2685	Another crack-really a burrow? Charateristics the same as the previous one, shrimp living in the burrow. Will be called "gashes"
145	116	2685	Small hummocks.
145	121	2685	Debris? Small hummocks. Biologically dense.
145	125	2685	Biological debris.
145	129	2685	Photos through #38.
145	132	2685	Hummocky. Base of slope approaching.
145	136	2683	Base of slope.
145	139	2673	Hummocky. Piles of fecal material. Biologically active.
145	144	2662	Hummocky. Photos through #40.
145	151	2646	Photos through #44.
145	157	2635	Hummocky. Many tracks.
145	204	2616	Collecting sponge.
145	217	2616	U/W again.
145	218	2616	Photos through #52
145	229	2591	Approaching the top of the slope. Taking a blade core (L-4).
145	241	2592	Blade core (No. 4) taken.
			"Don vs. the Volcano"
145	1248	1695.3	Lat. 6.27 Long. 94.44 Susan writing for Tim's description- reached bottom. Poor visibility. Heading 70 degrees. Shelf-mudstone with silt. Material floating 079 degree heading.
145	1253	1700	Ledge
145	1254	1702	Stopped to see make up of bottom by poking it with claw. Took samples by suction.
145	1305	1702	Picking up a sample of black rock with white underneath. Irregular, angular, tear drop shape. "Size of a dinner plate." Collected in front basket

145	1310	1702	On the move again.
145	1311	1703	Stopped to break a piece off a ledge. Looks all black. Collected fist sized-angular fractured off. Dumped it and will pick up a larger sample. Size of a loaf of bread (Greek) half moon shaped.
145	1324	1703	moving toward flawks 107 degrees numerous small ledges (few cm high). Cobbled surface with little covering.
145	1328	1703	several ledges, trending 080, downward to North.
145	1332	1703	Stop for sample. Tenderloin shaped. Ledge with horizontal fabric.
145	1346	1703	Cobble fields alternating with small ledge, as ROV moves toward flanks of cone.
145	1350	1692	Boulderfield. Cracked through weathered boulder.
145	1414	1690	Cobble sample.
145	1416	1689	Moving up flank.
145	1419	1687	Large boulders with exfoliation
145	1427	1676	Moving up flank. Numerous boulders, several meters in size. Small fields of well-sorted cobbles.
145	1453	1630	Sample, dead coral.
145	1505	1608	Mosaic of fan coral. Vacuum sample of white coral. Hard, compact rock.
145	1527	1604	Moving on, up steep face, several meters tall. Large boulders with pitted tops. Cooling rind?
145	1600	1534	Levels out near ediface. Possible caldera? Rubble field, collect rock sample. Fist sized sample.
145	1614	1530	Sample secured. ROV moves on shot 515.
145	1622	1530	Still images of Bryzoan 523
145	1630	1522	move rounded blocks at the top.
145	1631	1521	still images 528
145	1632	1518	Still images to 530 (of bryazoan was the last shot)
145	1635	1510	going up again after a relatively “flat” interval
145	1636	1504	lots of dead coral
145	1640	1492	coming over the caldera
145	1643	1492	bennatulides-stills being shot up to #555
145	1647	1473	562 on the still shots
145	1650	1473	stopping at 1650 for pilot change
145	1649	1470	smoother surface that looks more like sheet flow #568 still image count
145	1707	1472	Descending into the summit caldera. Blocky terrane; steep wall.
145	1713	1479	At the base of the caldera; smooter surface- sheet flows. *may not be complete

145	1714	1482	Some sediment dusting. Small debris. 5.75 degrees C. Some dead coral. Heading SE.
145	1723	1505	Heading 050. Cobbles, edge of flow. More dead coral.
145	1728	1513	Rounded cobbles, uiniform size. More sediment cover (current speed 0.2 kts)
145	1735	1525	Blocky terrane stepped topography.
145	1737	1534	More debris than before.
145	1741	1555	Lots of coarse sand between 8
145	1745	1555	nubble dusted with sediment - turning around.
145	1748	1555	Chilled rinds on one side of block. Photos through 644
145	1750	1542	Surface of blocks have a web-like cracks in chilled rind, tightly packed pile of boulders.
145	1752	1542	Going along top of flow with chilled Margin and cooling cracks.
145	1801	1532	END DIVE

ocean.oce.uri.edu/seatos